Master's thesis

NTNU
Norwegian University of Science and Technology
Faculty of Engineering
Department of Geoscience and Petroleum

Marthe Jacquette Dalheim Ottem

The Longyearelva River-to-Ocean System

Monitoring an anthropogenic arctic fluvial system in changing climate over short and long timescales

Master's thesis in Geology
Supervisor: Bjørn Frengstad (NTNU) and Lena Rubensdotter (NGU)
Co-supervisor: Aga Nowak (UNIS) and Maria Jensen (UNIS)
June 2022

NTNU
Norwegian University of Science and Technology

UNIS
The University Centre in Svalbard

Marthe Jacquette Dalheim Ottem

The Longyearelva River-to-Ocean System

Monitoring an anthropogenic arctic fluvial system in changing climate over short and long timescales

Master's thesis in Geology
Supervisor: Bjørn Frengstad (NTNU) and Lena Rubensdotter (NGU)
Co-supervisor: Aga Nowak (UNIS) and Maria Jensen (UNIS)
June 2022

Norwegian University of Science and Technology
Faculty of Engineering
Department of Geoscience and Petroleum

NTNU
Norwegian University of
Science and Technology

Abstract

The influence of climate change on episodic and dynamic environments, such as the Longyeardalen source-to-sink system, is little documented. The Arctic responds two to six times faster to climate change than the rest of the world, underlining the importance of creating long-term data series to improve the scientific understanding of how climate change impacts the Arctic. This study aims to investigate the long-term geomorphological development of the arctic Longyear delta with respect to river-to-ocean interactions. The study is a part of a long-term monitoring project (RiS ID 11641). The hydrology, sediment transport, and erosion in Longyeardalen were investigated along with a twin master study by Pallesen (2022), who focused on the source and transport in the source-to-sink system. A large collection of remote sensing data, together with hydrological and geomorphological monitoring and mapping, were applied to investigate the aim and quantify the changes detected in the delta.

Results show seasonal and inter-seasonal trends in the discharge and the transport of suspended sediment. In Longyearelva it was hypothesized that the hydrological system was dominated by shifting controls through the melting season. The beginning of the season was dominated by snowmelt, suggested by low discharge and sediment transport. The middle of the season was dominated by glacier melt, suggested by high diurnal fluctuations and correlation between the discharge and sediment transport. The end of the season was dominated by thawing permafrost, suggested by high sediment transport and low discharge. The temperature was found to be the main controlling variable for the beginning and middle of the melting season.

Along the Longyeardalen coastline three sections were identified; 1) an erosional coastline west of the Longyear delta, 2) a fluctuating coastline along the Longyear delta, and 3) a depositional coastline east of the delta. The delta morphology is a result of the sediment transported, the depth of the fjord, and the transport mechanisms acting upon it. Two conceptual models of delta development are presented. The first showing delta progradation over the last 10 ka years, after the past glacial. The second illustrates how the progradation of the Longyear delta became asymmetrical with a large erosional and depositional zone because of longshore transport. The two main factors that alter the delta front position were found to be isostatic uplift and progradation due to sedimentation in the delta and coastal zone.

Short-term analysis shows rapid net erosion of the shoreline west of the delta and rapid net progradation east of the delta. The shoreline by the delta has been largely fluctuating and highly dynamic for the last 30 years. Long-term analysis shows no net erosion. The smallest progradation occurred west of the delta, with an overall large progradation in the east. The highest net progradation documented was up to 167 m in the delta front over the last 85 years. The long-term progradation is a result of combined natural accretion and anthropogenic interference. Areas that are already prone to erosion or deposition will likely continue to experience the same development in the future.

The Arctic is projected to become warmer with increased precipitation and reduced sea ice. The long-term consequences of climate change are difficult to foresee, although they will likely affect the entire source-to-sink system. Continued monitoring of the system is therefore highly recommended for a further understanding of the glacifluvial catchment system's effect on the river-to-ocean interactions and closing knowledge gaps.

Sammendrag

Påvirkningen av klimaendringer på episodiske og dynamiske miljøer, slik som Longyeardalen «kilde-til-avsetning»-systemet, er lite dokumentert. Arktis responderer to til seks ganger raskere på klimaendringer enn resten av verden. Dette understreker viktigheten av langtidsovervåkning, for en forbedret forståelse av hvordan klimaendringer påvirker Arktis. Denne studien tar sikte på å undersøke den langsiktige geomorfologiske utviklingen av det arktiske Longyear-deltaet, med hensyn til elv-til-hav interaksjoner. Studien er en del av et langsiktig overvåkingsprosjekt (RiS ID 11641). Hydrologi, sedimenttransport, og erosjon i Longyeardalen ble undersøkt sammen med en tvillingstudie av Pallesen (2022), som fokuserte på sedimentkilder og -transport i systemet. En stor samling av fjernmålingsdata, sammen med hydrologisk og geomorfologisk overvåking og kartlegging, ble brukt til å undersøke målet med studien, samt kvantifisere endringer oppdaget i deltaet.

Resultatene viser årlige trender, samt trender innad i sesongen, i vannføringen og transporten av suspenderte sedimenter. En hypotese var at det hydrologiske systemet var dominert av skiftende kontroller gjennom smeltesesongen. Begynnelsen av sesongen var dominert av snøsmelting, antydet av lav vannføring og sedimenttransport. Midten i sesongen var dominert av bresmelting, antydet av høye daglige svingninger og høy korrelasjon mellom vannføring og sedimenttransport. Slutten av sesongen var dominert av tining av permafrost, antydet av høy sedimenttransport og lav vannføring. Temperatur ble vist å være den viktigste kontrollerende variabelen for begynnelsen og midten av smeltesesongen.

Langs Longyeardalens kystlinje var tre seksjoner identifisert; 1) en erosjonskystlinje vest for Longyear-deltaet, 2) en fluktuerende kystlinje langs Longyear-deltaet, og 3) en avsetningskystlinje øst for deltaet. Deltamorfologien er et resultat av sedimenttilførsel, fjorddybde og de påvirkende transportmekanismene. To konseptuelle modeller for deltautvikling er presentert. Den første viser deltautbygning over de siste 10 ka år, etter siste istid. Den andre illustrerer hvordan asymmetrisk utbygning av Longyear-deltaet med erosjons- og avsetningsområder skjedde som et resultat av transport langs kysten (longshore transport). De to hovedfaktorene som påvirker deltafrontposisjonen er isostatisk landheving og utbygning på grunn av sedimentasjon i delta- og kystsonen.

Korttidsanalyser viser en rask netto erosjon av strandlinjen vest for deltaet, og rask netto utbygning øst for deltaet. Strandlinjen ved deltaet har i stor grad vært varierende og svært dynamisk de siste 30 årene. Langtidsanalyser viser ingen netto erosjon. Den korteste utbygningen var vest for deltaet, og en stor utbygning i øst. Den høyeste netto utbygningen som er dokumentert var opptil 167 m i deltafronten over de siste 85 årene. Den langsiktige prograderingen er et kombinert resultat av naturlig tilvekst og menneskeskapt påvirkning. Mest sannsynlig vil områder som allerede er utsatt for erosjon eller avsetning fortsette å gjennomgå den samme utviklingen i fremtiden.

Arktis forventes å bli varmere med økt nedbør og redusert havis. De langsiktige konsekvensene av klimaendringer er vanskelige å forutse, selv om de sannsynligvis vil påvirke hele «kilde-til-avsetning»-systemet. Det anbefales å fortsatte med overvåking av systemet for en ytterligere forståelse av den glasifluviale nedbørssystemets effekt på elv-til-hav interaksjoner, samt tette kunnskapshull.

Preface

This master thesis concludes my studies in the MSc program in Environmental and Geotechnology at NTNU. I decided to write my thesis in English in hopes that those who would find these results interesting would not be limited by a language barrier. After all, the climate change in the Arctic does not care about nationality or disciplinary fields. I am most appreciative of NTNU and UNIS for all the opportunities offered to me during my time as a master's student. It has been a year since I traveled to Svalbard for three months of fieldwork, not knowing how much I would cherish the memories I made there.

Lena Rubensdotter, you have exceeded all my expectations for a supervisor. I am grateful for the guidance and opportunities you have given me. You have inspired me, taught me, and encouraged me. All of which I am sure will make me a better geologist in the future. Special thanks must also be given to my supervisor Bjørn Frengstad for all the hours of discussions, support, and Twists. My co-supervisor Aga Nowak has been invaluable during the fieldwork, and the feedback you have given me has been much appreciated. Thanks to my co-supervisor Maria Jensen for the input and for including me in the coastal dynamics group for interdisciplinary discussions.

Thank you to my field partner Lene Pallesen, first for being a valuable friend, and secondly for support, proofreading, and everything else you have done for me. I am so glad I got to share this with you.

Three months of fieldwork in Longyearbyen and the opportunity to present preliminary results at the Svalbard Science Conference 2021 were possible thanks to the financial support of the Research Council of Norway (the Arctic Field Grant). Thanks must also be given to The Norwegian Water Resources and Energy Directorate for contributing to the project.

I must also thank Martin Løvaas and Juliano Hanna for granting me access to their data, the employees at UNIS and at NTNU Department of geoscience for helping me with field- and laboratory work, and Ashton for doing the heavy lifting of rocks.

To my family and friends, without your support, I would not be where I am today. A thank you to my partner Aleksander for always being there for me and helping me in my final hours of need. I am grateful to the third-floor unofficial party committee for evening diversions during the fieldwork. And lastly, my gratitude towards the coffee machine, working long hours with me during the final months of writing my thesis.

Marthe Jacquette Dalheim Ottem

Trondheim, 1st of June 2022

Cover photo

The cover photo shows Longyearelva and the Longyear delta in August 2021. It was taken from Platåberget towards Adventdalen. Photo by Lene Pallesen.

Contents

List of figures

List of tables

List of equations

Abbreviations and dictionary

Abbreviations	Meaning
DEM	Digital elevation model
DSAS	Digital shoreline analysis system
EC	Electronic conductivity
ETRS	European terrestrial reference system
GCP	Ground control points
GIA	Glacial isostatic adjustment
GIS	Geographic information system
GPS	Global positioning system
HWL	High water line
LGM	Last glacial maximum
NGU	Geological Survey of Norway
NPI	The Norwegian Polar Institute
NSM	Net shoreline movement
NTNU	Norwegian University of Science and Technology
NVE	The Norwegian Water Resources and Energy Directorate
Q	Discharge
RIS	Research in Svalbard
RSL	Relative sea level
SfM	Structure from Motion
SSC	Suspended sediment concentration
SSL	Suspended sediment load
SSY	Suspended sediment yield
Tif	Tagged image file format
UNIS	The University Centre in Svalbard
USGS	The United State Geological Survey
UTM	Universal Transverse Mercator
WMTS	Web Map Tile Service
xx-PT	*Location*-Passive tracer

Dictionary

Norwegian	English
Bre	Glacier
By	Town
Dal	Valley
Elv	River
Energiverket	Powerplant
Fjell, berg	Mountains
Fjord	Fjord
Lufthavn	Airport
Søppelfyllinga	Land fill
Veg	Road

1 Introduction

1.1 Aim of study

In 2018 a long-term project was initiated by UNIS. The monitoring of the Longyeardalen catchment system was continued as a part of a long-term monitoring project (RiS ID 11641) during the summer of 2021. The aim of the study was to investigate the long-term geomorphological development of the arctic Longyear delta with respect to the hydrological system in Longyeardalen. The development of the coastline and delta is affected by sediment transport and seasonal variations from a glacierized catchment. It is unknown how continued climate change can affect the future development of river-to-ocean interactions. A list of research questions is presented to be further discussed:

- Can a baseline dataset be extracted?
- Recent climate reports predict that erosion and sediment transport will increase, along with average air temperature, precipitation, and runoff (Hanssen-Bauer et al., 2019). How will this affect the Longyear delta and the coastline development?
- Does reduced sea ice slow down the delta progradation due to wave erosion?
- How does the sediment input in a changing climate affect the development of the delta?

1.1.1 Motivation

The interest in the Arctic has increased due to the influence of climate change on episodic and dynamic environments, such as arctic hydrological systems. The Arctic response to climate change is among the fastest on the planet. The Arctic experiences warming two to six times faster than the rest of the world(Nowak et al., 2020). Svalbard coasts and coastal dynamics are little documented. Furthermore, anthropogenic interference and human presence often coincide with coastal systems. Long-term data series significantly improve the scientific understanding of how climate change is impacting the Arctic. Long-term monitoring projects like this are therefore vital for closing knowledge gaps and for achieving a better understanding of the glacifluvial catchment system's effect on river-to-ocean interactions. To approach these facts, and present and future problems, the detection of change over time will be used to create baseline data.

A transformation of the coast is planned in Longyearbyen with further development of the city center and the industrial areas. According to the area plan (Longyearbyen Lokalstyre, 2017), sections of the coastline are assigned as recreational spaces. The plan includes securing the beach zone from the Longyear delta to Vestpynten for a potential large harbor. Hazardous areas regarding avalanches, fire, and flooding have been mapped, while the potential threat of coastal erosion and sea level rise has only been acknowledged. Recent reports have documented coastal erosion threatening cultural heritage sites in Adventfjorden (Nicu et al., 2021; Nicu et al., 2020), the road from Longyearbyen to the airport (Jaskólski et al., 2018), and the road to Bjørndalen (Guégan & Christiansen, 2017).

1.1.2 Collaboration

In 2018 this long-term project was initiated by The University Centre in Svalbard (UNIS). Cooperation between the Geological Survey of Norway (NGU) and master's students from the Norwegian University of Science and Technology (NTNU) arose in the following years. The

project called “Hydrology, sediment transport and erosion in Longyeardalen” was developed to investigate hydrological and geomorphological changes in Longyeardalen in a changing climate and is currently running under the RiS ID 11641. Both Longyearbyen Lokalstyre and The Norwegian Water Resources and Energy Directorate (NVE) have shown interest and support for the project.

There are several projects under RiS ID 11641 connected to the long-term monitoring of Longyeardalen. For the 2021 melting season it was decided to have two master's students studying the Longyeardalen source-to-sink system as twin-studies. Pallesen (2022) investigated the source and transport in the system in her thesis “Sediment source-to-sink in a warming Arctic; thawing moraines, slope processes and river erosion in Longyeardalen, Svalbard”. A joint effort was made in data collection and processing regarding drone operations, the hydrological monitoring station, and bedload transport.

1.2 Previous studies

Recent multidisciplinary climate reports from Svalbard (Hanssen-Bauer et al., 2019; Moreno-Ibáñez M et al., 2021) focus on long-term monitoring of key variables in the Arctic to observe, attribute and describe the effects of climate change, and make future projections. These highlight the importance of continued monitoring and documentation of the drastic changes already observed and future predictions.

Several hydrological and sedimentological studies (Etzelmüller et al., 2000; Stenius, 2016) and theses (Grønsten, 1998; Løvaas, 2021; Riger-Kusk, 2006) have previously been executed in the Longyeardalen catchment system. These studies used different techniques, localities for measurement stations, and varying temporal extents to calculate and estimate results. This makes it difficult to compare results and develop models for future predictions.

Studies of the Longyear delta are more limited. Coastal dynamics and morphology of the Longyear delta have only been partially described in a study by Dill et al. (2021) and in a thesis by Hergot (2021). The oldest documentation of the delta development was by Prior et al. (1981). A study by Jaskólski et al. (2018) investigated the scale of degradation of the coastal zone in Longyearbyen and examined the impact of coastal hazards on major elements of community infrastructure. Detailed studies have been done in Adventfjorden and the Advent delta (Guégan & Christiansen, 2017; Lønne & Nemec, 2004; Nicu et al., 2021; Nicu et al., 2020; Węsławski, 2011; Weslawski et al., 1999).

1.3 Climate and geographical setting

A formal definition of the Arctic is the region north of the Arctic Circle (66,5˚N). Characteristics are continuous summer daylight and polar nights with duration depending on latitude. The Arctic does not have strict geographical boundaries. The Arctic land is commonly divided into High Arctic and Low Arctic, where High Arctic is characterized as a polar dessert. Svalbard is defined as a High Arctic area. The mountains on Svalbard are characterized by steep valleys, active glaciers, little vegetation, and slope processes, supporting high erosion rates (Serreze & Barry, 2014). The Svalbard archipelago extends from 74˚N to 81˚N. Longyearbyen (Figure 2), the administrative center of the archipelago, is located in the Longyeardalen valley (hereby to as Longyeardalen) (Figure 1). Longyearbyen lies 78˚ 10’ N and has the highest number of citizens in Svalbard. Two glaciers can be found in the Longyeardalen catchment system. They are the main contributors to the glacial

meltwater in the river Longyearelva. Longyearbreen and Larsbreen have been described as cold-based glaciers with temperate patches (Etzelmüller et al., 2000).

Variable climates can be found in the archipelago Svalbard due to its extent. Longyeardalen is located in the central part of Svalbard, where the climate is more continental. The sea is a controlling factor of the Svalbard climate because of the location between the ice-covered Arctic Ocean and the warmer North Atlantic sector. The climate on Svalbard is vulnerable due to its proximity to the sea, exposing the land to maritime changes. Datasets from 1982 to 2015 are dominated by negative trends related to sea ice conditions and terrestrial snow melt. In Svalbard, the melting season is typically from May to October (Nowak & Hodson, 2013). The average start time of snow melt has advanced from late June to mid-June. The melting season is beginning earlier and freezing up. Over the last 40 years the number of days with temperatures above 0°C have almost doubled, and increasingly negative mass balances for the glaciers of Svalbard have been observed over the last twenty years (Nowak et al., 2020).

Conditions on Svalbard include scant vegetation, the presence of ice-rich permafrost and frost-susceptible marine sediments in the ground, and high glacier coverage. This affects the processes of erosion and sediment transport in the rivers on Svalbard compared to middle latitude systems. This also makes the environment very sensitive to disturbance from human activity. It is therefore important for management purposes to find out more about erosion activity and sediment yields in Svalbard rivers (Bogen & Bønsnes, 2003; Hanssen-Bauer et al., 2019). Naturally, Longyearelva was a braided river system taking up most of the valley floor in Longyeardalen. As the infrastructure in Longyearbyen developed, the lateral extent of the river was restricted. A lot of infrastructure in Longyearbyen is confined to areas prone to potentially hazardous processes (e.g., avalanches, solifluction, floods) (Hanssen-Bauer et al., 2019).

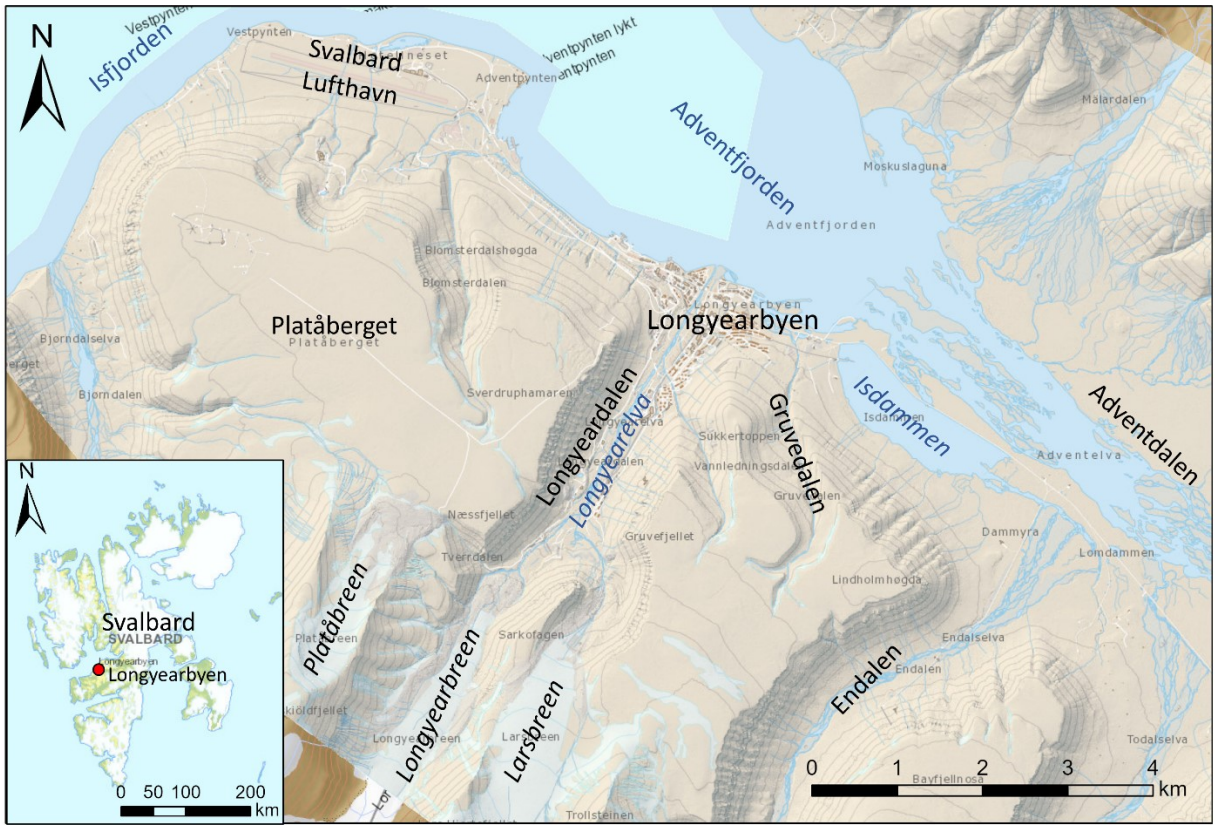

Figure 1 Overview of Longyeardalen and the surrounding area. The basemap was developed by NPI based on data from 2009 (Norwegian Polar Institute, n.d.-a).

Figure 2 Annotated drone image from 19/08/21 of Longyeardalen and the Longyear delta.

1.4 Svalbard's history

The discovery of Svalbard happened in the late 1500s during a Dutch expedition. In the following years the Arctic was considered an important resource for whale hunting and fur. Humans began to stay over the winter and eventually formed societies (Svalbard Museum, n.d.). The Svalbard Treaty gave Norway sovereignty of Svalbard in 1925. This resulted in rising motivation to develop Longyearbyen and the mining industry. Longyearbyen has a long history of mining. The first coal mining was started in 1903 by Trondhjem-Spitsbergen kulkompani, which was taken over by Store Norske in 1910. Store Norske still exists today and is responsible for mining coal and providing Longyearbyen with power (Store Norske, n.d.).

1.4.1 Anthropogenic influence in Longyeardalen

Early in the 1900s infrastructure was built in close proximity to the mines. Gradually the infrastructure expanded from the west side of Longyeardalen to the river mouth of Longyearelva and further to the east side of the valley. The settlement on the west side was completely destroyed in 1943, during the Second World War. After the war the development of the infrastructure continued on the west side and inwards in Longyeardalen. Nybyen was built in approximately 1970. From 1985 onward further expansion happened towards the valley Gruvedalen and the flood plain. When Store Norske took over the mining, the settlement changed from being a company town to an open community. As the town continued to grow, Longyearelva had to be continuously managed to run in a single channel to gain space for building more infrastructure (Figure 3). Recent building development has mostly taken place on the old riverbed (Hanssen-Bauer et al., 2019; Store Norske, n.d.). In 2017 measures to manage the river was taken over by The Norwegian Water Resources and Energy Directorate (NVE) to ensure that the river does not erode further into the riverbed and infrastructure. The measures also allow for further development and construction sites (Hanssen-Bauer et al., 2019; Longyearbyen Lokalstyre, 2017). Today the upper parts of the river system behave like a braided river originating from Larsbreen and Longyearbreen. From Nybyen and down to the sea, the river is confined to a single channel by mitigation walls (The Norwegian Water Resources and Energy Directorate, 2020).

Figure 3 Truck driving on the Longyearelva riverbed in the Longyeardalen valley, August 1920. From Store Norske (n.d.).

2 Theory

2.1 Arctic conditions

2.1.1 Climate

Temperature and precipitation are considered to be important variables for climate observations. Key forcings for climate change are the distribution of solar radiations, changes in the frequency of explosive volcanism, and changes in atmospheric greenhouse-gas concentrations. These factors can be amplified or decelerated by regional feedbacks that affect temperature and precipitation (Miller et al., 2010). The difference in elevation in a catchment can cause precipitation to change from rain to snow due to the potential temperature variation with altitude. Precipitation tends to increase with elevation, which has been verified in Svalbard. Strong winds, low temperatures, and precipitation in the form of snow often cause the observed precipitation to be lower than what it actually is (Killingtveit A et al., 2004).

Svalbard is located in a transitional zone of cold Arctic air from the north and mild maritime air from the south. This causes high cyclone activity, especially during the winter season. Topographic factors can locally alter the dominating wind direction, but northeastern winds tend to dominate in the archipelago (Hanssen-Bauer et al., 2019). Consistently higher wind speeds during the winter months compared to the summer months have been observed in Adventfjorden (Grochowicz et al., 2021). The dominating wind direction registered at Svalbard Lufthavn was from the southeast. The southeastern winds occurred more than 50% of the time from November to April 2021 (Klimaservicesenter, n.d.). Increasing numbers of cyclone events have been shown to have a connection with increasing air temperatures (Lambert, 2004). The 1971-2000 temperature average for Svalbard Lufthavn was -13,9°C in the winter, and 4,5°C in the summer (Hanssen-Bauer et al., 2019).

Relatively warm Atlantic water is brought into the Svalbard fjords, also during winter, as a result of the West Spitsbergen Current transporting warm water onto the West Spitsbergen Shelf. This is a consequence of recent changes in the large-scale atmospheric circulation patterns. Another consequence of this is surface warming and loss of winter sea ice (Hanssen-Bauer et al., 2019). The most severe reduction in land fast sea ice over the last 30 years was on the west coast of Svalbard, based on modeled and observational data. In Adventfjorden, the average land fast ice durations have decreased up to three months (Søreide et al., 2020).

2.1.2 Glaciers

The Legally (1932) – Ahlmann (1933) classification of glaciers is based on whether the body of a glacier is at a melting-point 1) throughout, 2) upper part, or 3) nowhere (Court, 1957). Glaciers with a melting point (1) throughout the body are referred to as temperate glaciers. Glaciers with (2) cold marginal regions but an inner and upper region of ice at melting point (temperate ice) will be referred to as polythermal. Glaciers that (3) do not have ice at the melting point (frozen throughout the entire body) will be referred to as cold glaciers. The different classifications of glaciers have different physical properties. The thermal regime of the glacier has a large effect on the development of glacial drainage systems.

Approximately 60% of the Svalbard landmass is glaciated (Lønne & Lysså, 2005). In Svalbard many glaciers are cold glaciers as a result of permafrost (Etzelmüller et al., 2000), which reduces the penetration of meltwater to the subglacial environment and the development of drainage systems. The glacial thermal regime is therefore a controlling factor for sediment

yield, meltwater runoff, and seasonal trends (Hodson et al., 1997). The glaciers in Svalbard are shrinking. Variations in glacier mass balance are mainly driven by the seasonal change from winter to the melting season (Hanssen-Bauer et al., 2019). For Longyearbreen and Larsbreen it has been documented that the drainage of meltwater occurs supraglacial and is routed to englacial and subglacial channels (Etzelmüller et al., 2000).

One of the most commonly found types of moraine in Svalbard is the ice-cored moraine. In the ice-cored moraine a layer of debris is covering a core of ice. The debris cover can originate from supraglacial sedimentation on clean glacier ice or melt-out of englacial debris. In Svalbard they can be up to 50 m in height and are an indicator of the outermost postglacial position. Development and preservation of this type of moraine in Svalbard are related to cold glacier front margins with a direct connection to the permafrost conditions (Etzelmüller et al., 1996). Meltwater channels from Longyearbreen and Larsbreen are routed through such ice-cored moraines (Etzelmüller et al., 2000).

2.1.3 Geology

Svalbard has complex geology dominated by sedimentary bedrock (Rubensdotter et al., 2015). In Adventfjorden the geology is relatively homogenous, while in Sassenfjorden it is more complex (Figure 4). Longyeardalen consists of sedimentary rocks from Cretaceous and Tertiary partially overlain by Quaternary sediments. The bedrock has a slight dip of horizontal layers with alternating sandstone and shale formations. The facies within the formations are marine, estuarine, and terrestrial. The lower sections of the stratigraphy consist of clastic sedimentary rocks with coal seams, e.g., marine sand- and siltstone from the Cretaceous. The upper part consists of clastic sedimentary rocks and coal seams, e.g., terrestrial sandstone (Major & Nagy, 1972; Norwegian Polar Institute, n.d.-b). This type of bedrock is considered to be mechanically soft and thus easily eroded (Etzelmüller et al., 2000). The marine limit is approximately 60-70 m above sea level (Rubensdotter et al., 2015).

In Sassenfjorden, a delta system similar to the Longyear delta can be located. The geology in the area of the Vindodden delta will therefore also be introduced. In Sassenfjorden a large fault can be seen dividing the geology in the Vindodden catchment. The stratigraphy in the lower part west of the fault consists of sandstone, siltstone, shale, and bituminous shale from the Early - Middle Triassic, while the upper part consists of shale and sandstone from the Late Triassic - Middle Jurassic. East of the fault, the lower part consists of chert, siliceous shale, sandstone, and limestone from the Permian. The upper part consists of sandstone, siltstone, shale, and bituminous shale from the Early - Middle Triassic (Norwegian Polar Institute, n.d.-b). The area is characterized by raised beaches and marine terraces up to an altitude of 80 m (Major & Nagy, 1972).

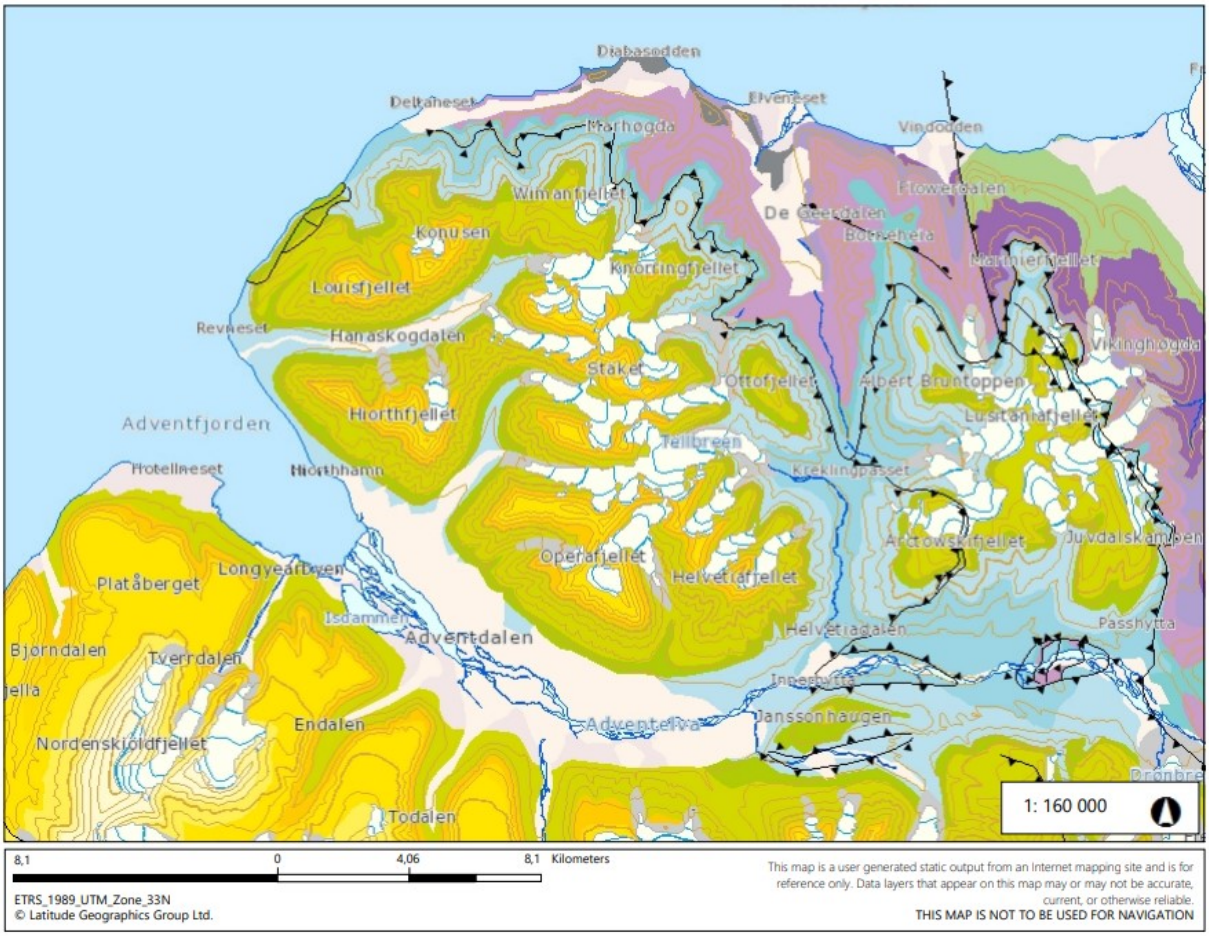

Figure 4 Geological formations in Adventfjorden and Sassenfjorden. The map is generated by the Norwegian Polar Institute (n.d.-b).

2.1.4 Permafrost

Permafrost is defined by ground temperature at or below 0˚C for at least two consecutive years (Humlum et al., 2003; Woo, 2012). The main factors influencing the distribution and extent of permafrost are air temperature, topography, geothermal heat flow, wind, lithology snow cover, and distance to the ocean (Humlum et al., 2003). The upper layer of the permafrost is called the active layer and is affected by seasonal freeze-thaw cycles. The permafrost occurs as ice in pores or as ice lenses (Rowland et al., 2010; Woo, 2012) and can function as a stabilizer in sediments. If the ground is frozen, it is protected against geomorphological processes that cause erosion (Rowland et al., 2010). Significant melting of the active layer can cause abnormally high instability in the ground (Nilsson et al., 2015). Precipitation, meltwater, and other erosional processes can easily erode sediments when ice in pores and ice lenses melt (Scott, 1978).

On Svalbard the permafrost is approximately 100-400 m thick and fairly continuous (Haldorsen & Heim, 1999; Humlum et al., 2003). In central Svalbard the permafrost near sea level is dated to be from the late Holocene (Humlum et al., 2003). The thermal regime in the ground of Longyeardalen was influenced by the sea temperatures up to 200 m inland from the shoreline. A transit zone from permafrost to non-permafrost environments is likely to occur in the shore area, suggesting the absence of offshore permafrost. By the coastline of Svalbard Lufthavn the active layer has a varying thickness of 1,5-2,5m (Guégan & Christiansen, 2017).

2.2 Arctic hydrology and sediment transport

2.2.1 The water balance

The water balance is the cycle of water movement. Through condensation and precipitation water moves from the atmosphere to the ground as snow, ice, and runoff. Via evaporation the water returns to the atmosphere. An example of a High Arctic water balance is illustrated in Figure 5 for a glacierized catchment. The hydrological year the water input and output from the 1st of October to the 30th of September (Nowak et al., 2020).

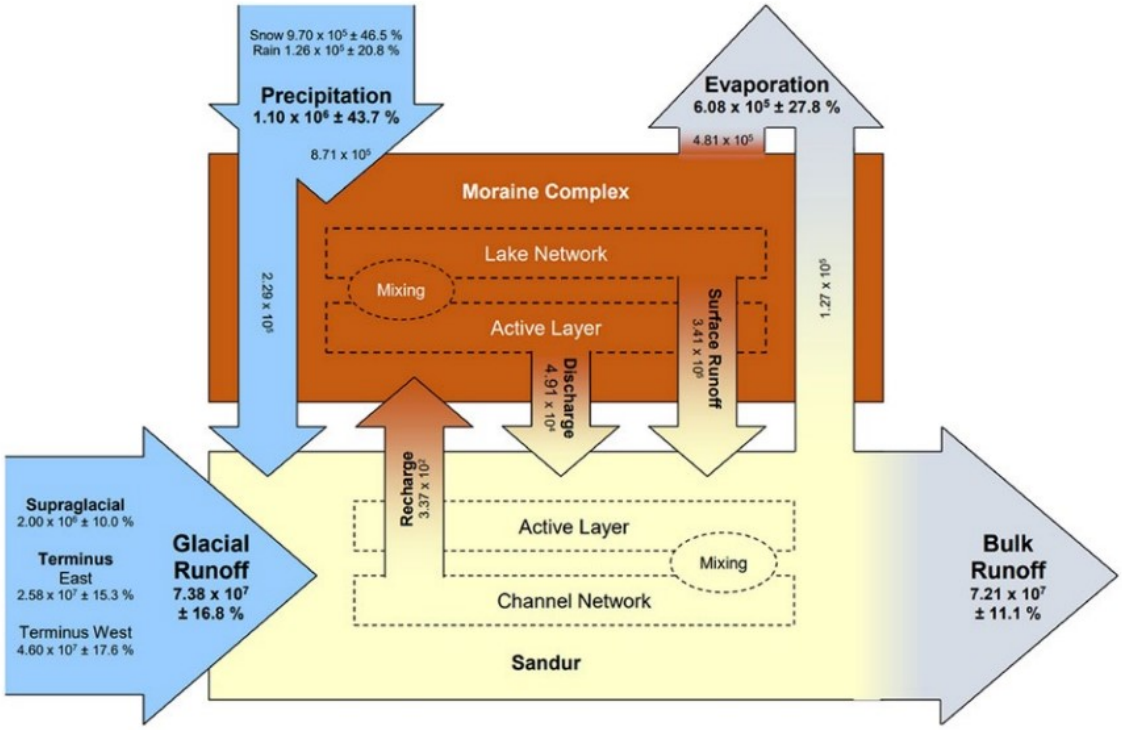

Figure 5 The water balance for the High Arctic, glacierized Finsterwalderbreen catchment. Blue arrows show water input. Gray arrows show water output. Other arrows show internal transfers. Dashed lines represent minor multi-directional exchanges and stores that have not been quantified due to limited data. Water fluxes (m^3) with probable errors are shown for water input and output. Channel discharge, active-layer discharge, and surface runoff are considered first-order estimates. Obtained from Nowak et al. (2020).

A modified version of the standard water balance (Equation 1) provides a more accurate description and results for glacierized catchments in a changing High Arctic (Nowak et al., 2020).

$$P_{winter\ (ngs)} + (P_{JJAS} + P_Q) + B_s + C - E_a \pm \Delta S = \varepsilon$$

Equation 1

Where $P_{winter(ngs)}$ [mm/yr] is the precipitation as snowfall in the non-glacierized areas, P_{JJAS} [mm/yr] is the precipitation from June to September, P_Q [mm] is the daily winter precipitation causing discharge, B_s [mm/yr] is the summer mass balance of glaciers the catchment, C [mm/yr] is the condensation, E_a [mm/yr] is the evaporation, ΔS [mm/yr] is the change in the

catchment's water storage, and ε [mm/yr] is the residual balance (Nowak et al., 2020; Nowak & Hodson, 2013).

The runoff in a catchment is dependent on the available water within a catchment. A representation of the volume of water in a catchment can be drawn from discharge measurements in a river. The discharge equals the volume of water flowing in a river in a time period. It can be measured or calculated based on the water stage (Dingman, 2015). The discharge can be used to create a hydrograph. The magnitude and form of a hydrograph can yield information about the hydrological processes within a catchment as it is an integration of spatial and temporal variations in water input, storage, and transfer processes within the system (Hannah et al., 2000). Factors known to influence discharge are temperature, precipitation, glacier- and snowmelt, and groundwater (Christiansen et al., 2020; Lafrenière & Lamoureux, 2019; Nowak & Hodson, 2013). In arctic glacierized catchments the annual hydrograph is generally inverse to that exhibited in temperate fluvial environments. This is typically a result of ice- and snowmelt causing maximum flow in the summer months (the melting season), when precipitation is low (Brown, 2002).

Groundwater discharge in the Arctic is strongly affected by the presence of the permafrost. Continuous permafrost in terrestrial areas causes implications for groundwater flow, as it can act as a barrier and/or limit flow in the active layer during the melting season. As temperatures increase and the active layer thaws, the permafrost may act as a water source for the groundwater (Christiansen et al., 2020; Lecher, 2017). The groundwater is not included as a part of the water balance (Equation 1) as the contribution has previously been assumed to be minimal.

2.2.2 Rivers

Fluvial processes, i.e., rivers, have been an important factor in the shaping of the Svalbard landscape through erosion, transportation, and deposition of sediments. Typical river morphology is illustrated in Figure 6. In an active river channel, bars and riverbanks can be found. Typical features on the floodplain are abandoned channels and flood deposits. The depth of the river is referred to as the water stage, and it is measured from the riverbed to the water surface. The thalweg is a line representing the deepest part of the river channel. The highest velocity in a river is found in the deeper part of the channel as the riverbed, riverbanks, and air creates friction (Nichols, 2009). Different river types have different behaviors, properties, and morphology. A summary of river types, behaviors, and typically transported sediment load can be found in Table 1.

Braided rivers are characterized by shifting river channels. Over time erosion causes the active channel(s) to shift paths, causing inactive and abandoned channel paths in the floodplain. This process happens over both short- and long periods of time. Channel bars are commonly formed depositional features. The morphology of braided river systems depends on the frequency of channel shifts, sediment supply, discharge, and topography (Miall, 1977; Nichols, 2009).

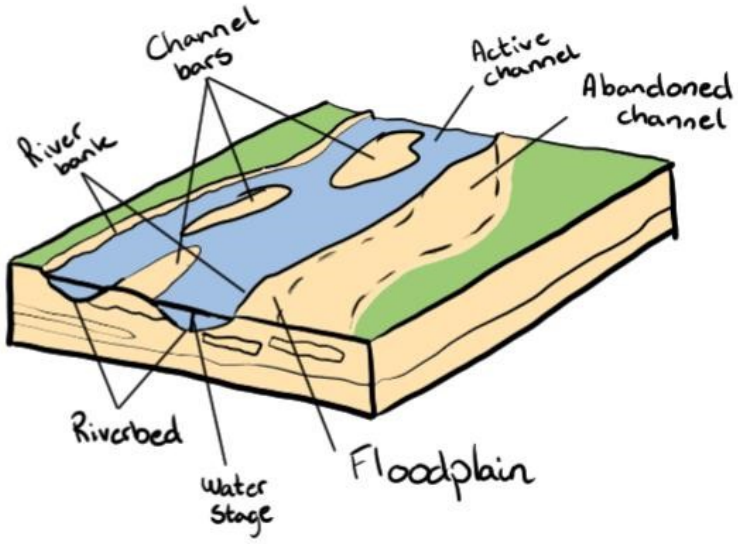

Figure 6 Illustration of the typical river morphology. Modified from Nichols (2009).

Table 1 Typical morphology, behavior, and sediment load found in different types of rivers. Modified from Miall (1977).

Type	***Morphology***	***Erosive behavior***	***Depositional behavior***	***Load type***
Braided	Two or more channels with bars	Channel widening	Channel aggradation, mid-channel bar formation	Bedload
Meandering	Single-channel	Channel incision, meander widening	Point bar formations	Suspension, mixed load
Straight	Single-channel	Minor widening and incision	Side-channel bar formations	Suspension, mixed load, bedload

Geomorphic processes of soil development, erosion, and deposition are closely linked to catchment morphology and hydrological processes. Water has an important role as a transporting mechanism for solutes and sediment. It is a major driving force in the development of catchment morphology through the influence it has on mass movement, soil creep, and weathering. Channel paths of water flow are critically dependent on hillslope morphology (Beven et al., 1988). Precipitation normally falls as snow in winter and rain in summer. Snowfall accumulates in snowbanks and glaciers seasonally. Rainfall and meltwater saturate thawed soil in the active layer. Excess water that cannot enter the ground retain as surface water and feeds rivers, wetlands, and lakes. Melting of ground ice can also be a contributor to runoff (Woo, 2012). It is projected that strong warming will cause an increase in runoff due to increased glacial meltwater and precipitation (Hanssen-Bauer et al., 2019).

Melting season in Svalbard is considered to be from May to October (Nowak & Hodson, 2013), whereas the discharge in the Arctic rivers are generally restricted to June-September. For the remaining months, the rivers are usually completely frozen (Killingtveit A et al., 2004). A large increase in discharge is common in the Arctic as the temperature increase (typically in early June) (Scott, 1978). In the Arctic the annual cycle and temperature variations are important for the runoff in rivers. During this time, meltwater from glaciers may largely contribute to high discharge in rivers. Towards the end of the season, discharge normally decrease with temperature until the river freezes, and the river system becomes stable until the next season (Bogen & Bønsnes, 2003).

2.2.3 Sediment transport and cycles

The two main forms of river transport are suspended load and bedload. The suspended load are particles in suspension moved by sufficient upwards motion from turbulence. Particles transported as bedload, move as saltation, sliding, or rolling on the riverbed (Figure 7).

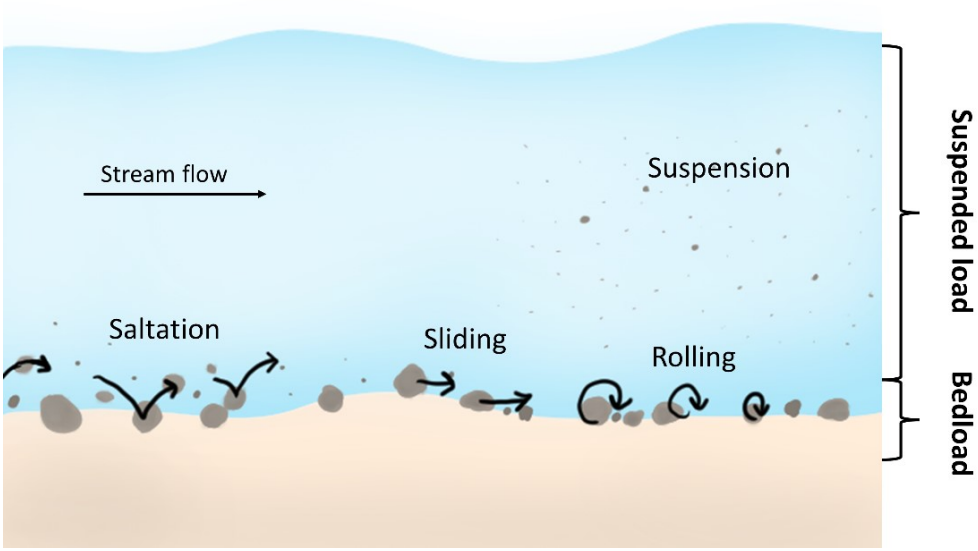

Figure 7 Sediment transport in fluids based on Nichols (2009).

The degree of erosion and deposition is depended on friction and flow speed (Hjulstrom, 1935). The relationship between grain sizes and flow velocities is illustrated by the Hjulström curve (Figure 8). The competence of the river is the maximum particle size that can be transported by the river. At low velocities finer particles (clay, fine silt) and low-density particles are kept in suspension. Larger particles are transported as bedload (Nichols, 2009). The competence is directly related to flow speed, which means that the transported particle size increase with increasing flow speed (Brattli, 2019).

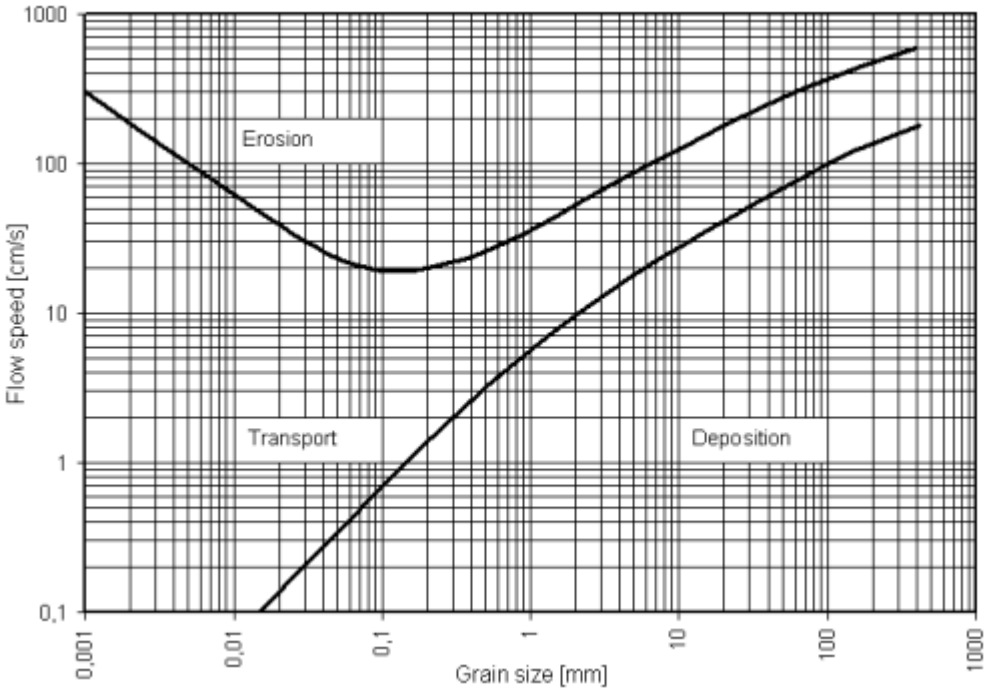

Figure 8 The Hjulström curve illustrating the relationship between flow speed [cm/s]and grain size [mm] with respect to the erosion-transport-deposition regime. From Hjulstrom (1935).

Suspended sediments are controlled by sediment availability, as opposed to bedload transport which is more hydraulically controlled. The floodplain of braided rivers may function as sediment storage as the channels shift and bedload is temporarily stored in inactive or abandoned channel paths. Braiding intensity, discharge, and flow velocity affect the rate of transport and deposition (Peirce et al., 2018). Measurements of suspended sediment concentration (SSC) can be used as a direct measure of input to a system (Hodgkins et al., 2003). Suspended sediment load (SSL) [tonne/yr] and suspended sediment yield (SSY) [tonne/km^2/yr] describe the total transport of suspended sediment with discharge through the hydrological year and the sediment load per area in a catchment, respectfully (Bogen & Bønsnes, 2003). It is expected that the suspended sediment flux will experience a larger effect of climate change compared to bedload transport as the suspended sediment is controlled by its availability (Hodgkins et al., 2003).

For the classification of grain sizes in this thesis, the Udden-Wentworth grain size classification (Figure 9) was used.

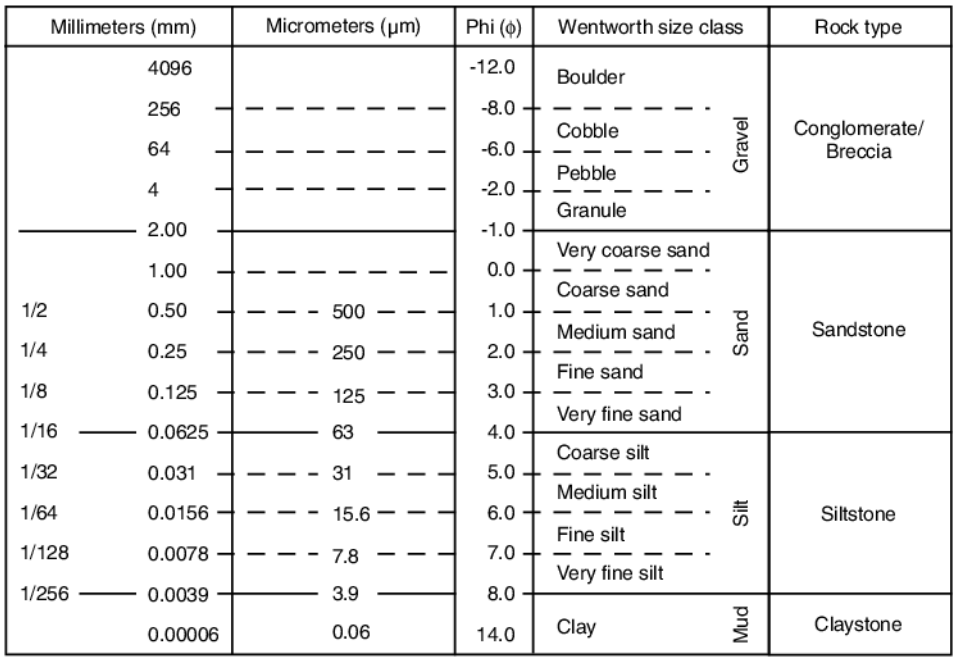

Figure 9 The Udden-Wentworth classification of grain sizes for terrigenous sediment. From Gallagher et al. (2017).

Seasonal variations in the Arctic

Glacial, colluvial, and fluvial deposits are considered the main sediment sources in cold climates (Orwin et al., 2010). The sediment budget in cold climates can be simplified into sediment input equals the output ± the change in sediment storage (Orwin et al., 2010). In general, the suspended sediment concentration varies directly with streamflow. However, strong seasonal and regional differences occur. To understand the movement of sediment in a river, the most important factors to consider are sediment storage and the time period of input and output to the storage. Over larger time scales (decades) the rates and release of sediment storage can have more impact on the sediment concentration in rivers than the rates of upland bedrock and soil erosion. This is because the upland erosion may be greater than the amount of sediment transported to the sink environment (Meade, 1972). In glaciated catchments sediment transport typically occur as large, discontinuous events with large seasonal and diurnal variations *(Hodgkins et al., 2003)*.

Studies in Norway and elsewhere have shown that sediment concentrations in glacial meltwater rivers are subject to large temporal fluctuations. This pattern of long- and short-term variations in sediment concentrations reflects the activity of the process of erosion and sediment delivery of glaciers in each catchment (Bogen & Bønsnes, 2003). The sediment transport in the Arctic is highly affected by discharge varying through the year (Ladegaard-Pedersen et al., 2017; Woo, 2012). The water phase transitioning between ice and liquid throughout the season dominates the transport process in cold climates. As fluvial processes usually dominate sediment transport in a catchment system, water shortage may have a big effect on the sediment flux (Orwin et al., 2010). The annual sediment cycle is largely dependent on the seasonal variability in temperature. Early in the melting season the ground is frozen, restricting the availability of sediment for erosion and transport. The upper, finer sediment layer deposited by the river at the end of the previous season, and the fine aeolian deposited sediment, are the first to be eroded at the beginning of the melting season. The

aeolian sediment is mostly deposited during fall and winter. Though the vegetation is sparse in the High Arctic, it can catch and store aeolian sediment (Serreze & Barry, 2014). The roots of vegetation can hold on to sediment in the ground and limit erosion. Later in the melting season, when thawing of the ground has caused an increased thickness of the active layer, more sediments become available for erosion and transportation. The sediments eroded from the active layer are often coarser material, which leads to further erosion as particles collide during transport. Erosion of the ground causes less protection of the active layer, and so the active layer deepens as a result of positive feedback (King, 1970).

The rate of melting is dependent on the grain size distribution and the amount of ice present. Higher ice content in the ground results in slower melting. Gravel and sand melt faster than silt and clay. The reason for this is that when fine-grained cohesive sediments melt, they create an isolating effect for the frozen material under and thereby reduce melting (Scott, 1978). It has also been shown that fine-grained, cohesive material has a lower maximum erosion rate, which can be seen in connection with the slower melting and the natural properties of cohesive soils (Brattli, 2019; Scott, 1978). The presence of permafrost increases the resistance of erosion in material with high content of silt and clay better than it does for coarse-grained material. Due to the limited melting season in the Arctic, the thickness of the active layer will largely depend on the grain sizes in the area. Studies from Alaska show that at the start of the melting season, the erosion of riverbanks is limited due to permafrost strengthening the ground (Scott, 1978).

Inter-seasonal variation in Arctic systems

The climatic conditions and a relatively short melting season strongly affect how sediments are transported in the Arctic. The main transport mechanism of sediments is through rivers. Ice builds up in river channels during fall and winter. This gradually melts at the beginning of the melting season in the summer months. The gradual melting can cause ice blocks in the river channel, leading to water flowing onto the floodplain. The presence of permafrost in the floodplain prevents infiltration and causes a high discharge coefficient. This may result in surface water flowing in areas that are normally not affected by surface runoff, causing erosion of exposed sediment. This is often suggested as a reason for observing high sediment concentration in the river at the beginning of the melting season (Bogen & Bønsnes, 2003). Another reason can be that the largest amount of sediments originates from the erosion of the riverbed. When the ice in the riverbed melts, an increase in sediment transport can be observed. The reasoning was suddenly increased access to available sediment combined with high runoff, which shows a correlation between discharge and sediment transport (Favaro & Lamoureux, 2015). Sediments can also be transported as ice-rafted material to the depositional environment. This mechanism can transport coarse sediment further than bedload transport before the material is deposited (Hasholt et al., 2006; Scott, 1978). Permafrost can decrease the transport length by freezing the coarser fractions in anchor-ice and frozen riverbanks, which hinder bedload transport (Hasholt et al., 2006)

Later in the melting season when there is no ice to block the river channel and water flow is no longer forced out on the floodplain. The increased thickness of the active layer results in a significantly larger infiltration rate. The period is characterized by high runoff, but less available sediment causes less erosion and transportation (Bogen & Bønsnes, 2003). Unstable sediments are transported by the river, and lateral erosion is likely to occur (Hasholt et al.,

2006). When sediments are being mobilized in the riverbanks, it is likely to cause changes in the channel path due to the erosive forces not being restricted by permafrost (Brattli, 2019). Down-slope processes and significant sediment transport generally occur later in the melting season due to the thawing of the active layer (Hasholt et al., 2006).

2.3 Arctic coasts

2.3.1 The source-to-sink system

The source-to-sink system is the entire sedimentary system from its ultimate upstream terrestrial source to deep basin plains (Figure 10). The original source of sediment in a millennial or longer time scale may be eroded upland soil, and the ultimate sink will be the deep basin plains. For shorter time scales it is important to consider storage sites along the system between uplands and coastal zone, for both source and sink. The original source of sediment in a catchment is the eroded soil//bedrock uplands, but the immediate source of most sediment transported in a river at a given time may well be from the storage sites in close proximity to the river. Similarly, even though the ultimate sink is the deep basin plains, the immediate sink for sediments can be the river flood plain, delta, or coastal zone (Meade, 1972).

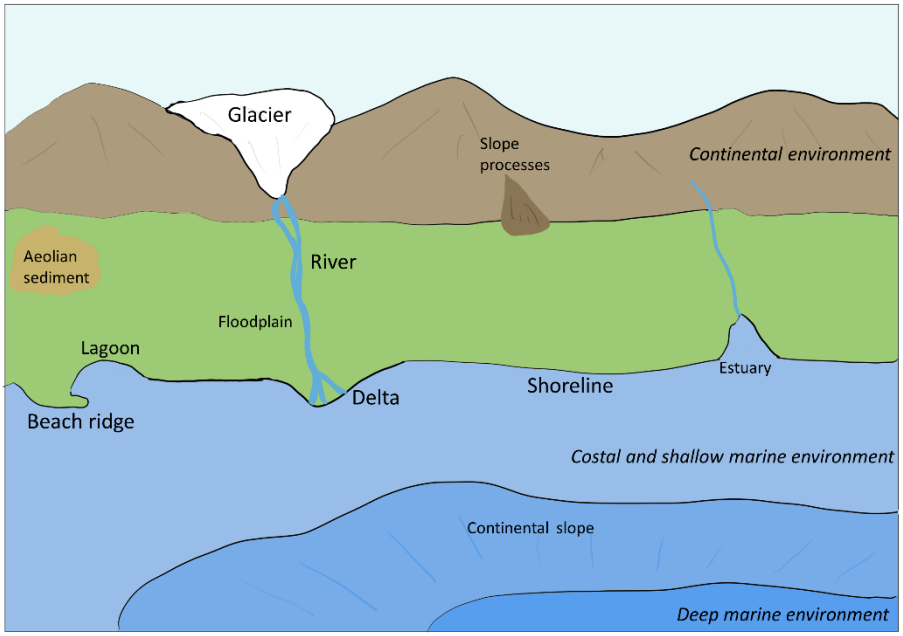

Figure 10 Conceptual sketch of principal sedimentary environments.

2.3.2 Coastal and delta geometry and development

In this thesis the coastline is used as a broader term to describe the area where land meets the sea and includes the shoreline and beach area. The shoreline is used for describing the specific line that separates the dry land from the sea. The river mouth is where the river reaches a standing body of water, e.g., the sea. The parts of the delta that can be observed above sea level are the delta front, found on the foreshore. The foreshore is normally slightly dipping in the seaward direction before it reaches the steeper delta slope in the shoreface. It is on the foreshore that waves swash and backwash (Nichols, 2009).

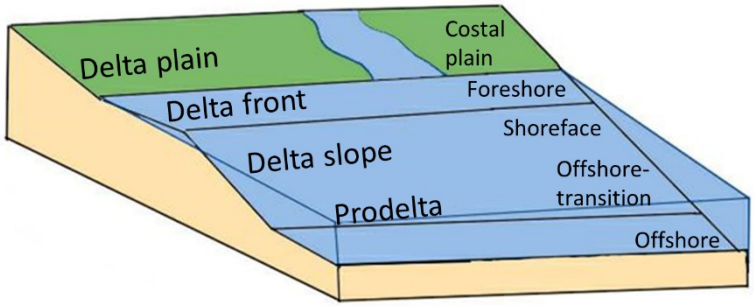

Figure 11 Conceptual sketch of delta and shore geometry. Modified from Nichols (2009).

The shape of a coast is determined by the following conditions. (1) The acting forces on the coast. Figure 12 shows how the connection between the forces of rivers, waves, and tides can contribute to coastal development. The coast shape is also largely dependent on (2) the geometry, e.g., bathymetry and the angle at which waves and currents hit the coast. Lastly, (3) the sediment supply and the resistance against erosion. These three conditions leave unique signatures which reflect the exposure of forces and sediment supply in the coastal morphology. These signatures change along with a potential change in conditions acting upon a coast. Often making it possible to track previous conditions in a changing environment in the area behind a current shoreline (Jensen & Rubensdotter, 2020).

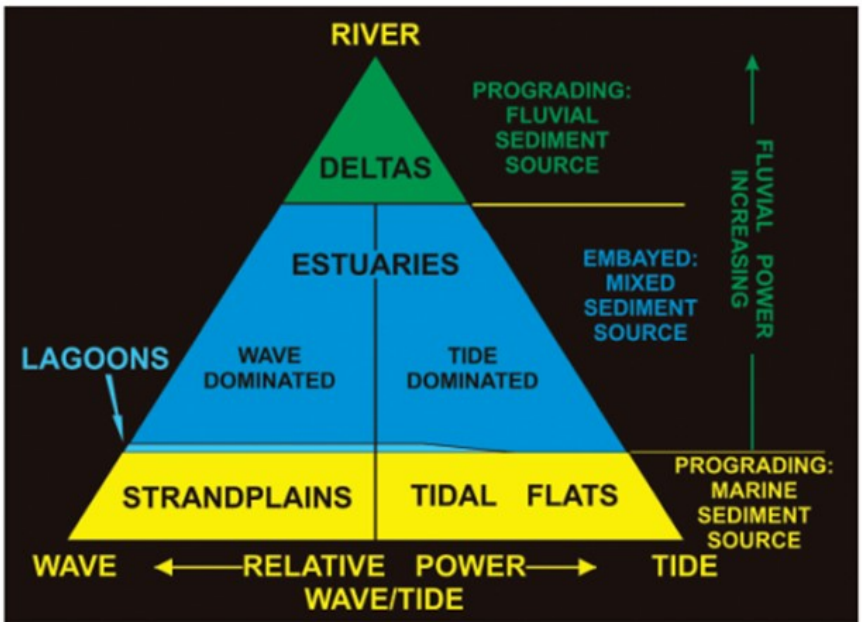

Figure 12 Examples of how interactions of rivers, waves, and tides create landforms and coastal signatures (Jensen & Rubensdotter, 2020).

Based on the gradient of the foreshore, two types of coasts can be identified. The first is the reflective coast, characterized by a steep gradient of the foreshore. Due to the gradient, the wave energy is reflected from the beach and back into the sea. Ocean processes as waves, tides, and currents dominate the erosion and redeposition of sediment along the coastline. The

second is a dissipative coast, characterized by a low gradient of the foreshore. The wave energy is reduced because of the shallow water stage. Longshore current is an important transport mechanism for the sediment to be redeposited and accumulated. The longshore current is typically caused by wind-driven waves coming in at an angle to the coast. The shape of the coastline is more dependent on the sediment accumulation, wave action, tidal differences, and climate (Nichols, 2009).

For the coastline, beach ridges are a commonly found feature, especially where it is dominated by coarse-grained material. They are built by waves depositing clasts ashore until enough sediment has been deposited to create a barrier. As the barrier is built up above sea level, water only crosses during stormy weather. The sediments that are washed over the barrier are called overwash. Overwash deposits are dipping landwards on the inner side of a barrier. Spits are a type of barrier partially connected to land. Spits require sufficient amounts of sediments (sand and gravel) to accumulate in areas where the tidal difference is small (microtidal). The accumulated sediments are usually a result of wave-driven longshore currents from a river mouth, and some sediment originates from erosion of the seafloor. Spits are often related to slow land rise (Nichols, 2009).

Marine deltas are created at the transition between continental and marine environments. For delta development, a river transport sediment toward the sea. As the flow speed of the river is reduced in the coastal zone, sediments are deposited. As the input of sediments continues, a progradation of the deposited sediments occurs, and the delta develops. The shape of the delta is a result of the same conditions affecting the shape of the coastline (Figure 12), in addition to the type of sediment transported to the delta. The coarse sediment is deposited when the flow speed is reduced (Figure 8), causing the coarsest sediment to be deposited in the delta front. The suspended sediment is often observed as a sediment plume, has a lower density than seawater, and is deposited furthest away from the river mouth. Deltas can be classified by the relative influence of processes, water depth, and dominating grain size (Nichols, 2009). Two types of deltas classified based on the dominating force are presented below.

- Wave-dominated delta (Figure 13): waves created during strong winds have the capacity to redistribute all sediments deposited on shallow water (especially during storms). This goes especially for river mouth and river mouth banks. Progradation of the river channel outwards is limited as subsea levees are not created, and bedload is redistributed by waves as soon as they are deposited. If waves are coming in from the side towards the delta front, it leads to lateral mitigation of sediments which are deposited as elongated spits and mouth bars oriented with the longest axis towards the coast (Nichols, 2009).
- River-dominated delta (Figure 14): microtidal and minimal waves. Controlled by fluvial processes. Developed channels, levees, and overbanks. Bedload and suspended sediments are deposited as submarine levees which build up the ocean floor and prograde the delta into the basin in a characteristic birdfoot-shape (a result of actively shifting channels). A characteristic of the fluvial-dominated delta is the instability of the channels due to a low gradient of the delta plain, which leads to the avulsion of river water and the development of new channels. Repeated channel shift leads to overlapping abandoned lobes (Nichols, 2009).

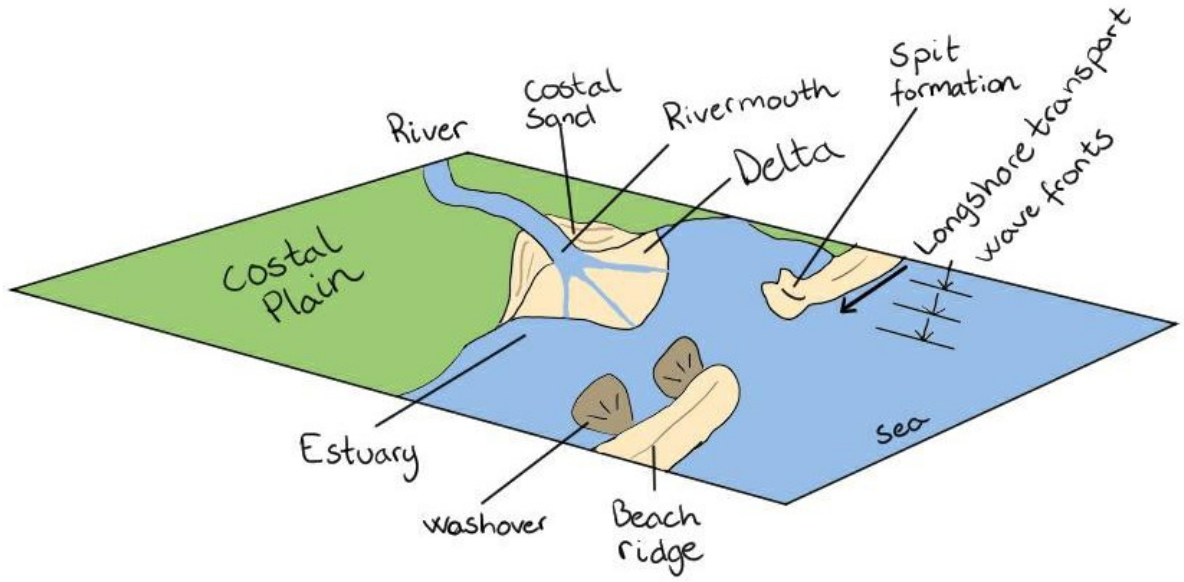

Figure 13 Sketch of a wave-dominated delta. Based on descriptions from Nichols (2009).

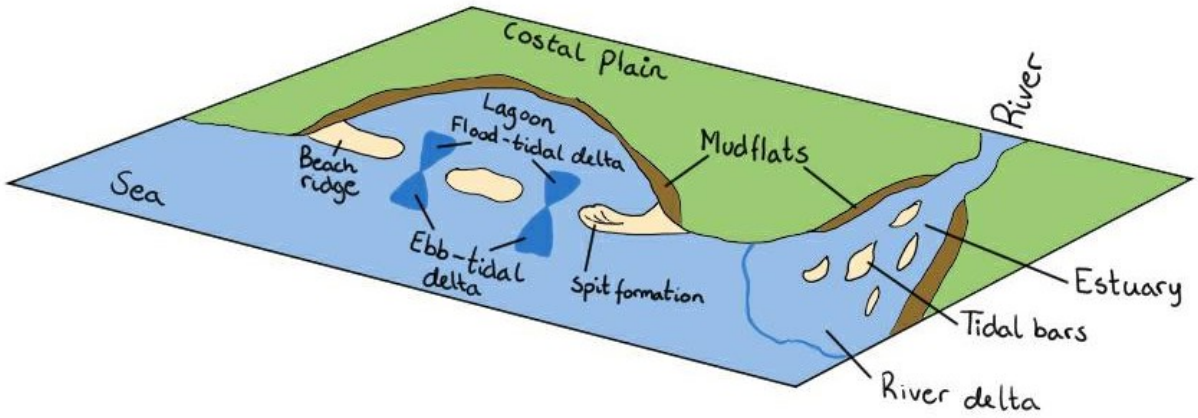

Figure 14 Sketch of a river-dominated delta and tidal-dominated lagoon. Based on descriptions from Nichols (2009).

Microtidal coasts are defined by a tidal range of <2 m, and mesotidal coasts are defined by a tidal range of 2-4 m. Generally, barriers occur along coastal plains close to slope edges of continents and marginal coasts. Factors like high sediment supply combined with moderate to high wave energy and small tidal ranges can cause exceptions. Barriers and river deltas are commonly best developed in microtidal coasts. The geomorphologic development has two significant controlling factors; wave energy and tidal current energy. Microtidal coasts are often dominated by wave energy, while mesotidal coasts show influences of being mixed-energy coasts. Typical features for microtidal and mesotidal coasts are presented in Table 2. It is not uncommon that barrier morphology may change from typical wave features at the entrance of the bay to tide-dominated forms in the inner part of the bay. Overwash features are the results of storms. A high frequency of overwash can be observed in microtidal barriers due to the lack of tidal inlets that allows for flow through the barrier during storm surges

(Hayes, 1979). Coarser sediments to cross beach ridges are reduced to overwash events during a storm (Nichols, 2009).

Table 2 General geomorphological features found in microtidal (<2 m) and mesotidal (2-4 m) coasts. Modified from Hayes (1979).

Microtidal	***Mesotidal***
Long, elongated barriers	Stunted, drumstick-shaped barriers
Abundant overwash terraces and overwash fans	Minor beach ridges or overwash terraces
Large flood-tidal deltas and small edd-tidal deltas.	Moderate to absent flood-tidal deltas and large edd-tidal deltas.

In Longyearbyen the mean sea level is 109 cm. The mean high water is 162 cm, and the mean low water is 57 cm (Kartverket, 2020b). The return height and period for extreme heigh waters in Longyearbyen are presented in Table 3.

Table 3 Return height for extreme heigh waters [meters above mean sea level] in Longyearbyen. Modified from Hanssen-Bauer et al. (2019).

Station	*20-year return height*	*200-year return height*	*1000-year return height*
Longyearbyen	1,33	1,44	1,51

2.4 Last glacial activity and the relative sea level response

2.4.1 The past glacial

During the last glacial maximum (LGM) the Svalbard archipelago was covered by a thick continental ice sheet. In valleys, fjords, and submarine shelf-crossing troughs, moraines indicate large glacial pathways created by grounded, temperate ice from the last glaciation. The glacial activity has varied both spatially and temporally, as it can locally be found very few traces of glacial processes (Lønne & Lysså, 2005). The LGM lasted for a relatively short period, as it advanced onto the western shelf after 22 ka and culminated between 19 and 15 ka. The deglaciation of the Svalbard west coast happened between 13 and 12 ka, and around 10 ka, the glaciers had withdrawn to all fjord heads (Landvik et al., 1998).

During and after the deglaciation, landforms and landscapes were reworked and dominated by running water and slope processes (Lønne & Lysså, 2005). A local glacial readvance happened around 12.4 ka west of Isfjorden before the glacial retreat continued through the Allerød period. Inner branches of Isfjorden were covered by outlet glaciers during the cold period of Younger Dryas. Fjord glaciers still connected to the Svalbard-Barents Sea ice sheet advanced. The climate warming at the transition to the Holocene caused rapid melting of the ice sheet around 10 ka for the northwestern Barents Sea. A large reduction of the glacial cover in Svalbard occurred early- and mid-Holocene. The Little Ice Age in the late-Holocene caused a small readvance of glaciers (Landvik et al., 1998).

2.4.2 Isostatic uplift and relative sea level

As a result of glacial isostatic adjustment (GIA) and the Earth's response to present-day glaciers, high land uplift rates can be observed in Svalbard. The isostatic uplift rates of west Svalbard vary between 7 and 10 mm/year (Table 4), with inter and intra-annual variations (Hanssen-Bauer et al., 2019).

Table 4 Uplift rates from permanent GNSS stations in Svalbard. Modified from Hanssen-Bauer et al. (2019).

GNSS station	*Period*	*Uplift rate [mm/yr]*
Longyearbyen	2008-2018	7,2 ± 0,6
Ny-Ålesund	1999-2018	8,0 ± 0,3
Hornsund	2009-2018	9,4 ± 0,7

The global sea level was approximately 120 m lower than the present sea level during the past glacial. As a result of rising ocean temperatures and mass loss from glacier and ice sheets, the global sea level rise. Over the last 10 ka years, the pattern in the relative sea level (RSL) reflects land motion in Svalbard. An overall fall in the RSL has been observed in Svalbard since the past glacial, suggesting a vertical uplift as a result of GIA dominating the past sea level changes. The RSL in west Svalbard has declined by 10s of meters. Furthermore, a decline of >100 m has happened in the east of Svalbard. From tide gauge records in Barenstsburg and Ny-Ålesund, a negative trend can be observed in the RSL (Table 5) (Hanssen-Bauer et al., 2019).

Table 5 Trends in relative sea level (RSL) based on tide gauge records for Barentsburg and Ny-Ålesund. Data from Hanssen-Bauer et al. (2019).

Period	*Barentsburg [mm/yr]*	*Ny-Ålesund [mm/yr]*
1992-2017	-0.3 ± 1.5	-7.1 ± 0.7
1948-2017	-2.7 ± 0.2	–
1976-2017	–	-4.5 ± 0.4

2.5 Remote sensing

Technological advances in the field of remote sensing, Global Positioning System (GPS), and Geographic Information System (GIS) have a clear advantage for field work in the Arctic. Remote sensing combined with photogrammetric techniques provides spatially explicit, digital data representations at local, regional, and global scales. GIS allows for efficient characterization and analysis of vast amounts of data (Sahu et al., 2015).

The accuracy of shoreline mapping is affected by the availability and quality of ground control points (GCP). The availability is strongly affected by the time period being studied and the development of the study site (Moore, 2000). This is important to account for when using remote sensing for measurement, sampling, and calculating statistics.

3 Methodology

In order to gather a base on which to investigate the research questions, several methods had to be implemented. In order to ensure continuity in the long-term project (RiS ID 11641), some equivalent methodology used in 2020 was applied to monitor hydrology, the suspended sediment, and bedload transport in Longyearelva. Other methods were applied for a comprehensive study of the river-to-ocean interactions.

To study the development of the Longyear delta the following data was collected:

- SfM to create orthophotos to be compared to previous years and quantify the shoreline movement
- Geomorphological mapping showing how the river and delta look now
- Monitoring of discharge, bedload, and suspended load to study the correlation between amount, grain size, and surface discharge.

3.1 Photogrammetry and Structure from Motion

A collection of imagery for Longyeardalen and the Longyear delta was put together through fieldwork, search, and inquiry. The collection includes ground photos, aerial imagery, orthophotos, and Digital Elevation Models (DEM) from 1936 to 2021.

3.1.1 Photogrammetry

To record inter-seasonal changes, photos taken with phone and camera are georeferenced (day/hour/position). Sedimentation dams, sills, bridges, and river mouths were regularly photographed from fixed points 1-2 times a week to monitor development throughout the season.

3.1.2 Drone

A drone is an easy, accessible, and cheap alternative for data collection in the Arctic. A Dji Mavic 2 Pro drone with a smart controller was used to monitor the river and the delta. Drone images were taken manually and automatically with different angles and elevations. When flying over the river, the application DJI Pilot PE was used on the smart controller for automatic flying sequences and automatic picture taking. Many automatic flight applications are restricted to smartphones and do not function on a smart controller. Although Løvaas (2021) was able to use the Pix4d Capture software on the smart controller, we were unsuccessful in the attempt to install it.

Drone photos were taken at varying locations at the beginning and end of the melting season. NVE began construction work in the river on the 19th of August, 2021. Drone imageries were immediately taken after to ensure that the imageries and orthophotos did not reflect the unnaturally high sediment supply to the delta. The settings used for automatic picture taking were intervals of five seconds with a margin of 0, side overlap of 70%, and frontal overlap of 80%, at ~80 m elevation and a 90˚ camera angle. The pictures were used to create orthophotos digital elevation models (DEM) and 3D-models of Longyearelva. Parts of the river system closer to the moraines were flown manually at 80-100 m elevation. Older aerial photos were recreated by manual flights with varying angles and elevations (50-120 m).

Many difficulties were related to drone flying. Parts of Longyearelva are within a No-Fly zone due to the short distance of the airport, which was solved by good communication with the airport tower. The melting season overlapped with nesting season for birds, which caused

difficult situations with drone-flying as birds actively tried to attack the drone. To achieve good quality drone photos the preferred weather conditions would be a thin cloud layer (no sun) and minimal wind. This was normally not the case, so some of the photos are affected by wind and sun disturbance.

3.1.3 Collection of aerial imagery and the construction of orthophotos and elevation models

For long-term monitoring of the study area, a collection of orthophotos, DEMs, and aerial imageries were assembled through online searching and contacting institutions and private individuals. For the 2021 melting season, drone images were processed in Agisoft Metashape Professional and ArcGIS Pro to create dense clouds, orthophotos, DEMs, and 3D-models. The structure from motion (SfM) technique was used to combine vertical drone images of the same elevation. The 3D-models were created over the selected areas by combining orthophotos and DEMs. This process has been repeated three years in a row, from 2019 to 2021. Problems that occurred were related to big tif-files and restricted hard drives. Therefore, a new hard drive was bought and formatted to export/import larger files, and the area of study was divided into smaller parts.

Accurate measurements cannot be made on uncorrected vertical aerial photographs due to distortion and displacement (Moore, 2000). The orthophotos, aerial imageries, and DEMs were orthorectified based on the NPI Web Map Tile Service (WMTS) server called NP_Ortofoto_Svalbard_WMTS_25833 (Norwegian Polar Institute, n.d.-a), and on ground control points (GCP) taken in the field with a Global Positioning System (GPS). Figure 15 shows an overview of when aerial images were last taken over Svalbard. These are the orthophotos included in the NPI WMTS server. In Longyeardalen (marked in red), the orthophoto is a combination of aerial imagery from 2009 and 2011. The projection used for orthorectifying was ETRS 89 UTM 33. The development in Longyeardalen from 1936 to 2009 was substantial, which made it difficult to orthorectify older aerial images based on recent orthophotos. The aerial imagery from 1936 was orthorectified by using both a 20 m resolution orthophoto named ortho_1936_all_Svalbard_20m.tif from Norwegian Polar Institute (n.d.-a) and the NPI WMTS server to achieve the highest possible accuracy. Both vertical and angled aerial imagery were attempted orthorectified.

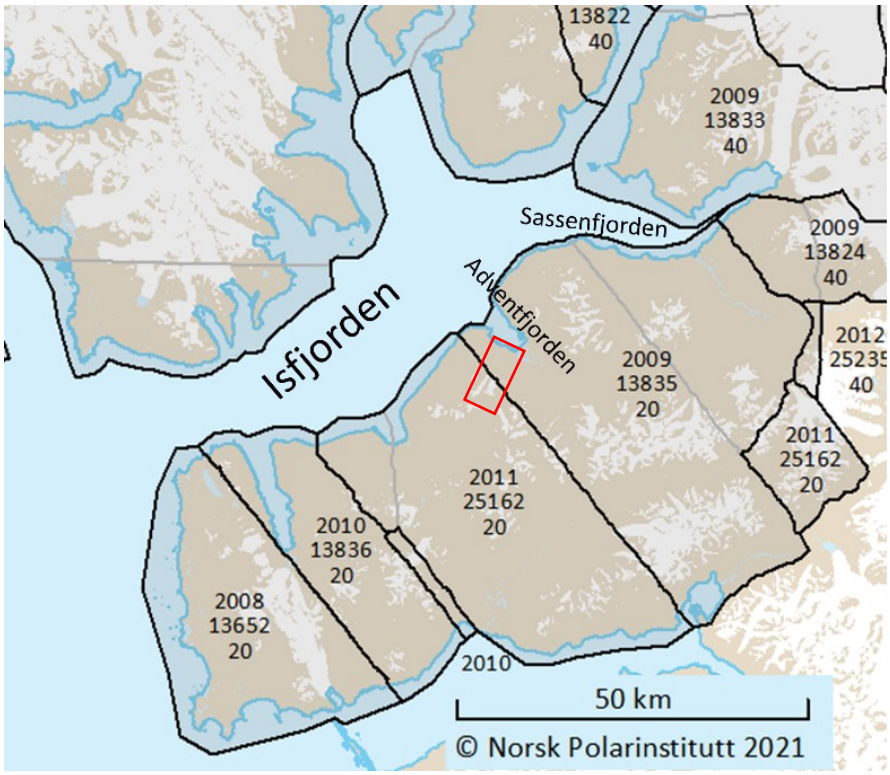

Figure 15 Overview of aerial imagery taken over Isfjorden, Svalbard. Showing the year, project id, and orthophoto resolution [cm]. Map data and orthophotos produced by NPI are based on these aerial imageries. All photos were captured between mid-July and mid-August. The red box shows the location of Longyeardalen. Modified from Norwegian Polar Institute (n.d.-a).

The orthophotos from 2019 had an elevation of 120 m and an 80° camera angle, while the orthophotos from 2020 had an elevation of 80 m elevation and a 90° camera angle. When comparing these two orthophotos, it is important to be aware of this spatial distortion. The orthophotos from 2019 cover most of the 2021 study area, while the orthophoto from 2020 has a limited spatial extent from the Longyearelva river mouth to Huset (upper-middle river). The dataset used to create the 2019 orthophotos was not available, but the datasets collected in 2020 were accessible.

3.2 Field observations and geomorphological mapping

Geomorphological features in the study area were recorded using a Garmin eTrex 10 GPS. GPS points were used to collect the location of the coastline morphology, placement, and movement of passive tracers, sills, bridges, and GCPs. GPS points were taken at varying locations along the coastline at the beginning and end of the melting season. They included notes describing active and abandoned beach ridges and spits, grain sizes, erosional and depositional features, and the high water line (HWL) (Figure 16).

Figure 16 Mapping of the high water line (HWL) on the Longyear delta. During mapping, trash was collected along the coastline. Photo taken eastward in front of Søppelfyllinga.

A Quaternary geological map of the Longyear delta was produced based on field observations, orthophotos from 2021 and 2009, and multiple ground and drone photos from around the Longyeardalen coastline. The mapping was done in ArcGIS Pro using the Norwegian SOSI classification system for Quaternary geological maps (Geological Survey of Norway, n.d.). This classification system is used by NGU (the Geological Survey of Norway) for classifying sediment types, lines, and point features. Adjustments to codes and classifications were necessary to capture variations in the Svalbard sediments.

The area of the Longyeardalen catchment was estimated by using appropriate hydrology tools in ArcGIS Pro. The estimation was made in collaboration with Pallesen (2022). Firstly, the flow direction (cardinal direction) for all slopes in the area was generated using the 2009 DEM (Norwegian Polar Institute, n.d.-a). Secondly, the flow direction raster was used to automatically generate a catchment area. The area was then manually modified based on the slope directions. The calculation of the area of Longyearbreen and Larsbreen was achieved with polygons drawn from the 2009/2011 orthophoto (Norwegian Polar Institute, n.d.-a). Both glaciers lie within the section of the orthophoto taken in 2011 (Figure 15).

A Rangemaster laser was used to measure the angle and distance between each sill in Longyearelva. The distance was measured between two sills, from the upper side of each sill to the lowest sinking part. Between each sill, three to six observations were made for the dip and distance to calculate the average. The results from this are not included in the thesis as it was not essential for the research questions.

3.3 Delta quantification

3.3.1 Digital Shoreline Analysis System

An important aspect of this thesis was shoreline mapping and change detection. An extension pack to ArcMap *10.7.1* developed by the United States Geological Survey (USGS) called Digital Shoreline Analysis System (DSAS) was applied to calculate the development of the Longyeardalen shoreline over time (Himmelstoss et al., 2021). It requires an input of at least three polylines representing shorelines at different positions in time and a constructed baseline.

The shorelines were based on the HWL for a specific year. They were drawn as polylines in ArcGIS Pro based on GPS points and georeferenced orthophotos and aerial imagery. The polylines were imported into ArcMap for access to the DSAS extension pack. Due to the lack of aerial images and restricted drone flights, shorelines were drawn from the years 2021, 2019, 2009, 1990, and 1936 based on aerial imagery. When interpreting the location of HWL it is important to be aware of potential errors. A commonly used proxy for shoreline position is the line between wet and dry sand, which is often seen as a tonal change in aerial photographs. Error related to the use of this line results from short-term natural mitigations, such as seasonal and tidal changes, beach slope, sediment size, wind, and waves (Moore, 2000). Therefore, it was decided to draw the HWL polyline based on erosion marks left by summer storms. These marks lay slightly above the wet-dry line and were the upper limit for dried kelp.

The baseline was constructed by the user and served as the starting point for all transects cast by the DSAS application. The distances from the baseline to each intersection point along a transect are used to compute selected statistics. The intersection points provide information on location and time, which was used by DSAS to calculate the rates of change. The baseline was constructed onshore parallel to the shorelines. Transects were cast at a user-defined spacing perpendicular to the baseline. The transect spacing length was 5 m, with a smoothing distance of 1000. The uncertainty and confidence interval were set as DSAS default values of 10 and 90, respectively (Himmelstoss et al., 2021).

From DSAS multiple statistical calculations can be made for change detection of the shoreline development. Net Shoreline Movement (NSM) was chosen to display the result. NSM is the distance in meters from the oldest to the youngest shoreline for each transect. This was chosen because of the limited aerial imagery over time.

3.3.2 Volume estimations of beach ridges and spits

Volume estimations were made for the beach ridges and spits closest to the river mouth of Longyearelva. The area of each beach ridge and spit was calculated in ArcGIS Pro based on orthophotos from June 2021 (Esri, n.d.) and August 2021. Equation 2 shows how volume estimations were made.

$$V = \frac{A * 1{,}05 + 0{,}3}{2}$$

Equation 2

Where V [m^3] is the volume estimation of the beach ridge/spit, A [m^2] is the area of beach ridge/spit, 1,05 m is the difference between mean high water and mean low water (Kartverket,

2020b), and 0,3 m is the approximate height of spit above mean high water based on field observations. All volume calculations have an assumed uncertainty of 20% due to the estimation of past material, approximate height above sea level, and quality of available imagery.

3.4 Hydrological monitoring

The melting season is considered to be from May to October (Nowak & Hodson, 2013). Streamflow in Longyearelva is normally restricted from June to September. A monitoring station (Figure 17) consisting of a data logger for hydrological monitoring and a pump to collect water samples for suspended sediments was installed by Veg 600. Measurements were initiated at the beginning of the melting season, on the 22nd of June 2021. For the hydrological monitoring, the measurements were stopped at the end of the melting season on the 25th of August 2021. Ideally, measurements should begin when streamflow starts and should end when the temperature falls below 0˚C and the river freezes.

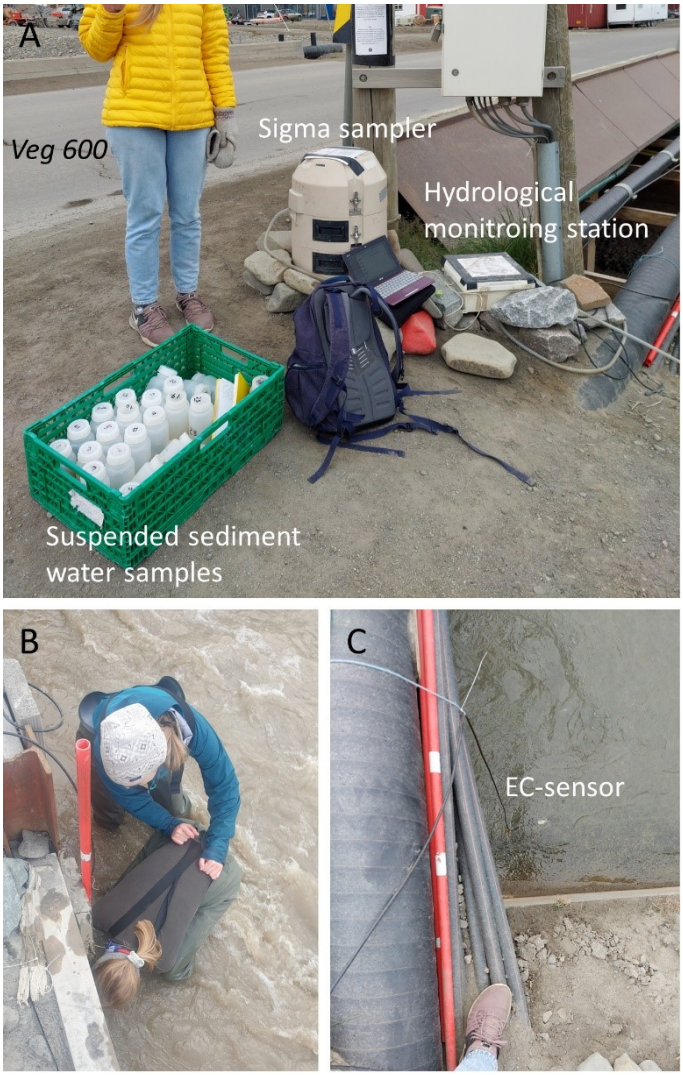

Figure 17 Monitoring station by Vei 600. A) Sampling area showing Sigma sampler and hydrological monitoring station. B) Installation of temperature and depth sensor 5 m downstream of the bridge. Photo by Aga Nowak. C) Electronic conductivity (EC) sensor connected to a hydrological monitoring station. Placed under the bridge of Veg 600.

3.4.1 Data logger

A Campbell Scientific (CR800 CX10) data logger was installed as a part of the hydrological measuring station. It included one sensor to measure the electric conductivity (EC) in the discharge and a Campbell pressure transducer to measure temperature and water stage (Figure 18). It was regularly checked that the EC-sensor did not lay on the riverbed or float on the surface because the sensor requires a constant stream through it to measure the electric conductivity. In periods with high discharge, a weight was mounted on the sensor. Air or lack of stream through sensor could cause incorrect results. The data logger was programmed to find the hourly average discharge (Q) from 10-minute readings of the water stage. The Campbell pressure transducer was installed with straps at a fixed location on the anthropogenically constructed riverbank, approximately two fingers above the riverbed. The battery level was checked regularly.

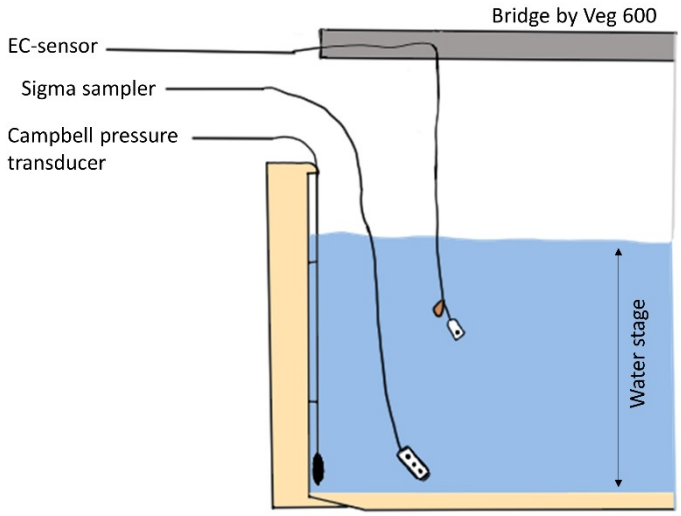

Figure 18 Schematic illustration of the hydrological monitoring station by Veg 600. The electronic conductivity sensor and the Campbell pressure transducer for the hydrological monitoring station, and the mouthpiece of the water sampler (Sigma pump) were placed in the river below a bridge.

3.4.2 The salt dilution method

The salt dilution method is the most commonly used method for studying the discharge for open channels in difficult and/or remote areas. It is applied when it is difficult to achieve a high-quality hydrological profile or measure the flow speed (Radulović et al., 2008). A known weight of salt dissolved in water was used as a slug injection to estimate the discharge in Longyearelva. Streamflow measurements by slug injections can be as precise as ± 5% (Day, 1976), but typically the uncertainty using this technique is ± 10% (Hodson et al., 2016). In this thesis, an uncertainty of ± 10% is assumed. Complete vertical and lateral mixing at the sampling site and a long stretch of unbraided river are requirements for this method. Since Longyearelva has been anthropogenically shifted into a relatively straight channel, it is possible to meet these requirements between Polarriggen and Veg 600 (Figure 19C). Here, Longyearelva has a long, unbraided stretch, which is easily accessible. An electronic conductivity meter (EC-meter, Figure 19A) was placed in the river downstream of the slug injection (Figure 19C). Before the injection was made, the readings of the EC-meter had to be stable. When they were sable, a signal was made to slug the saltwater into the river.

Recordings from the EC-meter were taken every 5 seconds from the slug injection was made until the EC in the river returned to the stable values.

Prior to the salt injection, the EC-meter was calibrated with salt solutions of different concentrations; 0, 10, 20, 40, and 80 mg/L. The solutions had the same temperature as the river when the calibration was executed.

Figure 19 The salt dilution method in Longyearelva for discharge calculations. A) Calibration of electronic conductivity (EC) meter. B) Measuring the EC in the river. Photo by Aga Nowak. C) The long, unbraided stretch of Longyearelva by Polarriggen, where slug injections of salt and the measuring EC were made.

To calculate the discharge using the results from the salt dilution method, Equation 3 was applied.

$$Q = \frac{kM}{((T_2 - T_1) * (EC_{mean} - EC_b))}$$

Equation 3

Where k was a constant, M [g] was the mass of salt added, T_2-T_1 [s] was the duration of tracer passage, EC_{mean} was the mean conductivity during tracer passage T_1 to T_2, and EC_b was the stable EC value.

The equation was used for every measurement from the salt dilution method. The discharge calculations obtained from Equation 3 were further used in a rating curve with the water stage measurements from the hydrological monitoring station. From the rating curve, Equation 4

was created. To find the hourly discharge in Longyearelva for the entire monitoring period Equation 4 was applied to the hourly EC measurements from the data logger.

$$y = 2{,}549e^{0{,}0396x}$$

Equation 4

Where y was the discharge [m^3/s] calculated from Equation 3 and x [m] was the water stage in Longyearelva.

3.5 Sediment transport

Monitoring of bedload and the suspended sediment concentration (SSC) are necessary for understanding a source-to-sink system as it gives indications of available sediment, erosion, and transport. From long-term data it is also possible to relate trends to climate change.

3.5.1 Bedload monitoring

In the Arctic, where glacifluvial braided rivers are dominating, it can be challenging to find a reliable method for bedload monitoring. Passive tracers were used as it is a part of the long-term monitoring project, and it is a cheap and accessible option for monitoring bedload transport.

In order to establish a monitoring series of comparable data, the same method and locations as Løvaas (2021) were used. Sediments the sizes of pebbles, cobbles, and boulders were placed in three different locations on the Longyearelva riverbed to monitor bedload transport (Figure 20). From Longyeardalen and Endalen, 138 rocks were collected and divided into six different classes (Table 6). Ideally, each rock should have been well-rounded and spheric. Due to the soft sedimentary rocks found around Longyeardalen, this was difficult to acquire. The rocks were washed, painted with environmentally friendly red paint, and labeled with unique values. The tracers were placed on the riverbed in three different localities. It was decided that location Ha-PT (Figure 20) would have all the rocks from class 6 since this area seemingly had a deeper channel and higher streamflow compared to the other two locations. The initial location was GPS marked at the beginning of the melting season. At the end of the melting season the positions of the passive tracers which could be located were registered to find the transport distance (if any).

Table 6 Size and distribution of passive tracers on the Longyearelva riverbed for the 2021 melting season.

		Number of passive tracers		
Class	**Size (mm)**	**Hu-PT**	**Ha-PT**	**Pr-PT**
1	50	10	10	10
2	100	10	10	10
3	150	10	10	10
4	200-250	10	10	10
5	300-350	5	4	5
6	400-450	4	-	-

The passive tracers placed at the location Ha-PT were removed on the 19th of August. This was earlier than planned due to construction work by NVE (The Norwegian Water Resources and Energy Directorate) on the riverbed. The remaining passive tracers that could be located

were removed from the river channel on the 26th of August, at the end of the melting season. The removed passive tracers were stored at UNIS for future participants in long-term projects. Some of the passive tracers were missing and were therefore not retrieved. Due to the heavy weight of the passive tracers from Class 6, they were not removed from the river channel.

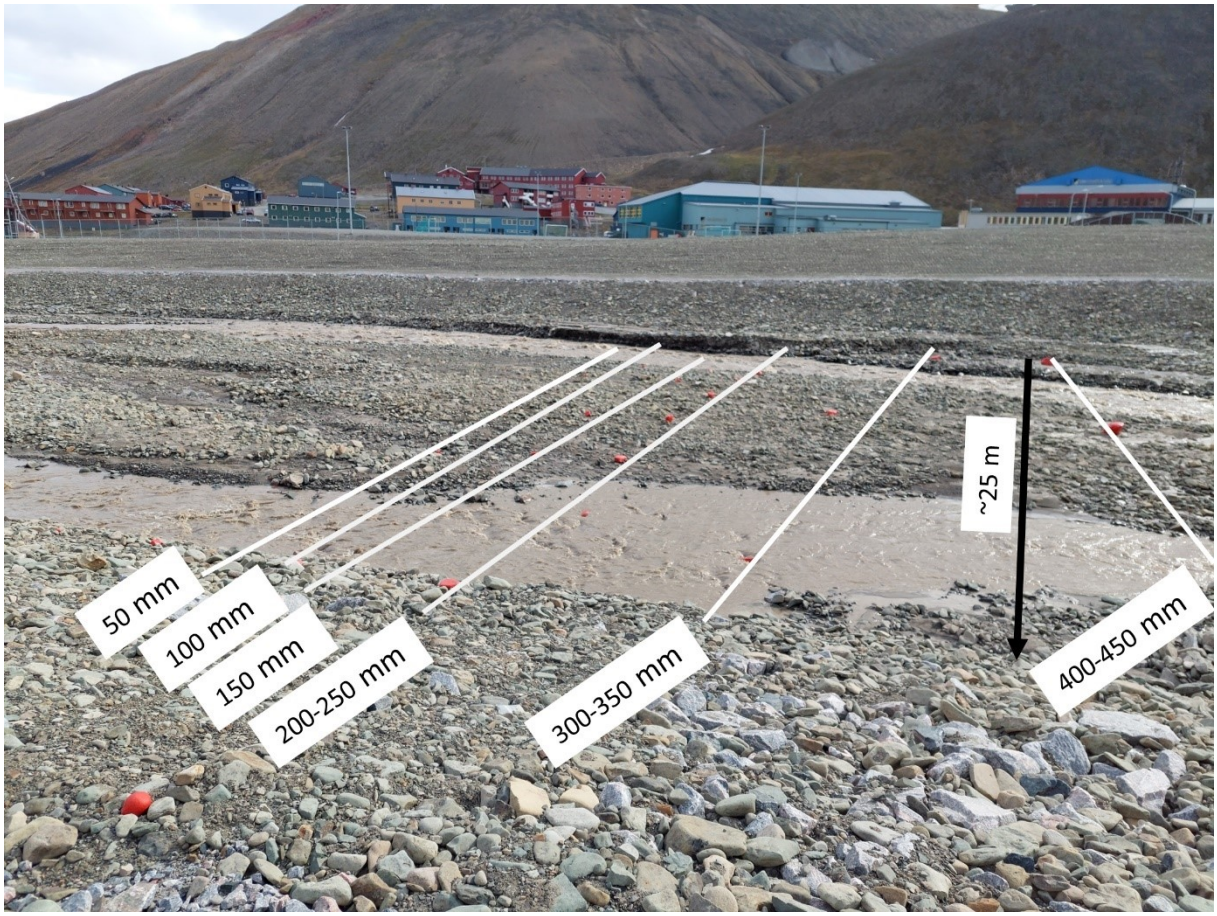

Figure 20 Passive tracers (red-painted rocks) placed on the riverbed in Longyearelva at the location Ha-PT (Hallen). Six classes of passive tracers were spread across the 25 m wide river channel. White lines indicate the placement of each class across the riverbed.

3.5.2 Suspended sediment concentration

A standard method for sampling suspended sediments was used. Sampling strategy and laboratory methods followed the procedures established by the NVE, as described by Bogen (1992). An automatic Sigma 900 Max Portable Sampler was used to obtain water samples with suspended sediment. The water samples were collected from the 23rd of June 2021 at 14:00 until the 31st of August 2021 at 08:00. The sampler had a programmed sampling frequency of four times a day, at times: 08:00, 14:00, 20:00, and 02:00. This was decided as an interval that can capture representative results while still taking into consideration the cost of filter papers used for filtering the water samples. The sampler could only contain 24 samples before it was full and needed to be reprogramed. The sampler was emptied and reset approximately every fifth day. The battery received regular checkups, approximately every other week. This turned out to be insufficient as the battery died one time. The hose from the Sigma sampler was not attached to a fixed point on the riverbank. As a result, the loose hose collected samples at unknown elevations above the riverbed. The mouthpiece of the hose (Figure 21B) has some weight to it, so it does not float. It has likely followed the flow

direction of the water current. The mouthpiece collects water samples through the small holes, which restricts larger grain sizes from entering the sampler.

Due to a misunderstanding when programming the Sigma Sampler, eight samples got lost between 30/06/21 at 14:00 and 02/07/21 at 08:00. From 03/07/21 at 14:00 until 06/07/21 at 08:00, a sampling delay of 1,5 hours occurred for 12 samples. Another 21 samples were lost between 20/08/2021 at 02:00 and 25/08/2021 at 14:00 due to a dead battery in the Sigma sampler. The lost samples in August had little significance for results as the construction work by NVE began on the 19th of August in the river by Veg 106. This caused unnaturally high suspended sediment concentration in the river, and the samples after this day were disregarded. In August, the sampler had a reoccurring problem with water leakage, resulting in smaller sample sizes in the collection bottles and sediment-laden water in the middle of the sample container (Figure 21C). The reason for leakage was not discovered.

Throughout the 2021 melting season, 240 water samples were collected. In a laboratory at UNIS the water samples were filtered, dried, and weighed. The filters used were Whatman GF/F 0,7 micrometers, 47mm diameter. Between 100 ml and 400 ml of each water sample was filtered. The suspended sediment collected in the filters from the water samples was dried at 100°C for 24 hours. When the filters with the suspended sediment had dried, they were weighted. To find the suspended sediment concentration [g/ml], the known weight of the filters was subtracted, and the suspended sediment was divided by the volume of the water sample.

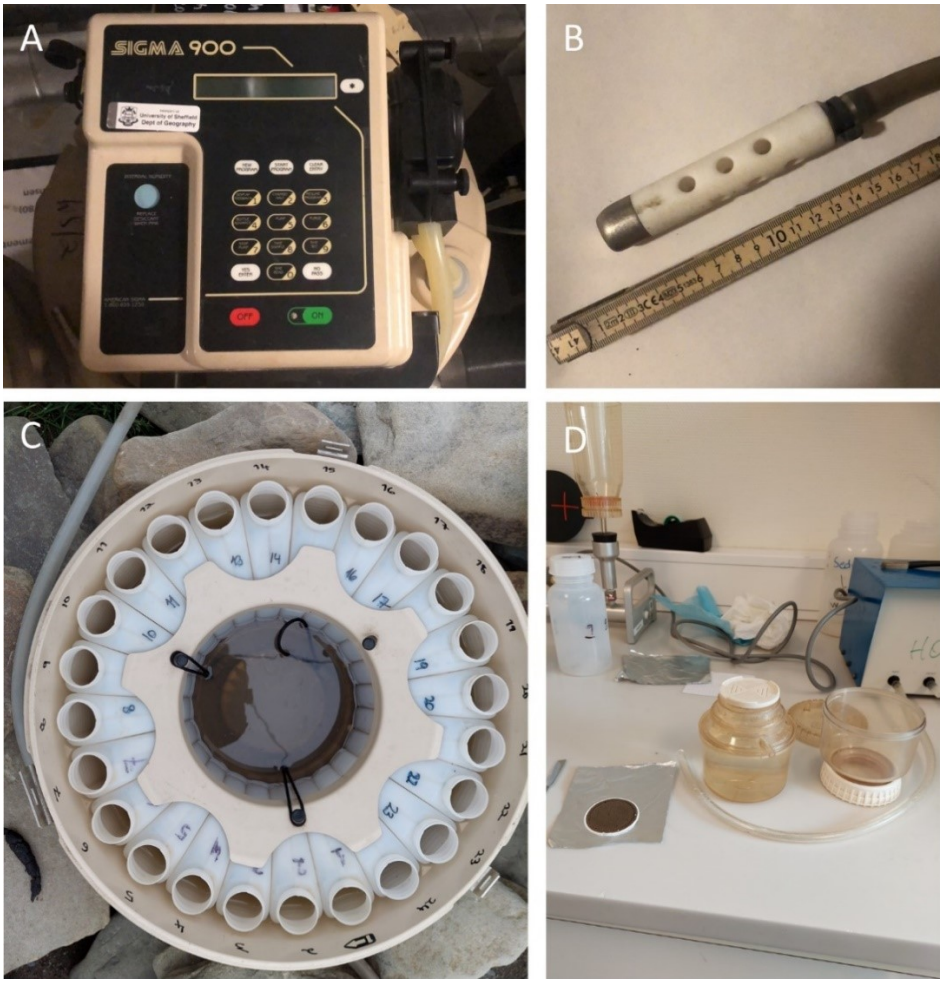

Figure 21 An automatic Sigma 900 Max Portable Sampler was used for collecting water samples with suspended sediment from Longyearelva every 6 hours. A) Programming of the pump. B) Mouthpiece of hose that was placed in the water to extract water samples with suspended sediment. C) Sample collection bottles are placed at the bottom of the pump. D) Water samples were filtered in a laboratory to study suspended sediment concentration.

An attempt to incinerate the filters of two sediment samples was made to study the grain size of the suspended sediments and how it correlates with discharge. Unfortunately, Whatman GF/F filters are too resilient to be incinerated. Firstly, an attempt to burn the filters at 550˚C for two hours was made without any results. Secondly, an attempt of 800˚C for two hours resulted in the filter papers turning light brown. Lastly, an attempt of 1000˚C for two hours was made. This resulted in filter papers turning thin and porous with a brown-red color, partially melted into the cup. It was not possible to see any traces of the sediments on the paper. Figure 22 shows the attempt to incinerate one of the filter papers of a test sample. No remains of sediment were visible.

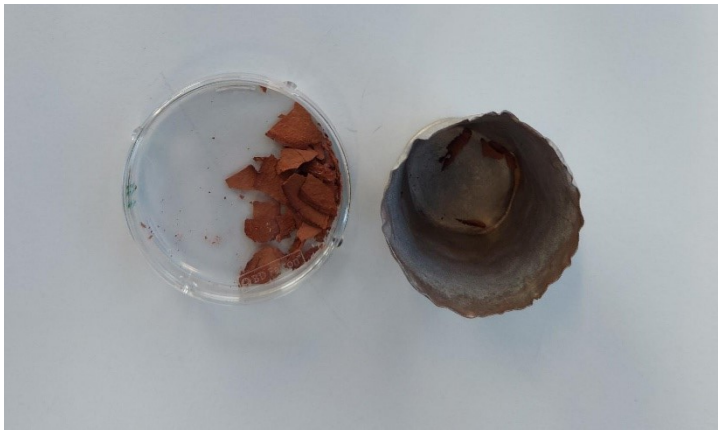

Figure 22 From the failed attempt to incinerate the filter paper to access sediments for further analysis.

3.5.3 Sediment samples from the Longyear delta

Sediment samples were collected in the delta area to study the grain size in the glacifluvial-marine environment (Figure 23). Eight samples (Table 7) were collected with a sediment probe and placed in sample bags. Samples were taken in places where a visible difference in grain size distribution could be observed, e.g., tidal flats, riverbanks, channel bars, and the inside of spits. When locations were selected, manual drilling was initiated. Initially, it was decided that each sample should be approximately 20 cm long or until the ground was too resilient to penetrate. This method of sampling was not ideal for all the locations. In the field it was discovered that the ground at some of the locations was hard to penetrate, and some of the locations had such high water content in the sediments that the sample collapsed before capture. A handful of sediment was taken from each of the boreholes for samples 004, 005, and 009 and mixed with the remains of their drilling cores. After collecting the samples, they were dried in open sample bags at room temperature for approximately one month. Due to a counting error sample 006 does not exist.

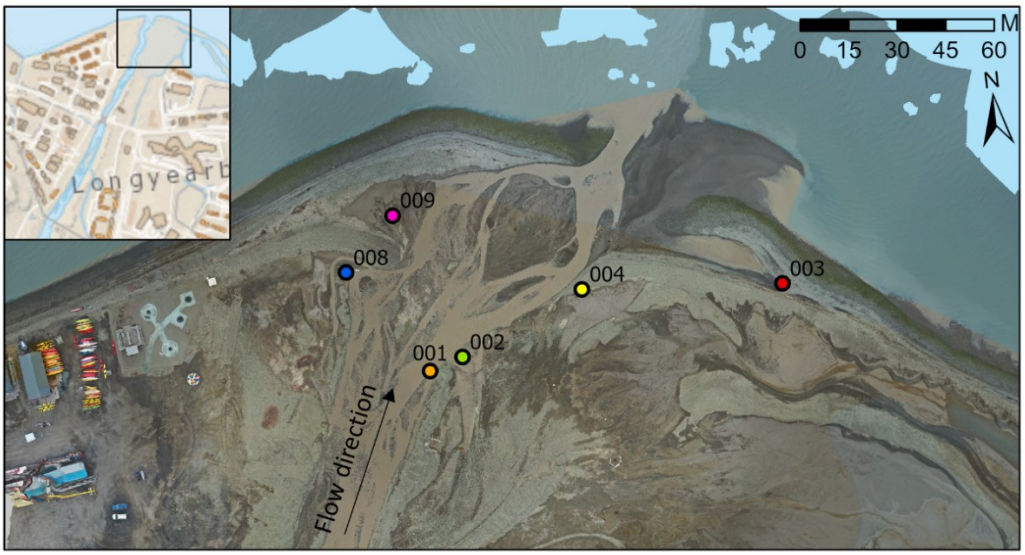

Figure 23 Location of delta samples collected from the Longyear delta at the beginning of the 2021 melting season. The background image is a 2021 orthophoto made from drone images. Overview map from Norwegian Polar Institute (n.d.-a).

Table 7 Information about sample depth, weight, and area of delta samples collected from the Longyear delta at the beginning of the 2021 melting season.

Sample Nr	***Sample depth***	***Sample weight [g]***	***Area***
001	20 cm	155,73	Riverbank
002	25 cm	325,9	Riverbank
003	20 cm	126,2	Spit
004	21 cm	124,3	Tidal flat
005	10 cm	199,61	Channel bar
007	3 cm	24,6	Channel bar
008	23 cm	164,1	Riverbank
009	23 cm	221,2	Tidal flat

The sediment samples from the delta were sieved after a standard method described by Vegvesen (2016). The samples were first weighed, mixed with water, and wet sieved with 1 mm – 63µm sieves (Figure 24A). The sieved, wet material was sorted into two glass bowls based on the grain size; 1) for sediment <63µm and 2) for sediment >63µm. The two glass bowls for each sample were dried at 45˚C for several days.

Secondly, the dry samples with sediments >63µm were dry sieved with 19 mm – 63µm sieves in an RX-29 H&B machine for 15 minutes each (Figure 24B). The 63µm sieve was included as wet sieving does not remove all particles finer than 63µm. Each sieve was manually shaken by hand over a paper sheet until no or little material fell through the sieve after the use of the machine. The material on the paper sheet was added to the underlaying sieve. When the sieving process was over, each sieve and the collection bucket were weighed with and without sample mass to create grain size distribution curves in Excel.

Figure 24 Sediment samples collected from the Longyear delta were first (A) wet sieved and dried, and then (B) dry sieved.

To ensure the quality of the results, a control check of the sample loss was necessary. If the difference between the weighted dry mass and the sum of separately weighted masses after sieving is larger than 1% of the weighted dry mass, the sieving should be repeated with a new sample. All samples had a loss of less than 1%, so this was ultimately deemed unnecessary. Table 8 shows the recommended sample sizes for samples where the largest grain size is of a certain size. If the collected sample size does not concur with this table, the achieved grain size distribution is not up to the Norwegian Standard (Vegvesen, 2016). From Table 7, none of the samples collected for the delta were big enough to meet the requirements of the Norwegian Standard. This must be taken into consideration when looking into the results. Due to the very small sample size, samples 005 and 007 will be excluded from any further discussion.

Table 8 Recommended sample size for grain size distribution for the Norwegian Standard. Modified from Vegvesen (2016)

Largest grain size (D) [mm]	***Sample size [g]***
22	5000
16	2600
11	1400
8	600
≤4	200

3.6 Climatological data

Temperature and precipitation data were downloaded from The Norwegian Meteorological Institute (n.d.). Temperature data was registered at two locations; Adventdalen and Svalbard Lufthavn. For the summer of 2021 the temperature and precipitation data from Svalbard Lufthavn were incomplete. It was decided to use temperature data from Adventdalen and precipitation data from Platåfjellet for the 2021 melting season. The Adventdalen and Platåfjellet monitoring station have not been active for long, so data from Svalbard Lufthavn was used to study long-term trends.

4 Results

To explore the research questions around the arctic delta dynamics while continuing the monitoring of the hydrological conditions in Longyeardalen several methods were applied. Firstly, the results from the aerial imagery and orthophoto collection will be presented. Secondly, the results regarding the Longyeardalen source-to-sink system with complementing discharge and sediment transport data from the 2021 melting season. The results are focused around delta geometry and development over time with respect to the sediment input.

Through the 2021 melting season, multiple monitoring points and stations were located in Longyeardalen. Figure 25A shows the points where ground photos were taken on a regular basis in Longyeardalen. Figure 25B shows the study area of the Longyear delta and the locations of passive tracers, hydrological monitoring stations, and where the salt dilution method was applied.

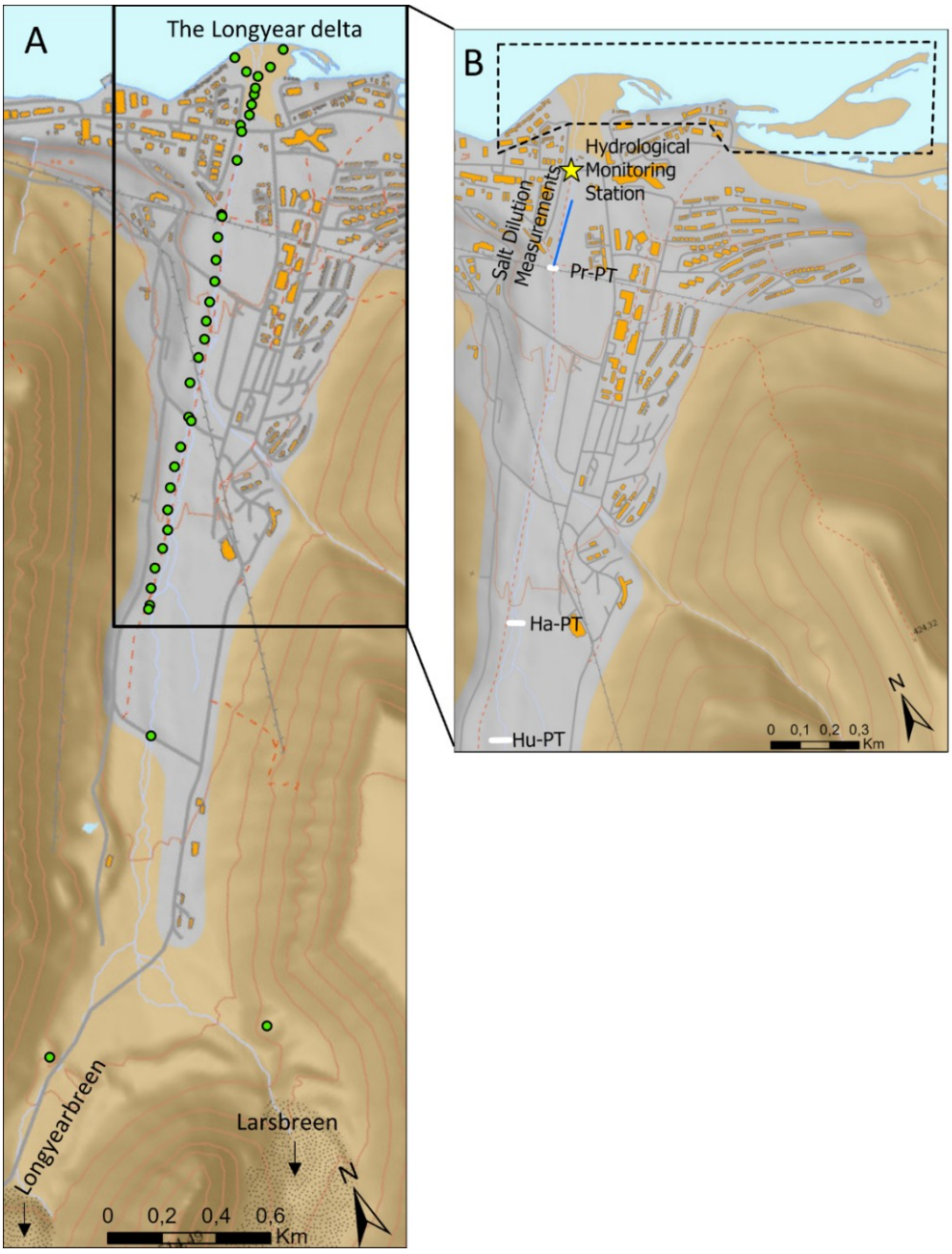

Figure 25 An overview of monitoring points and stations in Longyeardalen. A) Monitoring points where ground photos were taken every 1-2 weeks. B) The Longyear delta and coastline study area is marked with a black box. The yellow star shows the location of the hydrological monitoring station. The blue line represents the area where the salt dilution experiment was conducted. Pr-PT, Ha-PT, and Hu-PT show the initial location of passive tracers.

4.1 Collection of aerial imagery and orthophotos

A large collection of aerial imagery, orthophotos, and Digital Elevation Models (DEM) from Longyeardalen was assembled to study the long-term development of the Longyear delta. The collected overview of files from Longyeardalen, the Longyear delta, and Adventfjorden is presented in Appendix A. All files from 2021 were produced from fieldwork, with the exception of one orthophoto provided by Esri (n.d.). The files from previous years (1936-2020) were acquired from The Norwegian Polar Institute (NPI), the University Centre in Svalbard (UNIS), and previous UNIS students Martin Løvaas and Juliano Hanna.

From the collection of aerial imageries, orthophotos, and DEMs, only a certain selection has been used in this thesis. Table 9 shows the name, year, type, and source of the selected files. The numbers of each file will be used as a reference for figures to follow.

Table 9 Overview of orthophotos, aerial imageries, and digital elevation model (DEM) used in this thesis. Løvaas (2021) and Hanna (2019) are considered the UNIS source. The NPI source is the Norwegian Polar Institute (n.d.-a), and the source Esri is from Esri (n.d.).

Nr	***Name***	***Year***	***Type***	***Source***
1	S90	1990	Orthophoto	NPI
2	S90 3682	1990	Orthophoto	NPI
3	NP_Ortofoto_Svalbard_WMTS_25833	2009/2011	Orthophoto	NPI
4	Ortho_Low	2019	Orthophoto	UNIS
5	LongyearElva_Ortomosaic_07.08.20	2020	Orthophoto	UNIS
6	World Imagery	2021	Orthophoto	Esri
7	Ortho_delta_aug_21	2021	Orthophoto	UNIS
8	endofseason_delta_lower_river_ortho	2021	Orthophoto	UNIS
9	S36_2295	1936	Aerial imagery	NPI
10	S36_1358	1936	Aerial imagery	NPI
11	S36_3039	1936	Aerial imagery	NPI
12	DJI_0624	2020	Aerial imagery	UNIS
13	NP_S0_DTM20	2009	Digital elevation model	NPI

4.2 The Longyeardalen catchment

It was necessary to define the catchment area before the development of the delta in the Longyeardalen source-to-sink system (Figure 26) could be studied. For delta development, the availability of source material plays an important factor. The sources in the catchment will be briefly mentioned as it is important for the delta but got further investigated in the twin-study Pallesen (2022).

Figure 26 Flow chart of the Longyeardalen source-to-sink system. This chapter is centered around the source. The main focus is transport in Longyearelva and sink in the Longyear delta.

To find the area of the Longyeardalen catchment a flow direction raster was generated from the 2009 DEM[13] (Figure 27B). Each color in the raster represents a cardinal direction in which water flows. The calculated total area of the Longyeardalen catchment was 22,9 km^2, using hydrology tools and manual modifications based on flow directions in ArcGIS Pro (Figure 27A). The calculated area of Longyearbreen was 2,4 km^2 while Larsbreen was at 2,7 km^2, both based on the 2009/2011 orthophoto[3]. The glacierized area covers 5,1 km^2 (22%) of the catchment, and the non-glacierized area covers the remaining 17,8 km^2 (78%).

On the border of the catchment, a third glacier named Platåbreen is located. It is a part of a secondary catchment system. A little stream can be observed west of the Longyearbreen forefield originating from Platåbreen in the summer months. The hydrological and sedimentary input from this secondary catchment is assumed to be insignificant and was disregarded as a result.

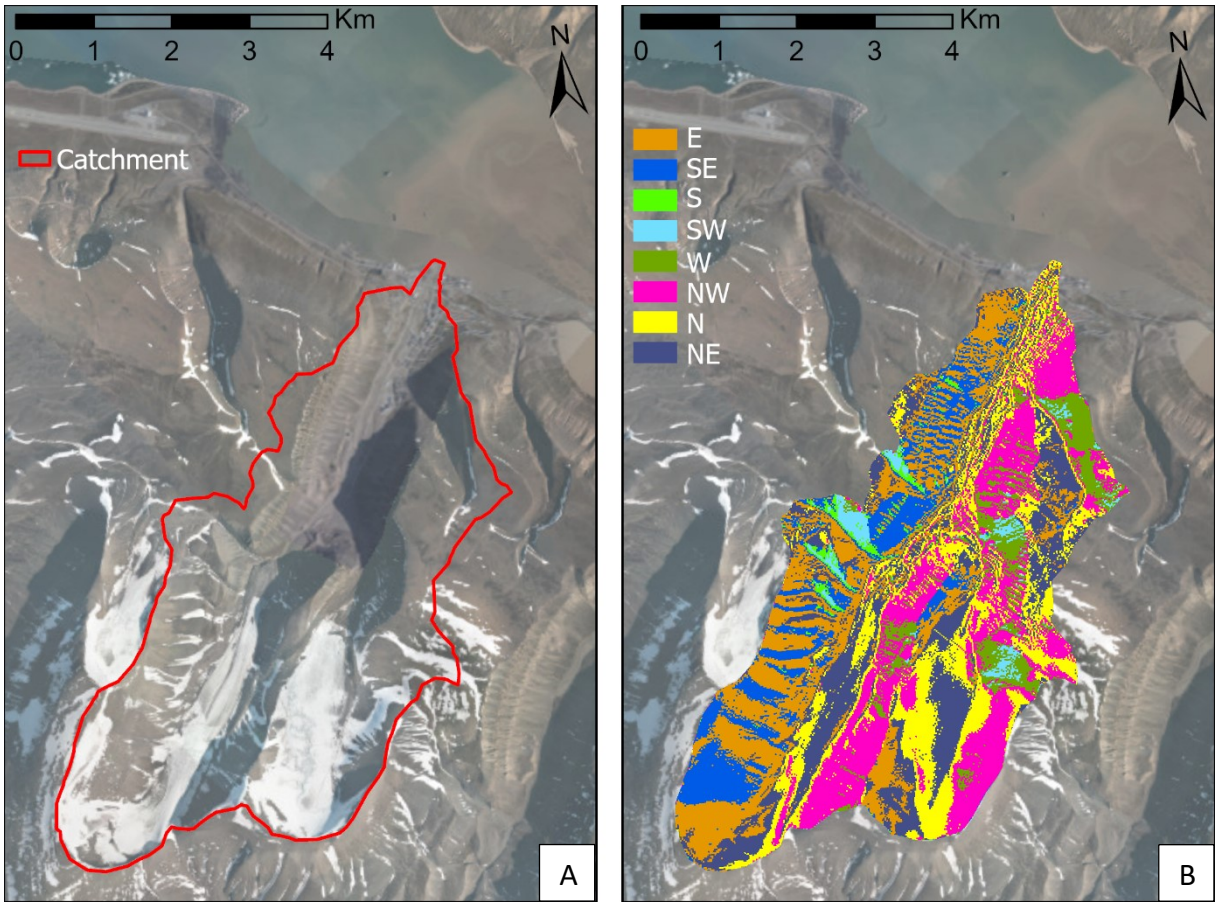

Figure 27 The calculated Longyeardalen catchment based on a 2009 digital elevation model (DEM)[13] in collaboration with Pallesen (2022). The background image is from the 2009/2011 orthophoto[3]. A) The red outline shows the Longyeardalen catchment. B) A flow direction raster illustrating the cardinal direction of slope faces in which surface water flows.

The percentage of the cardinal directions in the catchment was calculated (Table 10) from Figure 27B. The dominating slope directions are east, northwest and northeast, making up a total of 61% of the catchment system. South, southwest, and west-facing slope directions are barely present in the catchment system, making up a total of 10%.

Table 10 Percentage of cardinal flow (slope) directions in Longyeardalen catchment. Generated from 2009/2011 digital elevation model (DEM).

Cardinal Direction	**Percent**
East	22
Southeast	12
South	1
Southwest	2
West	7
Northwest	20
North	17
Northeast	19

4.3 Transport; the river system

Longyearelva and the ocean processes are the main transport mechanisms in the Longyeardalen source-to-sink system (Figure 28). The factors affecting the river transport, including temperature, precipitation, and discharge, will be presented, along with the results from the monitoring of bedload and suspended load.

Figure 28 Flow chart of the Longyeardalen source-to-sink system. This chapter is centered around transport. The main focus is transport in Longyearelva and sink in the Longyear delta.

4.3.1 Climatology

All fluvial systems are dependent on the climate of the region as input to the hydrological system. Precipitation and temperature are considered important variables for variations in discharge.

From June to August 2021, an average temperature of 5,2°C was registered (Table 11) at Svalbard Lufthavn. This was lower than the average temperatures registered in both the 5-year and 30-year periods. An increase of 0,6°C in the average temperature at Svalbard Lufthavn can be observed from the 30-year period to the 5-year period. The precipitation for the same period in 2021 was registered as 60,4 mm. It was higher than the average precipitation for a 5-year and 30-year period (The Norwegian Meteorological Institute, n.d.). Although the precipitation was higher than the average summer precipitation, it did not cause any flooding.

Table 11 Average summer (June-August) temperature and precipitation for a 30-year, 5-year, and 1-year period measured at Svalbard Lufthavn (The Norwegian Meteorological Institute, n.d.).

Years	*Temperature (°C)*	*Precipitation (mm)*	*Period*
1992-2021	5,6	51,4	30-year
2017-2021	6,2	55,3	5-year
2021	5,2	60,4	1-year

The daily total precipitation measured at Platåberget during the summer of 2021 is illustrated in Figure 29A. The maximum daily total precipitation registered was 8,9 mm on the 18th of July. The second highest value registered was the following day with 5,5 mm. Short, reoccurring periods of precipitation could be observed throughout the summer. The daily average air temperature from Adventdalen is illustrated in Figure 29B for the same period. At the end of June and beginning of July, the temperature rose from 3,2°C to 7°C. From mid-June to mid-August the temperature varied between 5,2°C and 9,8°C. The highest peak was registered at 9,8°C on the 16th of July. After the 11th of August the temperature began to decline. Peaks in temperature can be observed in the following weeks after the decline began, but they were not as significant as those observed between mid-July and mid-August.

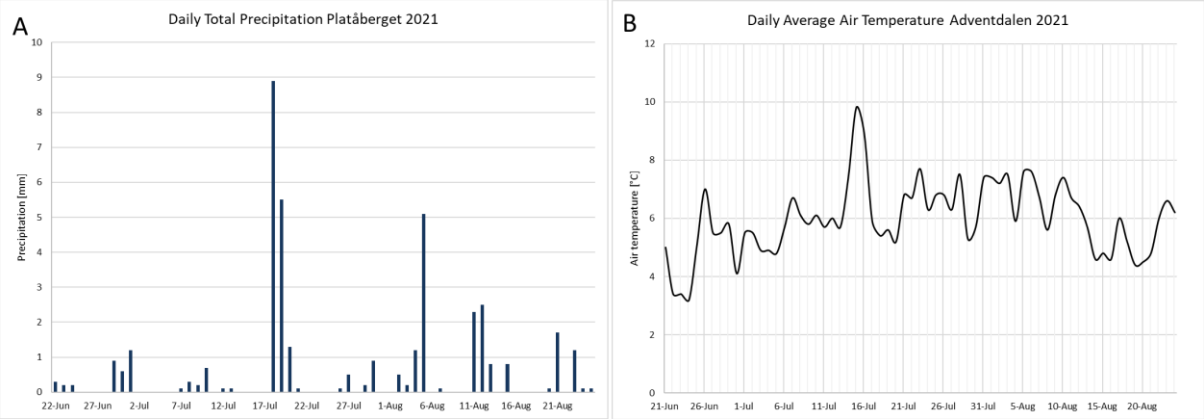

Figure 29 Precipitation and temperature data for the 2021 summer months (The Norwegian Meteorological Institute, n.d.). A) The daily total precipitation from 22/07/21 to 25/07/21. From the measuring station at Platåberget. B) The daily average air temperature measured in Adventdalen.

4.3.2 Discharge

The discharge (Q) was calculated for Longyearelva from the 22nd of June to the 25th of August. The hourly discharge (Figure 30) was calculated from the average of 10-minute readings of the water stage in Longyearelva. There were small variations in the hourly and daily discharge in June. The discharge normally varied between 1,2 m^3/s and 1,6 m^3/s. One small peak of 2,4 m^3/s occurred on the 26th of June. Early in July, an overall increase in discharge took place. The diurnal variations were larger than what was observed in June. The discharge normally varied between 1,0 m^3/s and 2,0 m^3/s, with repeated periods of rising and falling. Three peaks in discharge were observed in early, mid-, and late July. The highest peak of 3,2 m^3/s occurred on the 8th of July. From mid-July an overall decrease in the discharge began. The peaks were gradually changing from extended rising limbs and shorter falling limbs to shorter rising limbs and extended falling limbs towards the end of the melting season. At the beginning of August, the diurnal variations had small variations between 0,7 and 1,3 m^3/s. On the 11th of August, a peak of 2,7 m^3/s occurred. After the peak, the discharge returned to small diurnal variations.

The daily average discharge and the daily maximum discharge (Figure 31) were calculated from the hourly hydrograph (Figure 30). The low diurnal variations in June can be observed as a consistent gap between the daily average discharge and the daily maximum discharge. During July the gap between the two hydrographs became more irregular due to the diurnal variations. The highest daily maximum discharge was 3,2 m^3/s on the 8th of July, while the daily average discharge was 2,5 m^3/s on the same day. The gap between the two hydrographs was more consistent throughout August and gradually became smaller, though with the exception of the peak that occurred on the 11th of August.

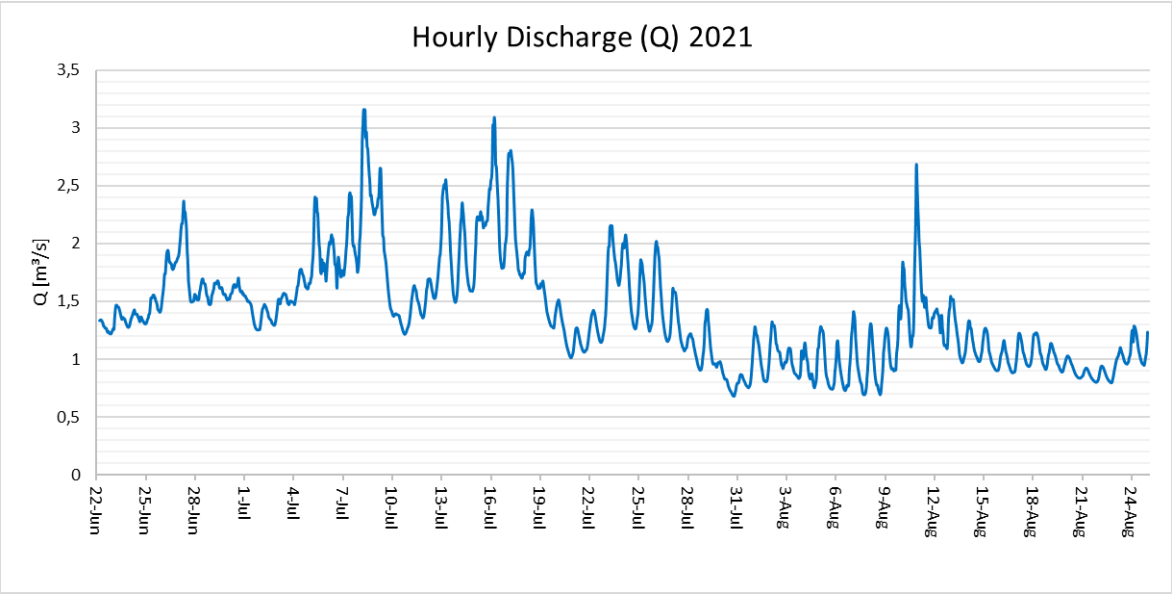

Figure 30 Hourly discharge measured in Longyearelva from 22/07/21 to 25/07/21. Three modes were constructed based on the inter-seasonal trends from the hourly measurements.

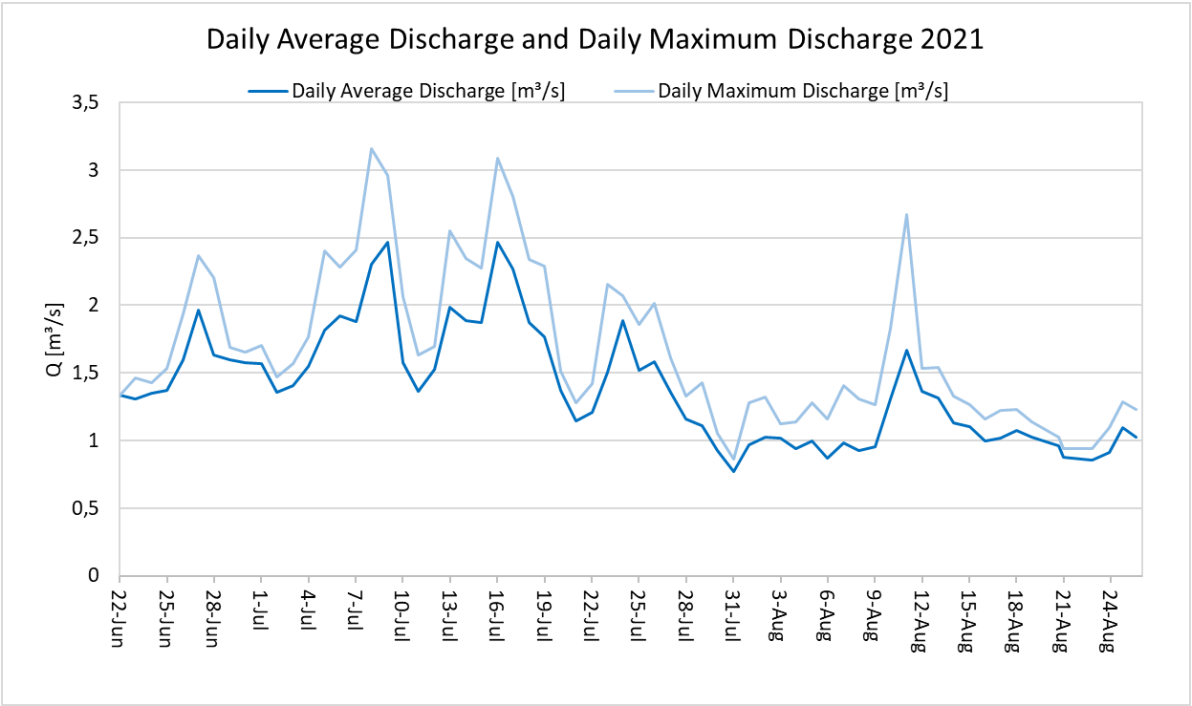

Figure 31 Daily average discharge and daily maximum discharge measured in Longyearelva from 22/07/21 to 25/07/21. Three modes were constructed based on the inter-seasonal trends in the hourly measurements.

4.3.3 Bedload transport

The Longyeardalen river system transport both coarse and fine sediment. To understand and measure the transport both studied. Firstly, the coarse sediment was observed transported as bedload. Secondly, the fine sediment was observed transported as a suspended load.

Passive tracers were placed in three locations for measuring the bedload (Figure 25B) on the Longyearelva riverbed. At the location Hu-PT the river channel has been anthropogenically reworked, but the width of the river channel allows for the river to behave in a braided channel pattern. At the locations Ha-PT and Pr-PT, the river has been anthropogenically forced into one narrow channel. In total 8 out of 138 passive tracers were registered as transported downstream from their initial position during the 2021 melting season. This shows a retrieval rate of 5,8% for the passive tracers registered as moved. The remaining 94,2% were either missing, buried (Figure 32), or still in the initial position.

- Hu-PT (Huset): Passive tracers were placed across the river channel. As the river channel shifted in a braided pattern, the tracers were moved or became missing. Seven tracers were registered to move downstream at this location. The longest downstream movement registered was 74 m by a 200-250 mm sized passive tracer. However, the movement along the stream was likely to be larger due to the braided pattern. The largest passive tracer transported was 300-350 mm, which occurred at this location. It was transported 65 m downstream.
- Ha-PT (Hallen): One passive tracer was registered as transported in this location. The size was 200-250 mm, and it traveled 21 m downstream. The four largest tracers (400-450 mm) were placed here, but no movement was registered.
- Pr-PT (Polarriggen): Passive tracers were placed in the active and inactive part of the river channel. All the passive tracers placed in the active part of the river channel were missing (sizes 50-350 mm).

Figure 32 A partially buried passive tracer in the Longyearelva riverbed by the location Hu-PT at the end of the 2021 melting season. The active channel can be seen between the passive tracer and Huset (white building). Photo towards southwest.

A large rock was discovered in the river mouth close to the delta (Figure 33). The rock was approximately 300 mm in diameter, laying in the middle of the river channel. Based on the properties of the rock, it was assumed to be natural in the Longyeardalen catchment. The large grain sizes in the surrounding area (Figure 33A) suggest that the rock was transported by the river.

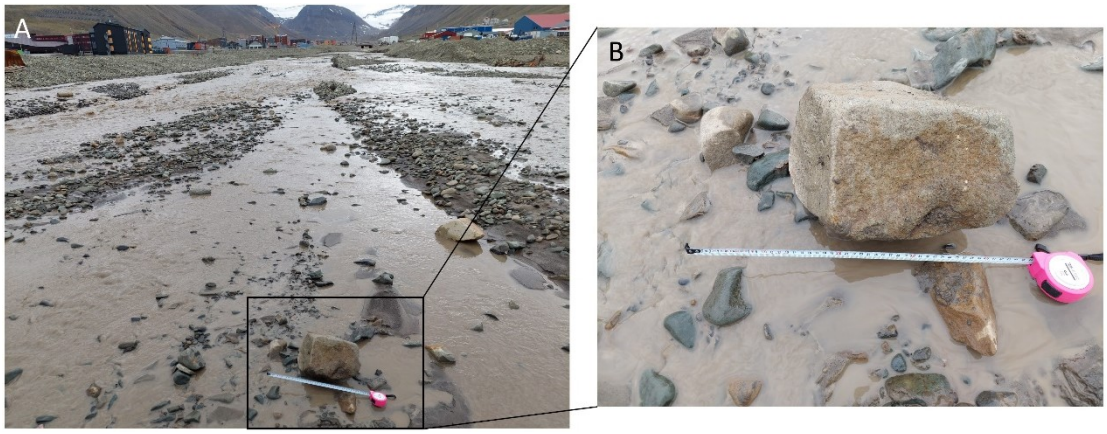

Figure 33 A large rock observed in the river mouth of Longyearelva, close to the Longyear delta. A) The rock was located in the middle of the river channel. The photo was taken upstream towards the south. B) Close-up of the rock with measuring tape for scale.

4.3.4 Suspended sediments

Studying the suspended load, suspended sediment concentration (SSC) was measured in Longyearelva. The suspended sediments were collected during the 2021 melting season between the 22nd of June and the 28th of August. In the following results, only data collected from the 22nd of June to the 19th of August are included because of construction work in the river by Veg 106. The construction work caused unnaturally high levels in the suspended sediment concentration, severely affecting the suspended sediment samples taken after the 19th of August.

The daily maximum SSC and the time of occurrence are presented in Figure 34. In June, the average daily fluctuations of the maximum SSC varied between 0,2 g/L and 0,9 g/L. One small, symmetrical peak of 1,8 g/L occurred around the 26th of June. In July, the maximum SSC had larger diurnal fluctuations, with average values between 0,6 g/L and 3,0 g/L. The period was characterized by several peaks of approximately the same order. The highest value registered for this month was 4,9 g/L on the 13th of July. The largest diurnal fluctuations occurred in August. The average daily values varied between 1,0 g/L and 3,0 g/L. Almost all the peaks observed in this period had values higher than 5,0 g/L. The highest maximum SSC for the entire monitoring period was 8,1 g/L and occurred on the 10th of August. The following day had the second-highest value of 7,1 g/L. The maximum SSC had extended rising limbs and shorter falling limbs from the beginning of the measuring period until approximately the 10th of July. Thereafter, a gradual change to shorter rising limbs and extended falling limbs could be observed.

In June and July, the daily maximum SSC occurred primarily at 20:00, with a few exceptions at 14:00 or 02:00. The daily maximum SSC was not registered to occur at 08:00 for the whole monitoring period. For August 12 of 19 days were registered to have the maximum SSC value at 14:00. The change in time of occurrence coincides with the high peaks of SCC in August.

Due to the loss of samples (see Chapter 3.5.2), it was chosen to display the daily maximum values instead of the daily average SSC. Many of the lost samples were supposed to be taken at 02:00, which was usually the lowest SSC registered in a day.

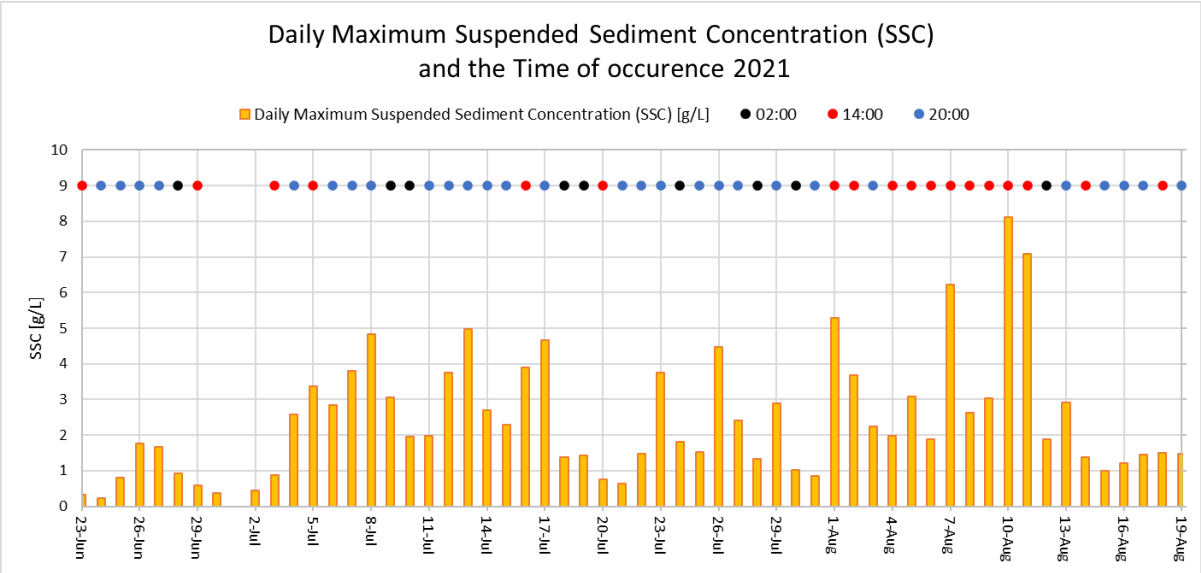

Figure 34 The daily maximum suspended sediment concentration (SSC) measured in Longyearelva from 22/07/21 to 19/08/21. Colored dots indicate the time of occurrence for each day.

The suspended sediment load (SSL) was calculated (Figure 35) from the daily average discharge (Figure 31) and the daily SSC (Figure 34). The highest daily SSL was 686 tonne on the 10th of August. The total SSL transported in Longyearelva was calculated to be at least 11 700 t/yr. The suspended sediment yield (SSY) was calculated as 510 t/km^2/yr by using the SSL and the calculated catchment size of 22,9 km^2.

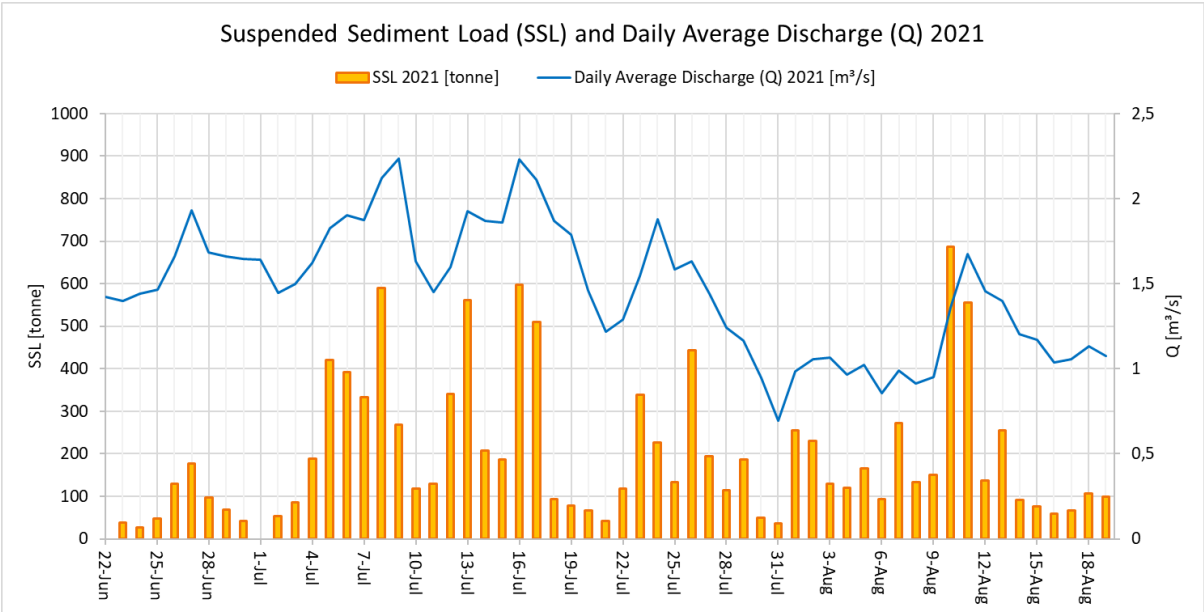

Figure 35 The daily average discharge (Q) and the suspended sediment load (SSL) in Longyearelva from 22/07/21 to 19/08/21.

Examples of two filtered water samples (suspended sediment) can be observed in Figure 36. The samples were taken between the 24th and 30th of June, but due to inexperience, the specific sample was not noted. Sample A had a normal distribution of grain sizes with a few coarse particles. The largest particles were ≤ 1,0 mm in diameter. Sample B had a bimodal distribution of grain sizes due to a large number of coarse particles. The particles were ≤ 1,5 mm in diameter. An attempt of a qualitative study of the grain sizes in the water column based on the suspended sediment samples was made. No valid results were achieved due to the choice of filter and placement of hose (See Chapter 3.5.2). As suspended sediment samples were taken at an unknown elevation over the riverbed, it was possible that the larger grain sizes in the filters were a result of saltation and not suspended load. After the samples had dried inside the filters, it was no longer possible to study the grain sizes without running the sample (Figure 22).

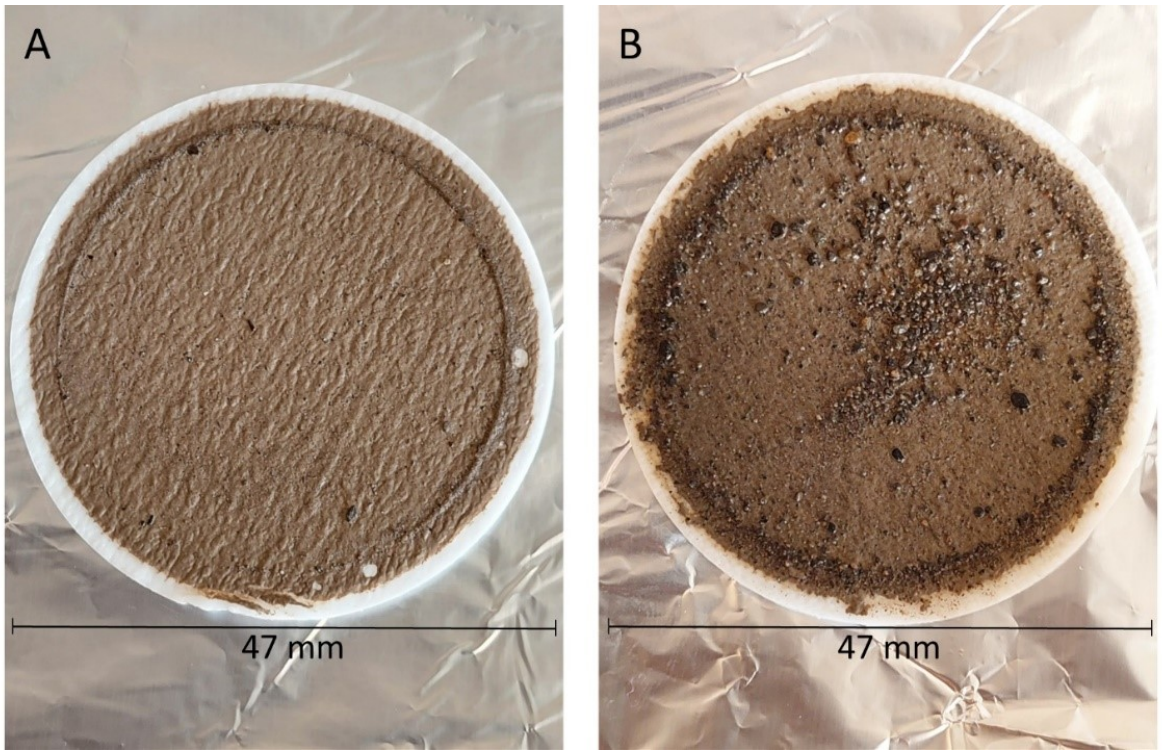

Figure 36 Examples of two filtered water samples to study the suspended sediment concentration (SSC). The filters with suspended sediment were taken in the period between 24/06/21 and 30/06/21. The filter diameter was 47 mm. Sample A had a normal distribution of grain sizes, and sample B had a bimodal distribution of grain sizes.

4.4 Delta as a depositional environment

Longyearelva transports glaciofluvial sediments down the river channel and to the Longyear delta. The Longyear delta and the deeper parts of Adventfjorden are the depositional environments in the Longyeardalen catchment system (Figure 37). Adventfjorden is a small fjord arm up to 60 m deep. The sediment reaching the fjord is deposited in the Longyear delta, including the coastal zone and deeper parts of the fjord. The final sink in the system is eventually the sea. Seasonal, multiyear, and permanent deposits in the delta area are considered secondary deposits. Long-term development was analyzed as it is possible through remote sensing of older aerial photographs. The study area includes the Longyear delta and the coastline on both sides of the river mouth (Figure 25B). The results of the delta and coastline development are restricted to the delta front above sea level due to the limited access to bathymetry data of Adventfjorden.

Figure 37 Flow chart of the Longyeardalen source-to-sink system. This chapter is centered around the sink. The main focus is transport in Longyearelva and sink in the Longyear delta.

4.4.1 Delta geometry

The study area of the Longyear delta and coastline is divided into three sections (Figure 38) based on field observation and orthophotos. From the west end of section 1 to the east end of section 3, the distance is approximately 1,5 km^2. In section 1, the coastline was observed as erosional. Section 2 is the Longyear delta. The Longyear delta was approximately 300 m wide, stretching 160 m into the Adventfjorden. The unlithified coarse material had an assumed depth of 2 m. Using these values, the approximate volume of sediments in the delta equals 48 000 ± 9600 m^3. In section 3, a depositional environment with a spit system was observed. In sections 2 and 3, 12 marine beach ridges were mapped with active and inactive spits. The beach ridges were raised approximately 30 cm above mean high water level. Erosion marks from wave action could be found on most of the beach ridges in sections 2 and 3.

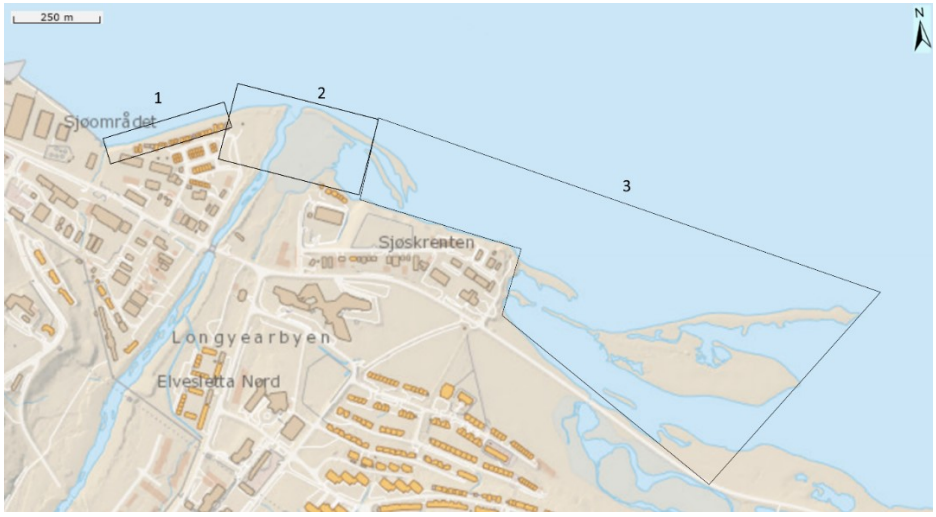

Figure 38 Map of the Longyear delta and coastline divided into three sections: 1) Erosive coastline west of the Longyear delta 2) The Longyear delta 3) Depositional area east of the Longyear delta. Basemap from (Norwegian Polar Institute, n.d.-a).

A Quaternary geological map (Figure 39) based on aerial imagery and field observations was produced in this study. The Norwegian SOSI standard for Quaternary geological maps was primarily used in creating this map (Geological Survey of Norway, n.d.). In section 1, a steep edge of anthropogenic fill mass could be found in the west. One inactive marine beach ridge was located close to the Longyear delta. Erosion marks from both summer and winter storms were observed along the coastline.

In section 2, the river and delta systems have been repeatedly managed by anthropogenic activity. Active and inactive channels could be found in the glaciofluvial deposits on the delta plain. The active river channel has mitigation walls on each side to confine it. Previously active river channels were located east of the currently active channel. Marine beach ridges formed on both sides of the river outlet. Five marine beach ridges were found, whereas four of them were active. Glaciofluvial sediment transported by Longyearelva was actively reworked in the tidal zone. Sediment transported by the river to the delta is strongly affected by the transport, sorting, and deposition of ocean mechanisms in the tidal zone. In the river mouth and eastward into section 3, glaciofluvial sediment from the river has been reworked in the tidal zone and deposited. Tidally active channels between beach ridges could be observed in the depositional areas.

Section 3 consists of large areas of actively reworked glaciofluvial sediment in the tidal zone and shallow marine sediment. A steep edge of anthropogenic fill mass was observed along the coastline. Six marine beach ridges were mapped. The east end of each beach ridge is curved towards land. Permanently deposited beach ridges have been anthropogenically disturbed in the east part of section 3. Old marine deposits mixed with fluvial sediment from a river originating from Gruvedalen were coved in peat and bog. These were deposited before the roads were built.

It has been acknowledged by Longyearbyen Lokalstyre (2017) that contaminated grounds can be found between Svalbard Lufthavn and Longyearbyen. The anthropogenic fill mass found in the study area is therefore suspected of containing pollution and waste.

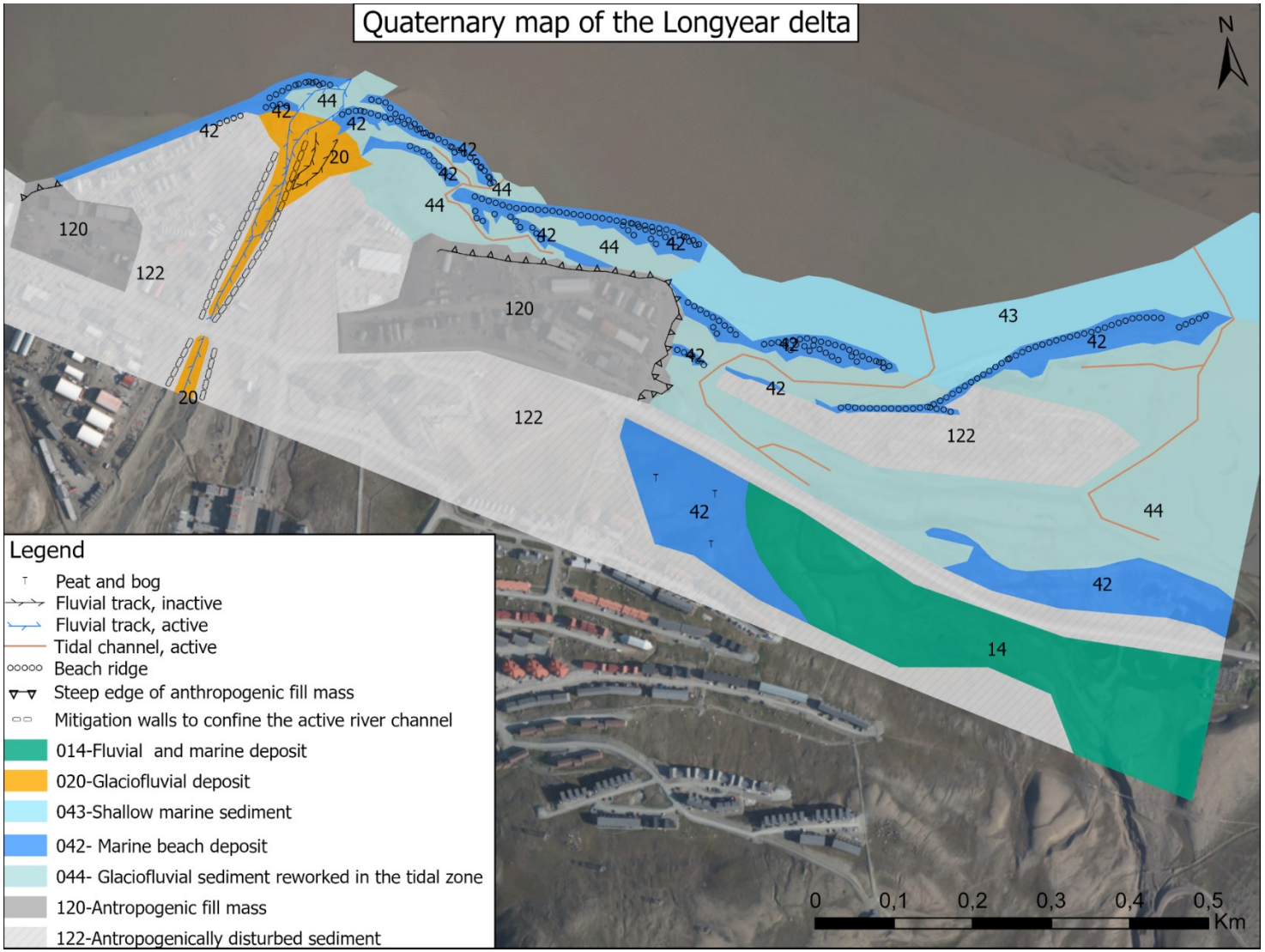

Figure 39 Quaternary geological map showing landforms and sediments found in the Longyear delta. Based on orthophoto from 2021 and field observations. The background image is a combination of the orthophoto from 2021[7] and 2009[3].

The approximate volume of the marine beach ridges and spits close to the river mouth was calculated (Figure 40, Table 12) based on field observations and orthophotos from 2021. In Figure 40 the orange polygons represent wave-formed marine beach ridges while the yellow polygons represent spits. The orthophoto from June was taken early in the melting season, so the river had barely broken through the beach ridges created by winter storms. The orthophoto from August was taken at the end of the season after the river mouth became more developed.

Beach ridge 1 and 2 had a big visual difference in the spatial extent from June (Figure 40A) to August (Figure 40B). Approximate volume calculations were therefore made for both the beginning and the end of the melting season. The remaining beach ridges and spits did not change as much through the melting season, so approximate volume calculations were only done for the end of the season. Beach ridge 1 had a volume of 1080 m^3 at the beginning of the season. Later in the season, this volume was reduced to 760 m^3, meaning 320 m^3 of sediment was eroded from the beach ridge during the melting season. Beach ridge 2 had a volume of 640 m^3 at the beginning of the season. Later in the season, this volume was reduced to 500 m^3, meaning 140 m^3 of sediment was eroded. Collectively, approximately 460 m^3 of sediment was redeposited from beach ridges 1 and 2.

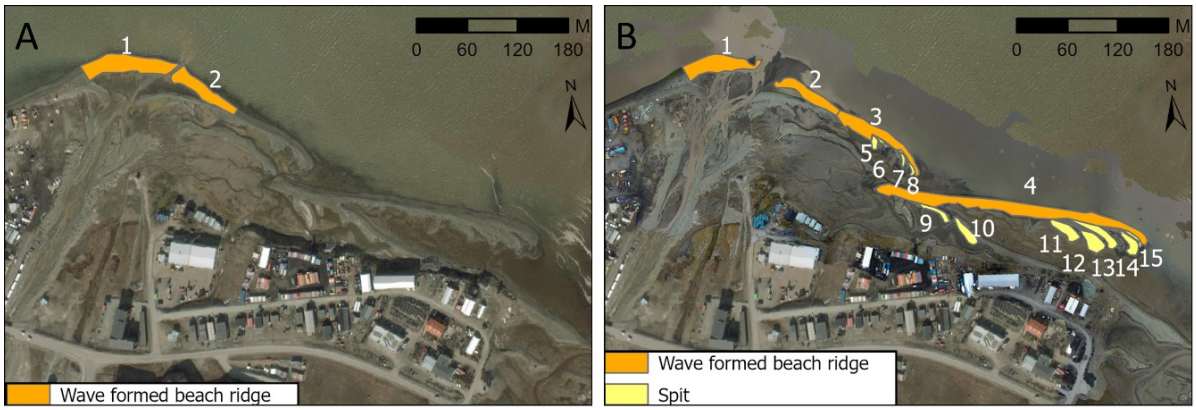

Figure 40 Wave formed beach ridges and spits in the Longyear delta in 2021. A) Last season's beach ridges formed by wave action mapped from 2021 orthophoto$_6$ from June. B) Beach ridges and spits mapped with GPS in August 2021. The background image is a combination of August 2021 orthophoto$_7$ and June 2021 orthophoto$_6$.

Table 12 Approximate volume calculations for beach ridges and spits around the Longyear delta during the 2021 melting season. The calculations include an uncertainty of 20%.

Nr	Feature	Vol [m³] June 2021	Vol [m³] August 2021	Active
1	Wave formed beach ridge	1080 ± 215	760 ± 150	X
2	Wave formed beach ridge	640 ± 130	500 ± 100	X
3	Wave formed beach ridge		710 ± 140	X
4	Wave formed beach ridge		2070 ± 415	X
5	Spit		55 ± 10	
6	Spit		25 ± 5	
7	Spit		35 ± 7	
8	Spit		50 ± 10	X
9	Spit		105 ± 20	
10	Spit		170 ± 35	
11	Spit		210 ± 40	
12	Spit		230 ± 45	
13	Spit		240 ± 50	
14	Spit		155 ± 30	
15	Spit		50 ± 10	X

Eight samples were collected to study the grain size distribution in the Longyear delta. Six of the samples were used to create grain size distribution curves (Figure 41). Samples 002 and 008 contained approximately 60% silt and clay. Samples 001, 003, 004, and 009 contained between 8% and 13% silt and clay. All the samples contained grain sizes larger than very coarse sand (>2 mm). The sediment samples with the highest amount of coarse material were found closest to the sea (samples 003 and 009). The samples show that the Longyear delta has a large grain size distribution over a small area.

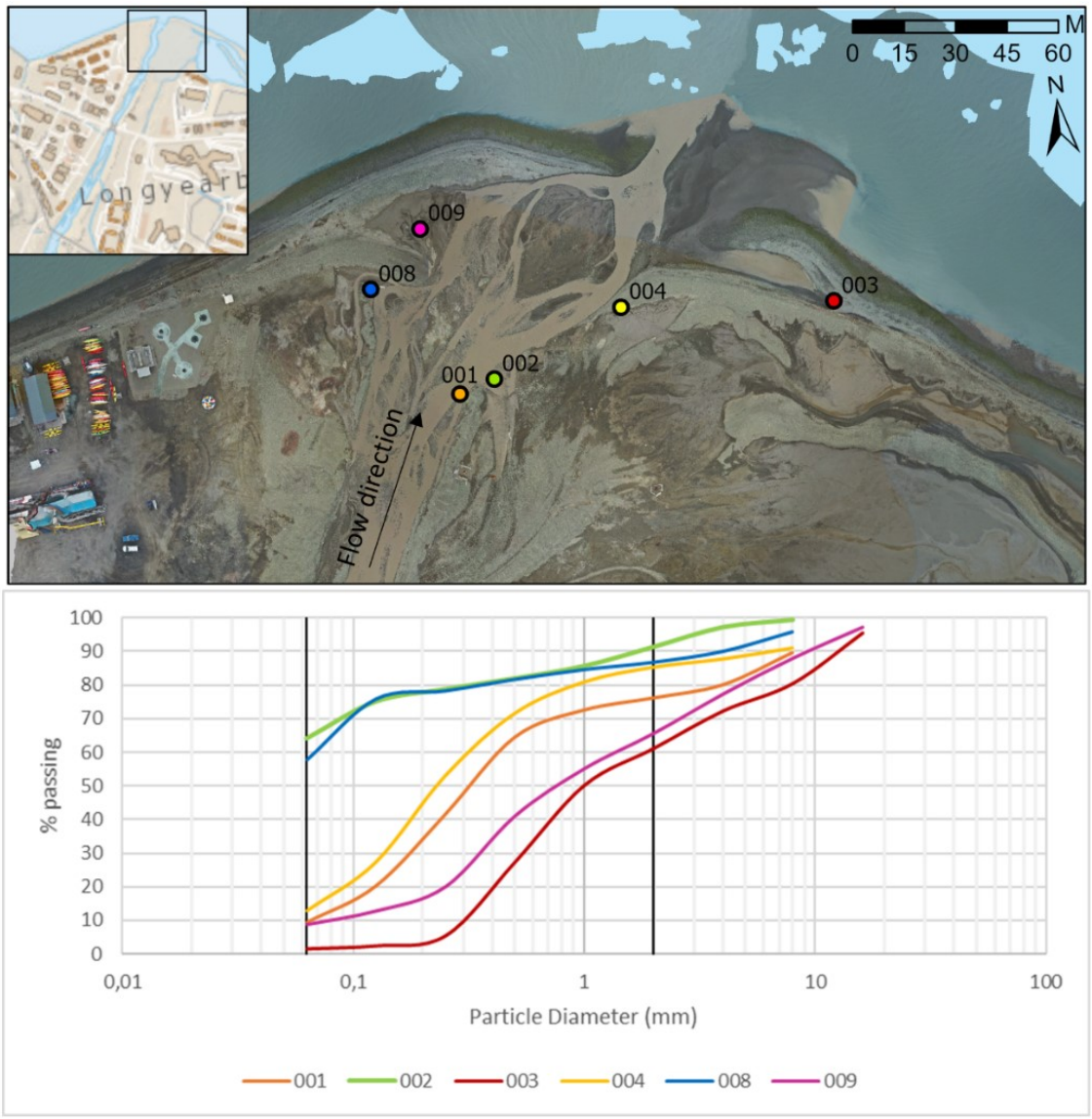

Figure 41 Orthophoto[7] of the Longyear delta with sample locations and the corresponding grain size distribution curves.

The coastline consists of both anthropogenically disturbed sediment and anthropogenic fill mass in the west of section 1. Figure 42A shows an approximately 3 m high steep edge of anthropogenic fill mass consisting of blocks of concrete, pink gneissic pebbles of mainland origin, and a mix of building materials. The pink pebbles (Figure 42B) were observed within the fill mass and along the coastline. The frequency of the pink pebbles was highest by the anthropogenic fill mass (section 1), and could be located along the coastline past Søppelfyllinga (section 2 and 3) with a decreasing frequency farther away from the fill mass.

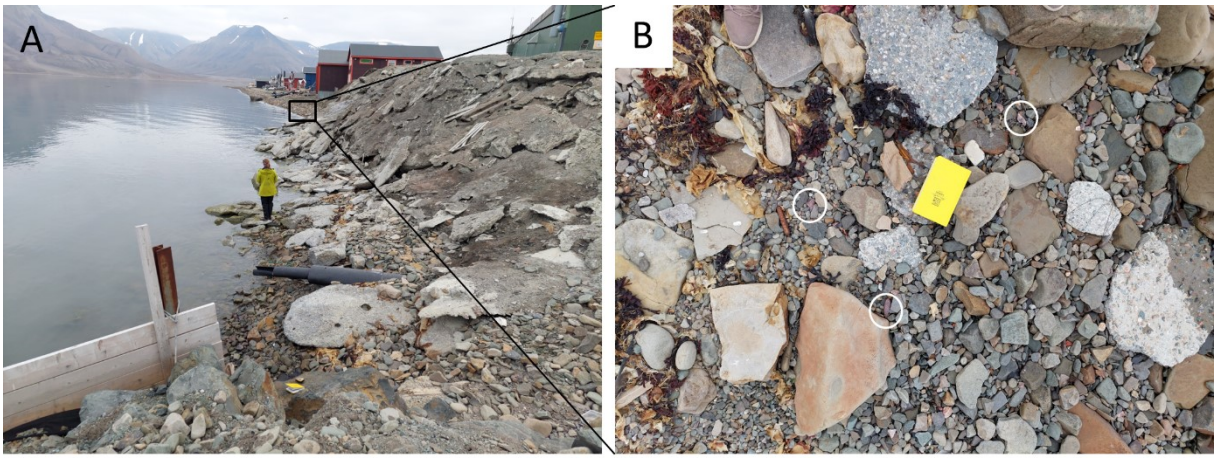

Figure 42 Photos of the coastline west of the Longyear delta in August 2021. A) Coastal erosion of a steep anthropogenic fill mass (person for scale). Photo towards east. B) Coarse, angular sediments in the tidal zone. Precise location shown in A. Grain sizes vary from coarse sand to boulders. Material is a mix of mainland and anthropogenic rocks (concrete), with pink gneissic pebbles of mainland origin. Pink pebbles are indicated in white circles.

In the beach ridges east of the Longyear delta, in section 3 (Figure 43A), the pink pebbles were no longer observed. The beach ridges consisted of coarse sediment (Figure 43B) with reverse grading. The outermost beach ridge in section 3 consisted of heavily weathered, coarse material. The material was mostly dominated by rocks natural to the catchment. Erosion marks from wave action could be observed.

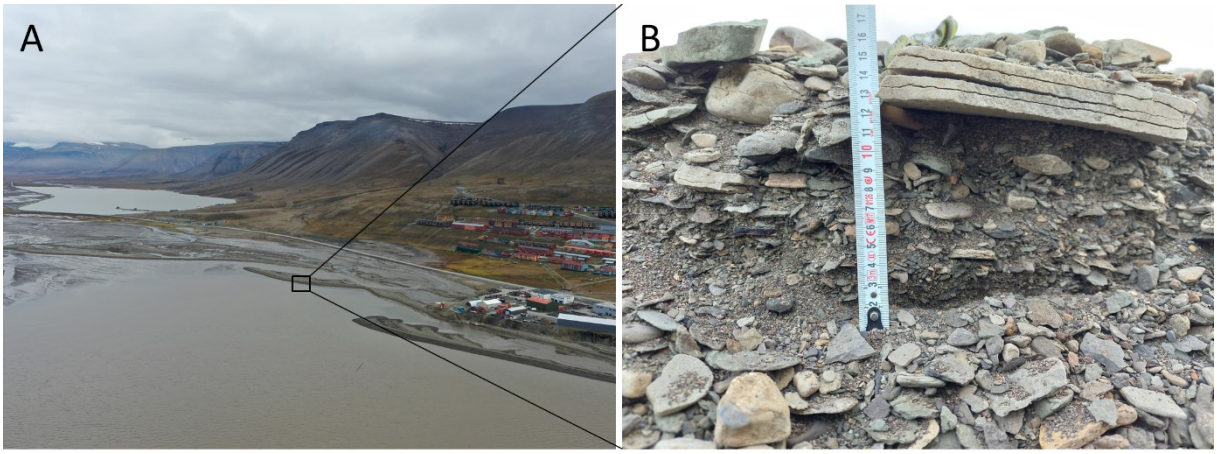

Figure 43 The coastline in front of Gruvedalen. A) Drone image showing several beach ridges and spits. B) Reverse-graded erosional scarps with weathered material, in the beach ridge furthest away from the Longyear delta. Precise location shown in A.

4.4.2 Development over time

The collection of orthophotos and aerial imagery has been essential in documenting the long-term development of the Longyear delta. Figure 43 shows a selection of the most important orthophotos and aerial imagery of the study area. The orthophoto from 2020 was not focused on documenting the delta area, and due to its limited extent, it was not used for calculations in this project. The orthophotos from 1990 to 2021 (A-F) have very high resolution, which is important when studying the development of landforms. The resolution of the 1936 aerial imagery and the infrared orthophoto from 1990 is lower compared to the other orthophotos, making detailed mapping of landforms more difficult.

The oldest aerial imagery available was from 1936 (Figure 44H). This is considered a baseline of what the natural system in Longyeardalen looked like before human interference. However, documentation of human activity in the river before this period exists (Figure 3: a truck driving on the riverbed in 1920). In the 1936 aerial imagery, a few small houses and a soccer field can be seen. Between 1936 and 1990 (Figure 44FG) measures to reduce the lateral extent of Longyearelva were present. More developed infrastructure can be observed close to the coastline on both sides of the river. Early in the melting season of 1990 (Figure 44F) the Longyear delta still had the potential to develop freely. Later in the melting season of 1990 (Figure 44G) measures were also implemented to restrict the lateral extent of the river with mitigation walls all the way into the sea. Between 1990 (Figure 44G) and 2009 (Figure 44E) large amounts of sediment from beach ridges and spits were dug out in section 3 (Figure 39). This information is known locally, but detailed documentation of this is difficult to acquire. From the limited extent of the 2019 orthophotos, it is still possible to observe beach ridges forming on both sides of the river outlet, similar to observations from 2021. Between 2009 and 2021 beach ridges have increased in size, and new ones have formed in sections 2 and 3. From 1990 until today (Figure 44A-E) more buildings and roads have been built along the river and seaside. Changes in the landforms related to the delta can be observed from 2009 to 2021, but they are not as significant as the ones seen from 1936 to 1990.

The aerial imagery from 1936 shows what Longyearelva looked like when it was running freely in the Longyeardalen catchment. Since 1990 the river has clearly been restricted by mitigation walls. By comparing the orthophotos from 1990 to 2021, the location of the active channel has barely changed. In Figure 44A Longyearelva has barely broken through the winter beach ridges at the beginning of the melting season. Figure 44B illustrates how the river mouth widened in the delta by the end of the season.

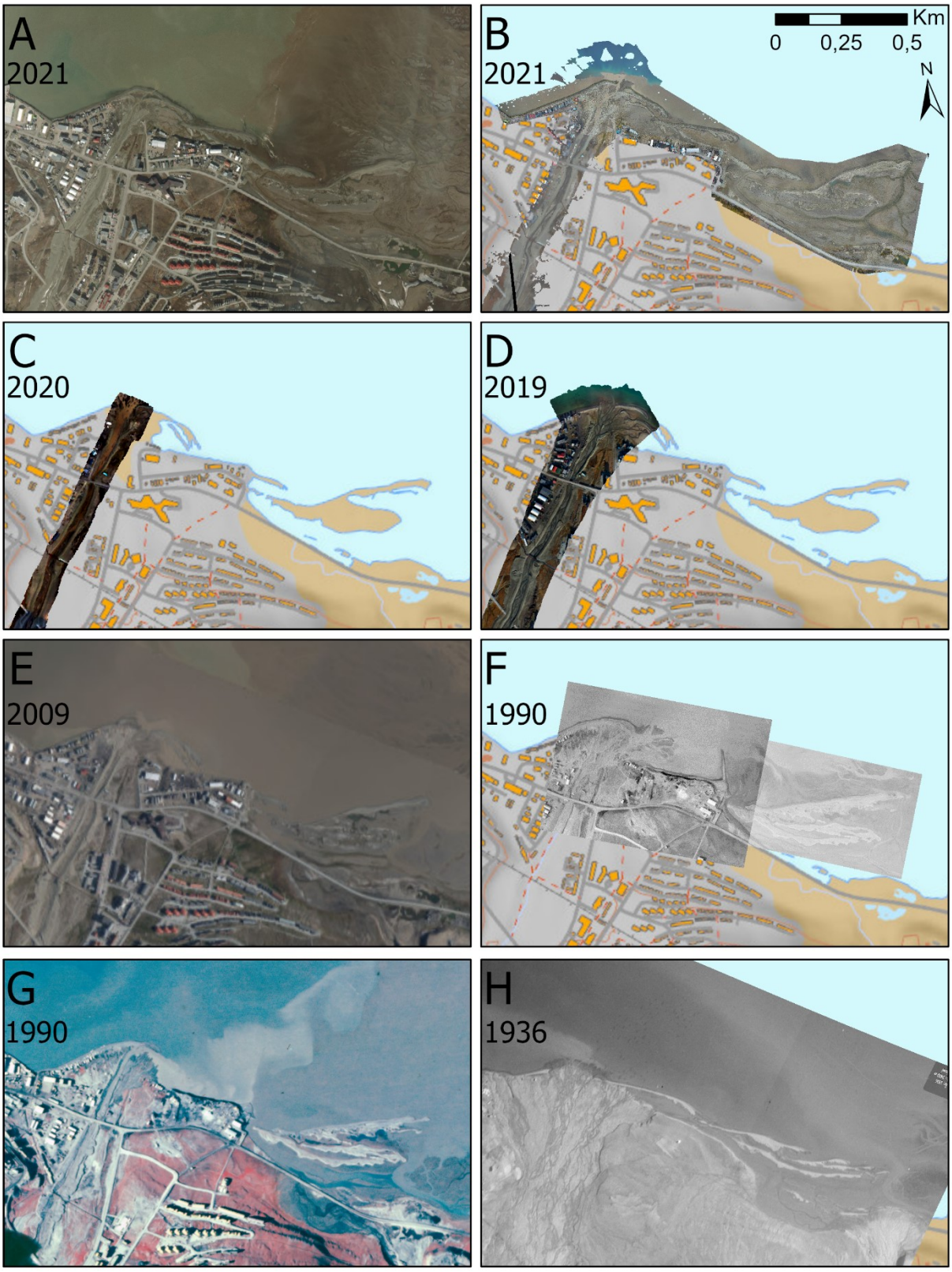

Figure 44 An overview of available orthophotos over the Longyear delta. The basemap used was based on data from 2009. A) Orthophoto$_6$ from the 18th of June 2021. B) Orthophoto$_7$ from the 19th of August 2021. C) Orthophoto$_5$ from 2020. D) Orthophoto$_4$ from September 2019. E) Orthophoto$_3$ from 2009. F) Orthophoto$_1$ from 1990. Likely taken early in the melting season. G) Clip of orthophoto$_2$ from 1990. Likely taken late in the melting season. H) Aerial imagery$_9$ from 1936, taken at an angle and orthorectified.

In addition to the orthophotos presented in Figure 44, angled aerial imagery of the delta can be an important tool for studying the system. Drone imageries from 2020 and 2021 were taken to recreate aerial imagery from 1936 (Figure 45). Note that all the images are taken at different tides. The 2021 aerial imagery was taken at low tide, and the 2020 aerial imagery was taken at high tide. It is unknown when the aerial imagery from 1936 was taken.

In 1936 a more natural state of Longyearelva and the Longyear delta can be observed. The braided river filled the Longyeardalen valley floor. Early settlement can be found west of the delta, and the old cableway ramp can be seen crossing the riverbed. The Longyear delta had a symmetrical fan shape. Sediment transported with the river during the melting season seems to have broken through marine beach ridges created by winter storms. This has similarities to the breakthrough seen in 2021 (Figure 44AB). From the recent imageries from 2020 and 2021 it is possible to determine that the beach ridges and spits close to the river outlet are constantly being reworked throughout the seasons. The beach ridges further away from the outlet to the east were more stable.

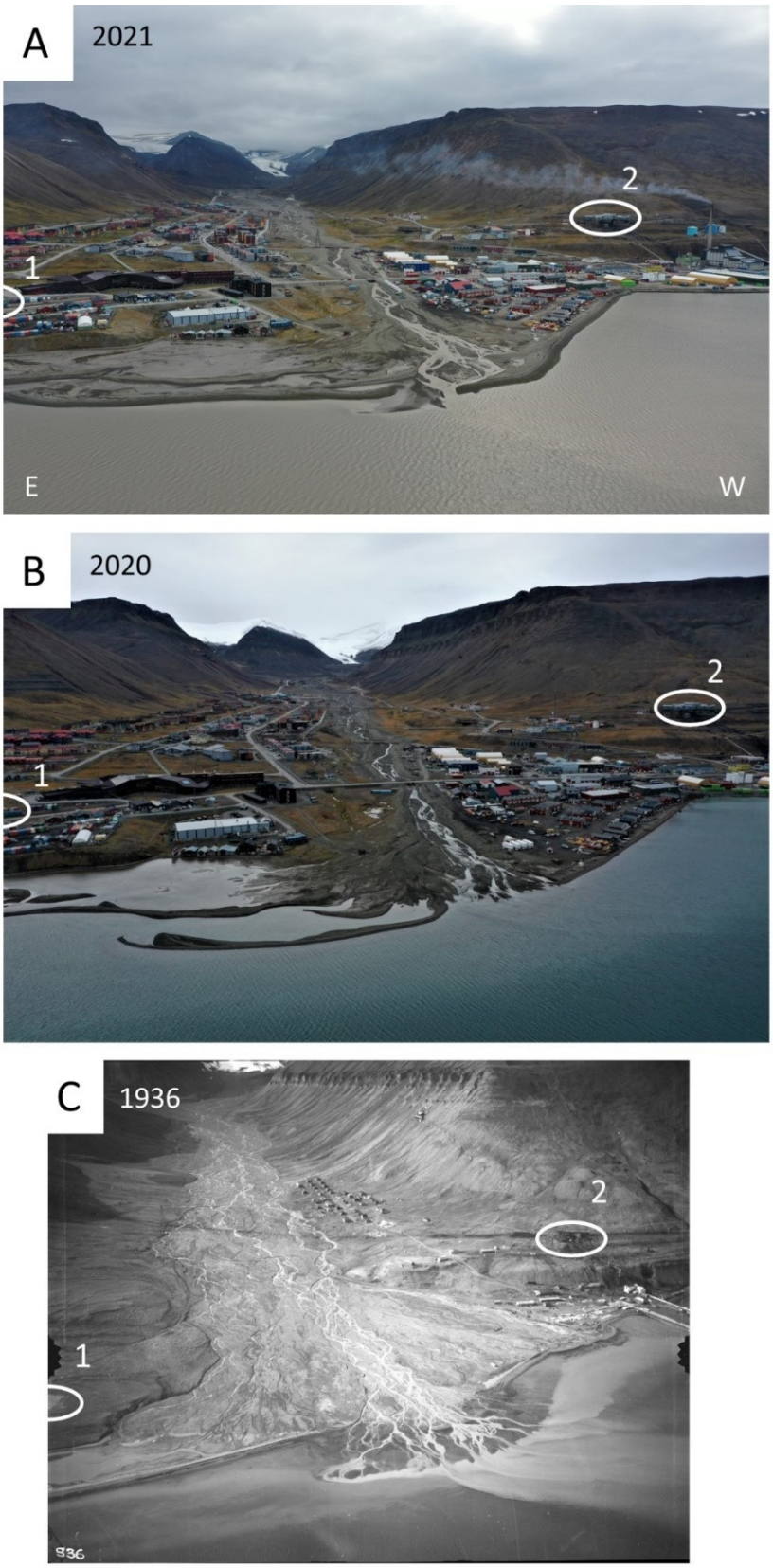

Figure 45 Aerial imagery of the Longyear delta from 1936 to 2021. Note that there is a varying photo height between AB and C due to drone restrictions. The white circles represent (1) the location of an old soccer field, which cannot be observed at present, and (2) the location of an old cableway station. A) Drone imagery taken at low tide in 2021. B) Drone imagery$_{12}$ at high tide in 2020. C) Aerial imagery$_{11}$ at an unknown tide from 1936.

4.4.3 Quantification of delta change

To study delta development over time, both the genetic understanding of the system and quantification of change is important. The latter was investigated using the DSAS, which assists in objectively quantifying shoreline change over time. The placement of shorelines from aerial imagery was studied. Shorelines were drawn from the following years: 2021 (late melting season), 2019, 2009, 1990 (early melting season), and 1936. The reason for choosing the late melting season in 2021 and the early melting season in 1990 was due to the resolution of the available imagery (Figure 44BF). Digital Shoreline Analysis System (DSAS) was used to compute the Net Shoreline Movement (NSM). The results are displayed in an automatically generated classification, showing in meters the net movement of the shoreline. Negative values indicate erosion, and positive values indicate progradation.

The analysis was executed four times with different inputs of shorelines and spatial extent (Table 13). The first three analyses had a spatial extent restricted to section 2 (Figure 38) due to the limited spatial extent of the 2019 orthophoto4. For the fourth analysis, the orthophotos with restricted spatial extent were excluded. It was important to include section 1 in one of the analyses as erosion marks were mapped in the field.

Table 13 Shoreline input and spatial extent used for Digital Shoreline Analysis System (DSAS). Sections as seen in Figure 38.

Nr	*Input- Shorelines*	*Spatial extent*
1	2009, 2019, 2021	Section 2
2	1990, 2009, 2019, 2021	Section 2
3	1936, 1990, 2009, 2019, 2021	Section 2
4	1936, 2009, 2021	Section 1 & 2

As DSAS requires a continuous shoreline for the analysis, a decision to draw the shoreline as a straight line where the river mouth meets the sea was made. Figure 46 and Figure 47 show the shoreline and orthophoto for the years in question. It is important to consider that NSM does not show inter-annual and annual movement or trends, so results are restricted to the input.

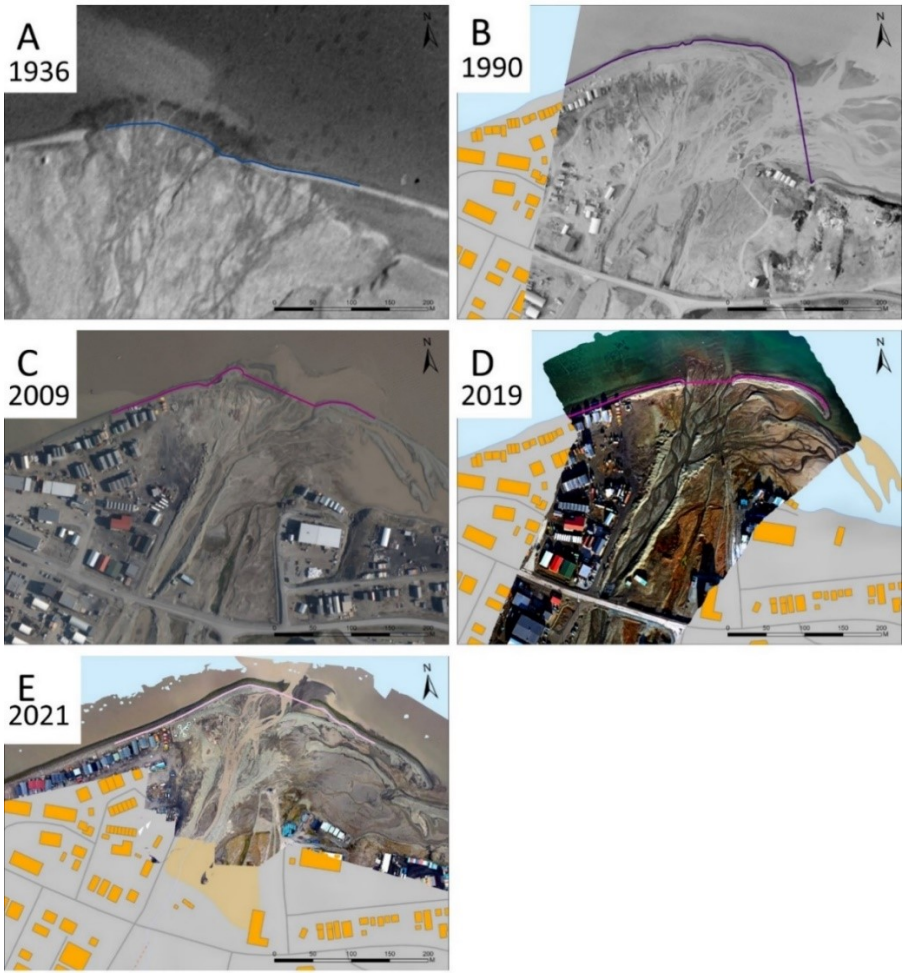

Figure 46 Shorelines drawn on aerial imagery and orthophotos as input for DSAS analysis nr. 1-3, from year A) 1936[9], B)1990[1], C)2009[3], D)2019[4], and E) 2021[7].

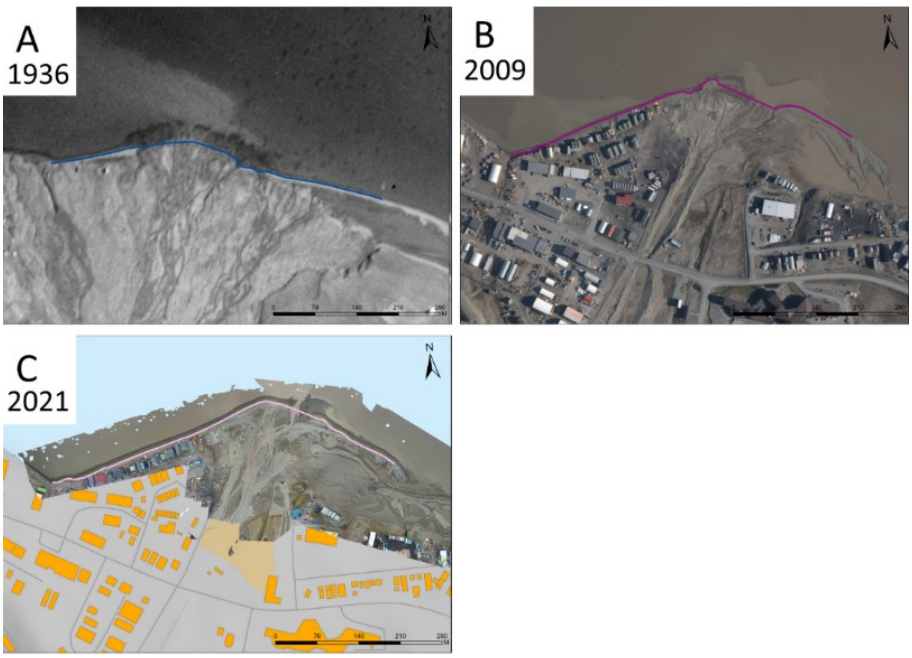

Figure 47 Shorelines drawn on aerial imagery and orthophotos as input for DSAS analysis nr. 4, from the year A)1936[9], B)2009[3], and C)2021[7]

1) Analysis of 2009, 2019 and 2021

The first analysis (Figure 48) includes the shorelines from the years 2009, 2019, and 2021. The analysis shows the Net Shoreline Movement (NSM) in recent years from 2009 to 2021. Negative NSM values are found to the west of the river mouth. Up to 7 m of erosion has occurred from 2009 to 2021. The orthophoto from 2009 with the 2021 shoreline shows how the erosion has already managed to affect constructions in the area. The local kayak club had to relocate stacks of kayaks further inland. In the river mouth, the Longyear delta has prograded up to 32 m. In the east the 2009 shoreline and the 2021 shoreline meet, which makes the NSM approximately 0 m for this area. The 2019 shoreline is not included in the calculation but indicates that the shoreline fluctuates between the years. The shorelines for all three years are straight in the west and largely fluctuate between progradation and erosion in the east.

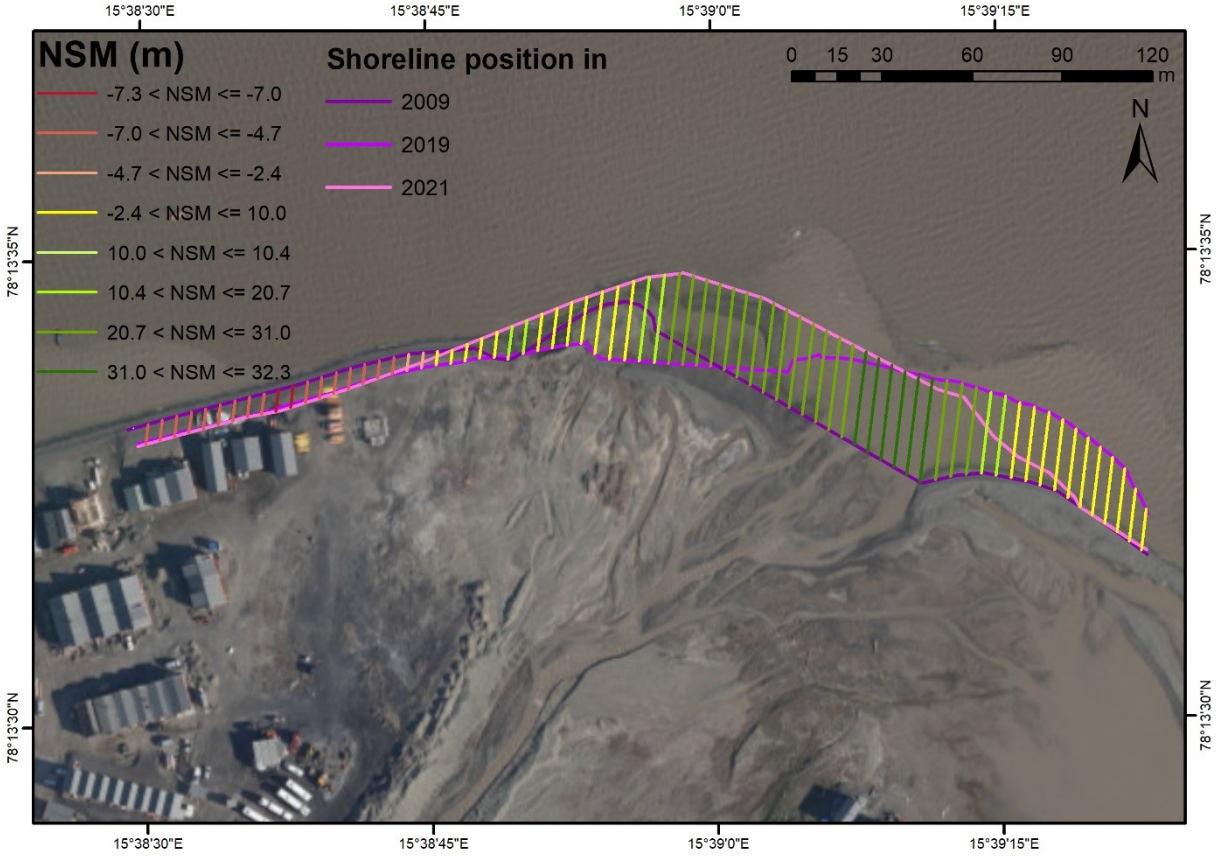

Figure 48 Net Shoreline Movement (NSM) of the Longyear delta from 2009 to 2021. Generated using Digital Shoreline Analysis System (DSAS) with shorelines drawn from orthophotos and aerial imagery. The shorelines from the years 2009, 2019, and 2021 are included. The background is the 2009 orthophoto[3].

2) Analysis of 1990, 2009, 2019 and 2021

The second analysis (Figure 49) includes the shorelines from the years 1990, 2009, 2019, and 2021. Over this approximately 30-year period, negative Net Shoreline Movement (NSM) values can be seen in the west and positive values in the east. From 1990 to 2021 erosion up to 21 m occurred west of the river mouth. In the river mouth all the shorelines were fluctuating and crossing each other. Resulting in both progradation and erosion in the area around the river mouth. In the east, positive values up to 116 m can be found as a result of progradation. The sudden change of the 1990 shoreline is considered in large part to be caused by the location of the river mouth (Figure 46B).

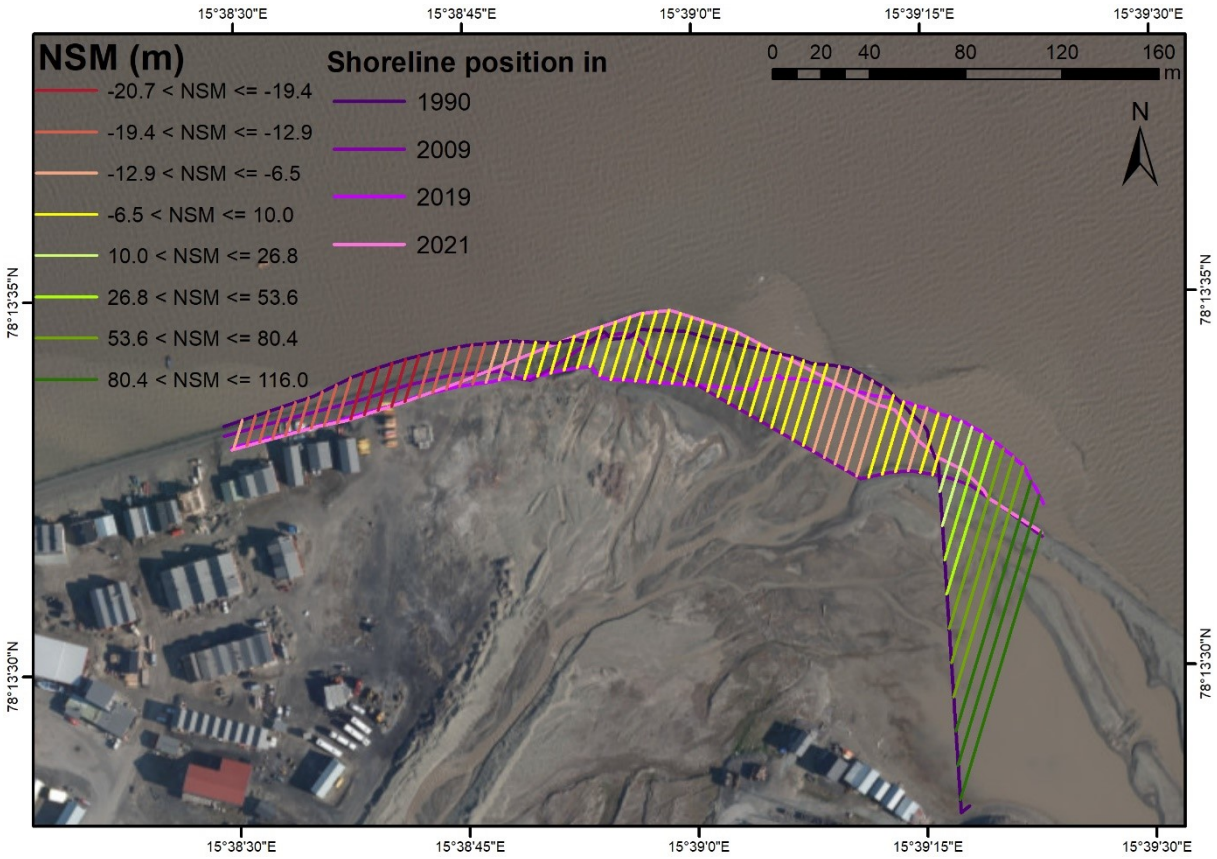

Figure 49 Net Shoreline Movement (NSM) of the Longyear delta from 1990 to 2021. Generated using Digital Shoreline Analysis System (DSAS) with shorelines drawn from orthophotos and aerial imagery. The shorelines from the years 1990, 2009, 2019, and 2021 are included. The background is the 2009 orthophoto[3].

3) *Analysis of 1936, 1990, 2009, 2019 and 2021*

The third analysis (Figure 50) includes the shorelines from all the available years; 1936, 1990, 2009, 2019, and 2021. For this 85-year period, only positive Net Shoreline Movement (NSM) values can be observed. The lowest values can be found in the west, where the progradation from 1936 to 2021 was 10 m. The highest values were in the river mouth, up to 165 m. In the east, the high NSM values continue to vary between 107 m and 160 m.

The 1936 shoreline was much straighter compared to the shorelines from the last ~30 years. Between 1936 and 1990 large amounts of sediment were deposited in the delta. Because few images between 1936 and 2009 exist, it is not possible to state the amount of progradation observed as a result of natural development or anthropogenic activity. From 1990 to 2021 the shorelines have shifted multiple times.

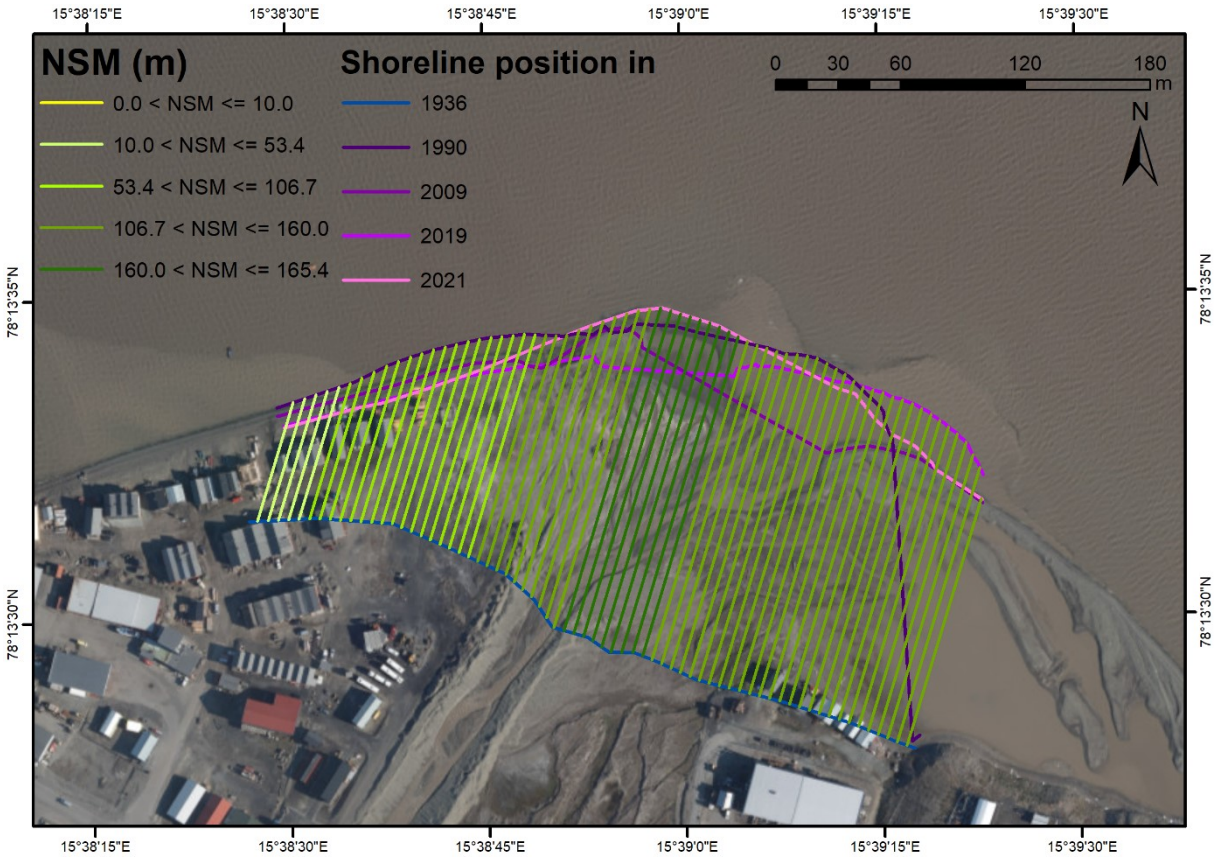

Figure 50 Net Shoreline Movement (NSM) of the Longyear delta from 1936 to 2021. Generated using Digital Shoreline Analysis System (DSAS) with shorelines drawn from orthophotos and aerial imagery. The shorelines from the years 1936, 1990, 2009, 2019, and 2021 are included. The background is the 2009 orthophoto[3].

4) Analysis of 1936, 2009 and 2021

The fourth analysis (Figure 51) includes the shorelines from the years 1936, 2009, and 2021. This analysis has a larger spatial extent compared to the previous analyses as it is not limited by the 1990 and 2019 shorelines.

From 1936 to 2021, only positive Net Shoreline Movement (NSM) values can be observed. The progradation of the shoreline in section 1 was much smaller compared to the delta area. The smallest progradation was between 0 m and 10 m in the westernmost part of the coastline, with increasing amounts towards the delta. The progradation was most substantial around the river mouth (as seen in the third analysis), with continued high values towards the east. In the east the NSM values ranged between 106 m and 159 m. The 2009 and 2021 shorelines have very similar positioning in the west and the east compared to the 1936 shoreline.

Figure 51 Net Shoreline Movement (NSM) of the Longyear delta from 1936 to 2021. Generated using Digital Shoreline Analysis System (DSAS) with shorelines drawn from orthophotos and aerial imagery. The shorelines from the years 1936, 2009, and 2021 are included. The background is the 2009 orthophoto3.

4.5 Similar river-to-ocean systems

Arctic glacial systems are complex and thus may be difficult to understand. The human impact on the Longyeardalen catchment system, in addition to the inconsistence of data, makes it even more complex to elucidate the main focus years in regard to end-members and trends. Two similar systems will be introduced to establish context related to Svalbard's setting with regards to delta development from small glacierized catchments; the spit system on the north side of Adventfjorden and a similar delta system in Sassenfjorden.

4.5.1 The Adventfjorden spit systems

On the northern side of Adventfjorden, on the opposite side of the Longyear delta, another spit system can be found. Figure 52 shows Adventfjorden in 1936 and in 2009. In the figure, the spit system related to the Longyear delta is marked as 2, and the similar spit system on the other side is marked as 1. Spit system 1 is assumed to be developed from the sediment originating from Adventdalen. The large spit in spit system 1 has been eroded at the base and accumulated in the outer part when comparing the aerial imagery from 1936 (A) to the orthophoto from 2009 (B). Both spits systems are prograding from the west towards the east.

From Chapter 4.4.3, it was shown that the shoreline has prograded up to 167 m from 1936 to 2021, indicating that spits system 2 has also been moved further out into the fjord. It is possible to observe in orthophoto (B) that the road from Longyearbyen to Isdammen has contributed to moving the spit system further out. The spits and beach ridges in 1936 are seemingly larger in extent compared to 2009 in spit system 2. This may be due to the river coming from Gruvedalen, east of Longyearbyen, which likely contributed to the input of sediments. After the road past Isdammen was built around 1950-1960, the input from this river was cut off. Between 1936 and 1990, sediments from the system were anthropogenically dug out, reducing the volume of the spit system.

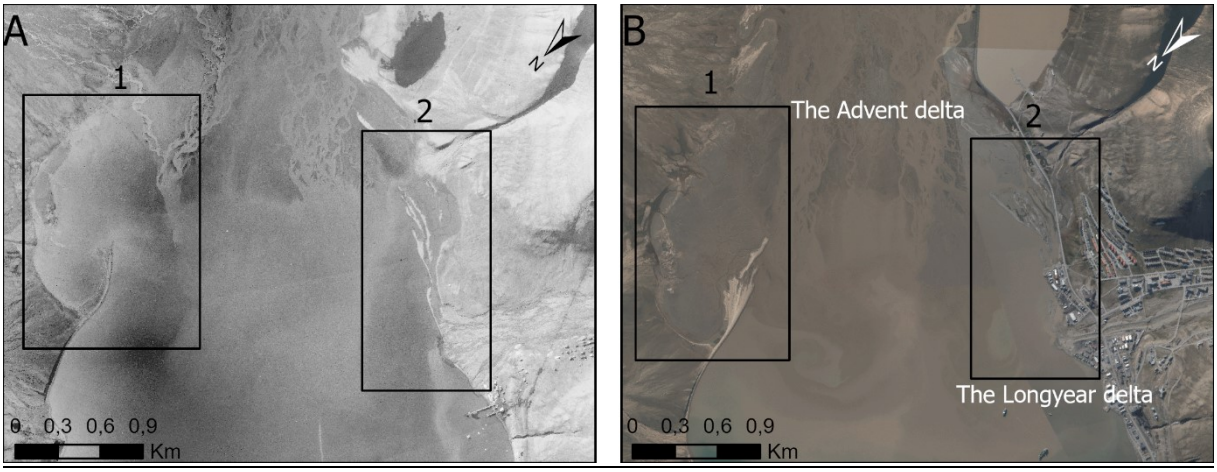

Figure 52 Aerial imagery of Adventfjorden. Marked in black boxes are two spit systems. A) Aerial imagery from 1936[10]. B) Orthophoto from 2009[3].

4.5.2 The Vindodden delta system

The Vindodden catchment system is similar to the Longyeardalen catchment system. The Vindodden catchment is approximately 21 km^2, which is 2 km^2 smaller than the Longyeardalen catchment. The Vindodden catchment has a river system fed by meltwater from one glacier. The glacier covers approximately 3 km^2 of the catchment, which is 2 km^2 less than the glacier cover in the Longyeardalen catchment. The biggest differences between the two delta systems are the geology in the catchments (see Chapter 2.1.3) and their exposure to wave action. The Longyear delta lies relatively protected in a small fjord, while the Vindodden delta is more exposed in a large fjord (Figure 53A).

The river mouth in the Vindodden delta is continuously shifting from east to west and back, causing an outwards, symmetrical progradation of the delta. Figure 53 is a comparison between the Longyear delta and the Vindodden delta. The dimensions of the Vindodden delta in 2009 were approximately 1590 m wide and stretching 790 m into the sea, while the Longyear delta was 300 m wide and stretching 160 m into the sea. The Vindodden delta was approximately five times bigger than the Longyear delta, although they have similar catchment conditions. In Figure 53DE the Longyear delta shoreline was placed on top of the Vindodden delta to illustrate how much bigger the Vindodden delta was compared to the Longyear delta.

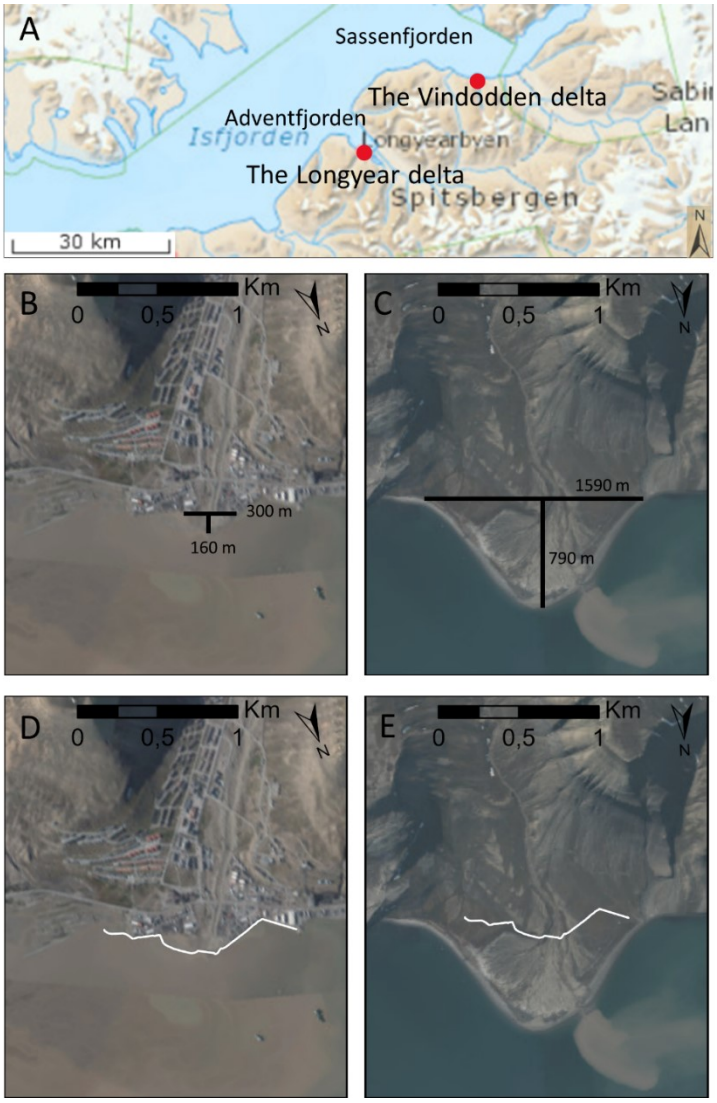

Figure 53 Orthophotos[3] of the Longyear delta and the Vindodden delta in 2009. A) Overview (Norwegian Polar Institute, n.d.-a). B) The dimensions of the Longyear delta. C) The dimensions of the Vindodden delta. D) The Longyear delta with the 2009 shoreline. E) The Vindodden delta with the Longyear delta shoreline from 2009.

5 Discussion

Svalbard coasts and coastal dynamics are little documented, and the understanding of how the glacifluvial catchment system effect the river-to-ocean interactions is limited (Nowak et al., 2020; Søreide et al., 2020). Human presence and thus anthropogenic interference often coincide with river-to-ocean systems. To approach these facts, the results from Chapter 4 will be used to discuss important factors for delta development, along with present and future problems.

The main parameters in the Longyeardalen source-to-sink system are summarized in Figure 54. Sediments come from glaciers, moraines, and a range of sources, as well as being added through river erosion during transport. This leads to a range of factors controlling the transportation and input of sediment to the sink over the melting season. This is further complicated by ocean processes that redistribute sediment along the coast. In the following chapters, the presented results of this study will be reviewed and discussed in the context of river transport and delta development. The discussion will follow the source-to-sink division, beginning with a short discussion about the sediment sources before river transport and the deposition in the sink. Uncertainties in the present results and potential future studies are mentioned, and lastly, the conclusion.

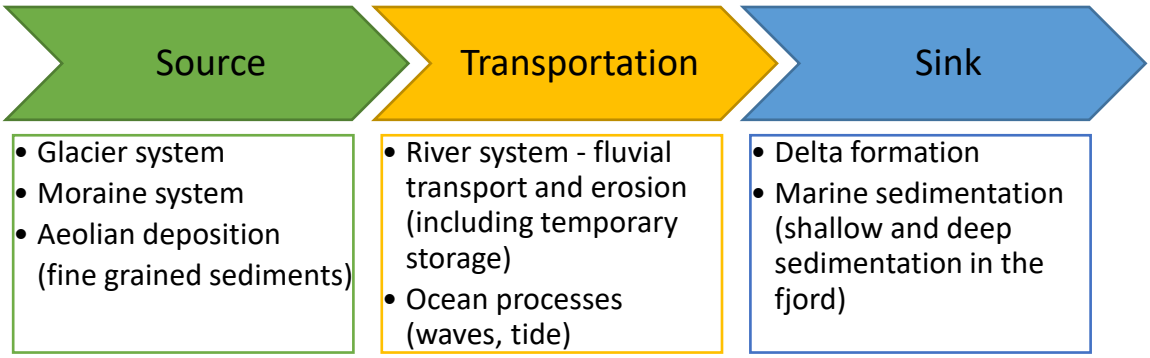

Figure 54 Flow chart of the Longyeardalen source-to-sink system with the most important mechanism for each part of the Longyeardalen catchment system.

5.1 The catchment and its sediment sources

The present study primarily focused on the transport and sink parts in the Longyeardalen catchment system. However, since hydrological transport of water and sediment also depend on the availability and sediment sources, the general setting will be discussed. For further details it is referred to the twin-study by Pallesen (2022).

Figure 55 Flow chart of the Longyeardalen source-to-sink system. This chapter is centered around the source. The main focus of this study is transport in Longyearelva and sink in the Longyear delta.

It was decided to modify the catchment size based on the flow direction generated from a digital elevation model (DEM) to include a larger area close to the sea (Figure 27). Different techniques and datasets have been applied in previous studies, where the focus has been to capture the source part of the catchment. In this study, the catchment size was found to be approximately 23 km^2, while previous studies calculated it to be 22 km^2 (Løvaas, 2021; Stenius, 2016). Permafrost may affect groundwater to flow in a different direction than the surface dip suggests. This usually only occurs in the active layer. Groundwater flow is typically not accounted for in the Arctic (Killingtveit A et al., 2004). Therefore, without much information, it is assumed that this approximation of the catchment size is reliable.

In the Longyeardalen catchment there are multiple sources of sediment input (Figure 56) to the sediment budget. The primary sources of sediment from the glacially controlled system are glacial processes, moraines, and aeolian deposition. Secondary sources are sediment from slope processes, river erosion, and weathering (Pallesen, 2022). Due to the location and shape of Longyeardalen, three out of four wind directions blow sediment into the valley. Only wind coming from the south can function as an output mechanism (Figure 56). The main output of sediment in the system is the glacifluvial river Longyearelva, which erodes and transports sediments into the delta. The sediment is eventually transported to the depositional environment in the sink, where it can be reworked or deposited.

Heavy rainfall and snowmelt contribute to debris flows and slope processes that can affect the suspended sediments in the river. In Longyeardalen many active and inactive slope processes were observed. The contribution of secondary sources to the sediment budget is likely to be occasionally significant, although less important than the sediment delivery from the glaciers and moraines. Events may cause sudden input in sediment transport. An increase in temperature and rainfall may promote frequent or higher amplitude slope events, thus increasing the probability of irregular high sediment input to the sink (Hanssen-Bauer et al., 2019; Pallesen, 2022). Events of short duration related to slides, the collapse of riverbanks and sills, or similar processes, may in some cases fail to be recorded with the sampling frequency chosen for suspended sediment concentration in this study.

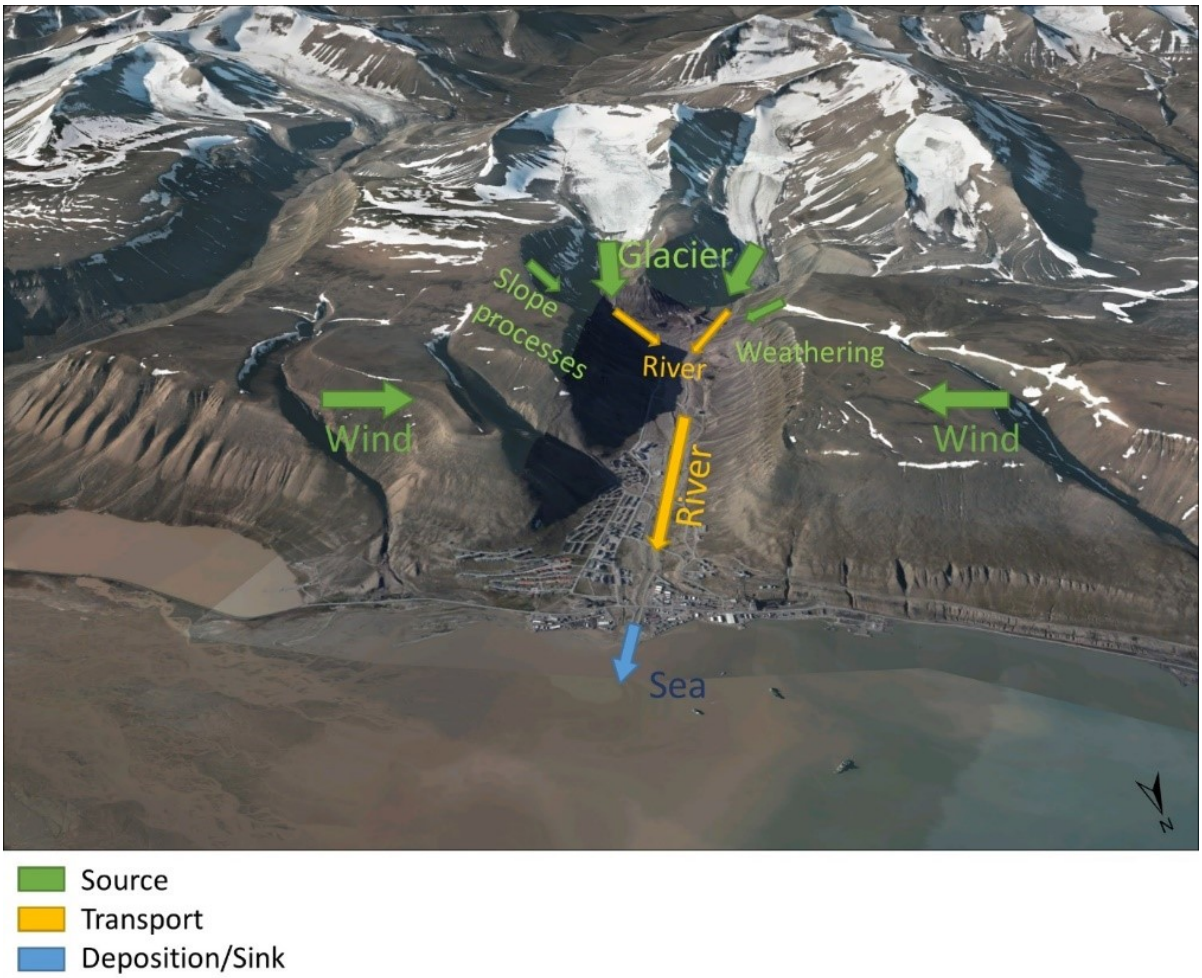

Figure 56 Illustration of sediment budget in the Longyearbyen catchment. The background is a 3D-model of Longyeardalen based on the 2009/2011 orthophoto[3].

From April to August, it is 24h daylight on Svalbard. Although this could imply equal warming and consistent melting around the clock, the sun warms the most around midday-early afternoon, when it is placed in the south shining at the N, NW, NE facing slopes. The generated flow direction over the Longyeardalen catchment shows that 56% of the slopes in the catchment face these cardinal directions (Table 10). These directions are therefore more exposed to chemical weathering. More active weathering is expected in areas where temperature reaches above 0°C. Since Longyeardalen consists of homogenous geology with mechanically soft bedrock (Etzelmüller et al., 2000; Norwegian Polar Institute, n.d.-b), this is expected to largely contribute as sediment sources for river transport.

5.2 River transport

The transport mechanisms in the system are mainly river transport and ocean processes (e.g., waves and tide). Trends in sediment transport in arctic glacierized catchments generally vary both seasonally and inter-seasonally (Bogen & Bønsnes, 2003; Favaro & Lamoureux, 2015; Serreze & Barry, 2014). Finding trends in the Longyeardalen transport system will help the understanding of the river-to-ocean interactions in the Longyear delta. No extreme weather (e.g., heat waves or precipitation) occurred during the 2021 melting season, making it possible to apply the collected datasets as baseline data for the catchment system.

Figure 57 Flow chart of the Longyeardalen source-to-sink system. This chapter is centered around transport. The main focus is transport in Longyearelva and sink in the Longyear delta.

5.2.1 Discharge

Factors like temperature, precipitation, groundwater, glacier- and snow melt are known to influence a hydrological system (Nowak et al., 2020; Nowak & Hodson, 2013), and thereby discharge and sediment transport. The discharge in Longyearelva varied daily and seasonally during the 2021 melting season. This is thought mainly to be related to variations in temperature, glacier- and snowmelt.

The temperature at Svalbard Lufthavn for the summer months in 2021 was slightly lower than the average seasonal temperature. Meanwhile, the precipitation was slightly higher (Table 11). In Longyearelva, an increase in discharge was observed in June and a decrease towards the end of the melting season in August, as is typical for arctic rivers. Temperature increase causes increase in snow- and glacier melt (Bogen & Bønsnes, 2003; Scott, 1978). The daily average discharge in relation to daily total precipitation and daily average air temperatures from 2021 are displayed in Figure 58. The hydrograph correlates with the air temperature. The rising temperatures in June cause increased snow and ice melt resulting in higher discharge. The correlation between discharge and air temperature is stronger as peaks in discharge often occur on the same days as peaks in temperature.

Precipitation is a known factor in influencing the discharge (Nowak et al., 2020). However, the observed correlation between the hydrograph and the precipitation was low (Figure 58). Precipitation did not seem to have any immediate effect on the discharge, with the exception of the peak in discharge on the 10th of August. The two consecutive days (18th and 19th of July) with the highest amount of precipitation had seemingly no effect on the discharge. The discharge was declining during the precipitation event along with the temperature, suggesting that temperature is the most important control in the system. This indicates a mostly glacially controlled runoff as ablation is directly influenced by temperature.

Note that the highest peak of 2,5 m^3/s on the 8th of July in the average hydrograph was measured on a day with little precipitation and low temperature. Around the 25th of July, a

significant drop in discharge can be observed over five days. Meanwhile, the temperature was stable at around 6,5°C, and precipitation was low. This indicates that the discharge can be controlled by factors other than temperature and precipitation, as discussed here. This might be a result of time delay due to the infiltration in the ground.

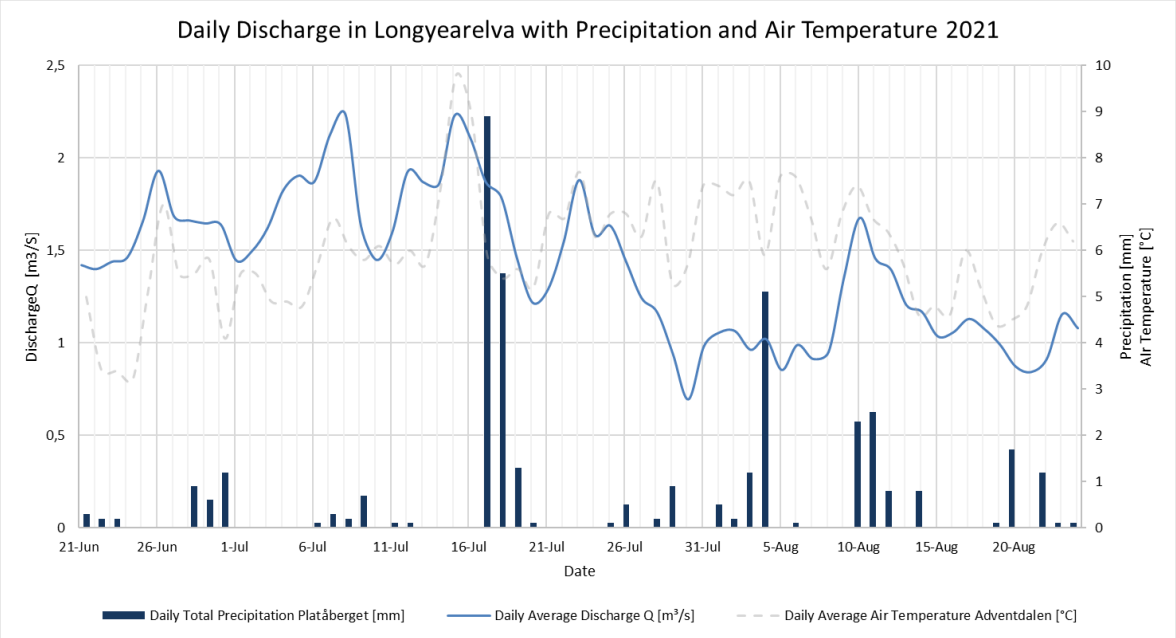

Figure 58 Graph showing the metrological conditions and discharge in Longyearelva from 21/06/21 to 25/08/21. The daily total precipitation data were measured at Platåberget and the daily average air temperature in Adventdalen (The Norwegian Meteorological Institute, n.d.).The daily average discharge was calculated from measurements in Longyearelva.

The discharge varied seasonally and daily. To better understand these variations, three modes were interpreted based on the hourly hydrograph from 2021 (Figure 59) in a twin-study collaboration with Pallesen (Pallesen, 2022). The interpreted modes from the 2021 hydrograph are used for the following graphs in an attempt to find seasonal and inter-seasonal patterns that might be linked to the general development of the source-to-sink system during the melting season. Mode 1 shows a trend of low discharge values and low diurnal variations at the beginning of the melting season (22/06 – 04/07). Within this mode, the diurnal variation was normally between 1,2 and 1,6 m^3/s, excluding the peak. Mode 2 was characterized by high diurnal variations with shorter reoccurring periods of high discharge in the middle of the melting season (04/07 – 31/07). From the 4th of July the diurnal variations were normally between 1,2 and 2 m^3/s, excluding peaks and drops. Towards the end of the mode, the average discharge dropped before it began to stabilize at lower average values in mode 3. Within mode 3 the discharge values stabilized at an average lower than previously measured during the melting season (31/07 – 25/08). There were overall small diurnal variations varying between 0,7 and 1,3 m^3/s, excluding one peak. The modes are expected to show indications of controlling factors in the hydrological system. The conditions within each mode are thought to reflect the seasonal snowmelt, glacial meltwater input, and thawing permafrost.

The modes were applied to the hydrograph from 2020 with the intention of detecting possible trends and differences between 2020 and 2021. From Figure 59, the three modes seem to fit with the seasonal changes in the 2020 hydrograph as well. In mode 1, the 2020 hydrograph

did not have any clear trend. In mode 2, the 2020 and the 2021 hydrograph show similar reoccurring periods of high and low diurnal variations. The 2020 hydrograph at the end of mode 2 was abnormally high because a heat wave occurred in Svalbard from the 24th of July to the 30th of July. Due to the considerable peak it created in the discharge, it was named the Late July Flooding by Løvaas (2021). After the Late July Flooding, the hydrograph for 2020 had a changed pattern, with large diurnal variation. The date of change correlates with the shift into mode 3. Although the pattern of the 2020 and the 2021 hydrograph was not identical to each other. Within the modes, the three modes do seem to fit the approximate dates where a shift in the system can be observed.

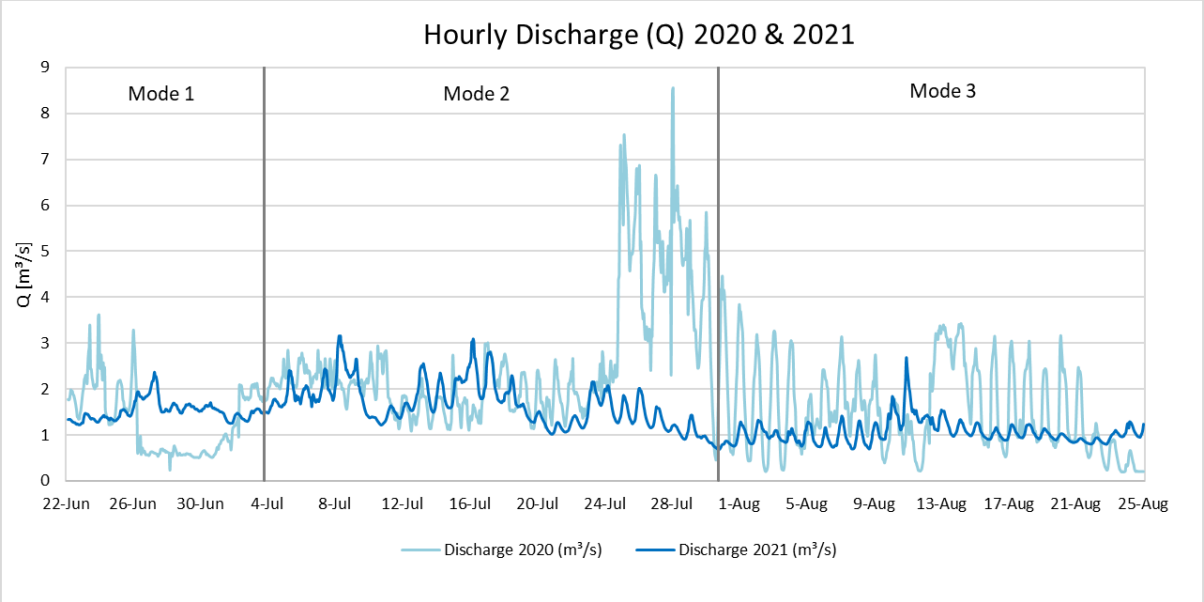

Figure 59 Hourly discharge data from 2020 and 2021 in Longyearelva. Modes based on data from hourly discharge in 2021.

The relationship between the discharge and the air temperature in Longyearelva is closely studied in Figure 60. Here, the daily average discharge data is plotted against the daily average air temperature for the 2020 and the 2021 melting seasons. Based on these observations, the temperature is the main controller of discharge for normal values. It is important to consider that other factors such as precipitation and groundwater can have a large influence on discharge during extreme events.

The differences highlight the inter-seasonal variability that is expected in Longyearelva. This also supports the idea of multiple controls on discharge, including glacier melt and precipitation. Based on the data presented, the main controller of discharge seems to be snowmelt in mode 1, glacier meltwater in mode 2, and thawing permafrost combined with glacier melt in mode 3. The list below describes what different types of the main controllers can mean for the hydrological system throughout the melting season.

- Snow insulates and delays the spring thawing of the ground and glaciers as temperatures increase at the beginning of the melting season. As the snow melts, surface runoff is initiated. As the protective layer of the snow melts, the permafrost and glaciers become exposed to the temperature increase and starts to melt as well.
- As the snow disappears, glacier meltwater dominates the runoff, which is strongly affected by the diurnal and seasonal variability of the temperature.

- Before the ground has thawed, meltwater from snow and ice will not be able to penetrate the ground and therefore lead to high surface runoff. When the ground thaws, water can infiltrate, causing less surface runoff and reduction of the potential for flooding. Although, it may cause increased erosion and sediment transport. The increase of the thickness in the active layer will eventually be able to affect the discharge and reduce the surface runoff. It will likely reduce the diurnal variability in the discharge as water penetrates the ground.
- Precipitation can affect both the diurnal and the seasonal variability of the discharge. Little to no precipitation will make the hydrological system dominated by other factors. Stable trends in precipitation (e.g., evening rain) could change the diurnal variations in the discharge, while event-based precipitation with high intensity can cause flooding.
- It is unknown how significant the impact of groundwater is on the Longyeardalen hydrological system. If the groundwater impacts the system to a significant degree, it will only be late in the melting season after active layer development from thawing permafrost.

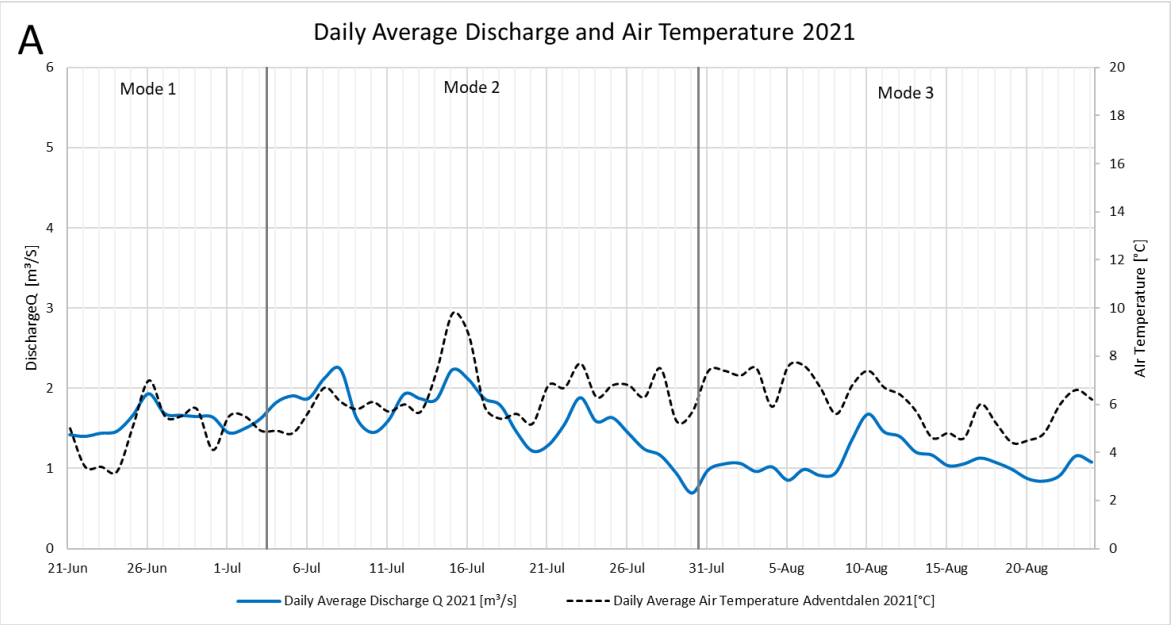

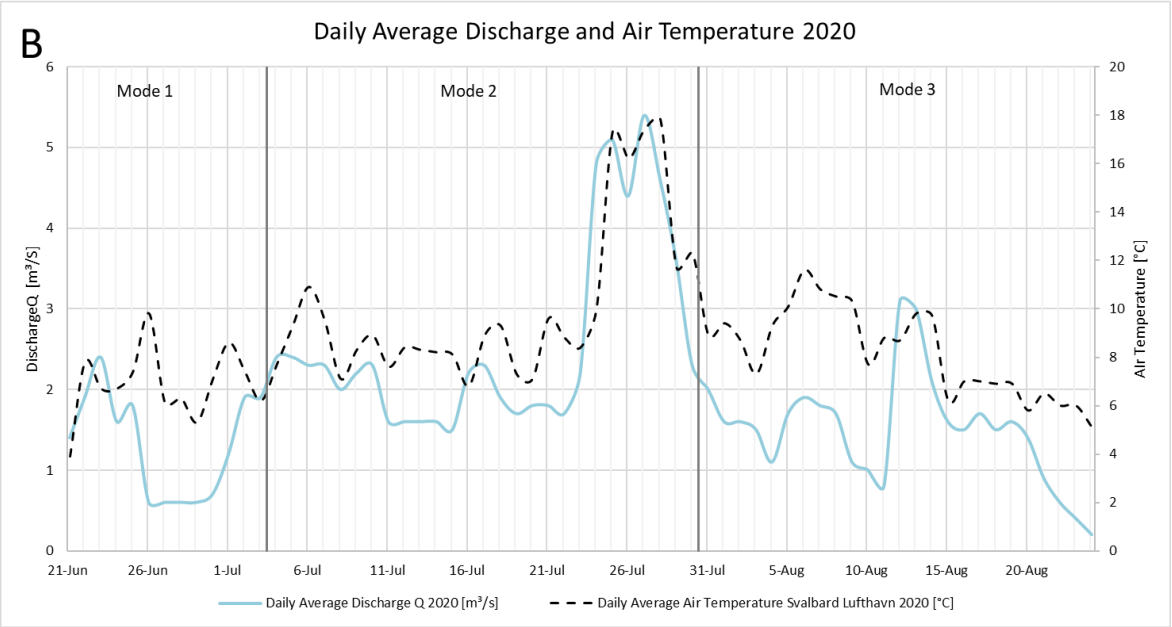

Figure 60 Daily average discharge data from Longyearelva and daily average air temperature from Adventdalen. Modes based on hourly discharge data from summer 2021. A) For summer 2021. B) For summer 2020.

To further illustrate what baseline discharge and event-based discharge mean for Longyearelva, a comparison of photos taken of Longyearelva in 2020 and 2021 are shown in Figure 61. Photo A shows a "regular" high discharge, and photo B shows a "regular" low discharge in the river in 2021. Photo C shows the river during the Late July Flooding, and photo D shows the river during the first snowfall in 2020 (Løvaas, 2021). The thalweg of the river was at the east side of the river channel in both years, during high and low discharge. During low discharge, the river covers approximately 35% of the river channel for both years (Figure 61BD). During a "regular" high discharge, it only covers approximately 50% of the channel (Figure 61A). During the Late July Flooding, the discharge takes up the entire river channel (Figure 61C). This illustrates that during extreme events, such as flooding, the runoff has the possibility to fill the entire mitigation channel and flood the riverbanks.

Figure 61 Photos taken from Veg 600 towards Polarriggen. A) High discharge in the beginning of the 2021 melting season (26/07/21). B) Low discharge in the end of the 2021 melting season (03/09/21). C) Highest discharge recorded discharge of 8,6 m^3/s during record high temperatures (28/07/20) (Løvaas, 2021). D) First snowfall with low discharge at <0,5 m^3/s (28/08/20) (Løvaas, 2021).

Climatic predictions for Svalbard indicate increased frequency and intensity of precipitation along with increased temperatures (Hanssen-Bauer et al., 2019). This will result in an even longer melting season. A possible outcome of this is that snow and glacier melt increase and last for a longer period. Precipitation can cause more frequent flooding and causes an overall higher degree of discharge in the river. On the other hand, it is known that water fluxes from catchments with smaller glaciers where ice has already retreated markedly have been decreasing for one or more decades. It has been suggested that small glacierized catchments in Svalbard, such as this one, have already reached "peak water" from the glaciers, and meltwater discharge will only decrease in the future (Nowak et al., 2020). This means that in the future, the hydrological system in Longyeardalen may become more controlled by precipitation and less glacially controlled.

5.2.2 Sediment sizes and their movement

Sediment transport in Longyearelva occurs both as suspended and bedload transport. Bedload transport is a useful measure of competence and indicates what sizes of sediment can be deposited in the delta.

Bedload transport has been measured in 2020 and 2021 using passive tracers. Only 5,8% of the tracers were registered after movement in 2021. Many tracers were not possible to relocate at the end of the melting season, and some tracers were placed on the inactive part of the

riverbed and had, therefore, no movement. However, tracers up to 300-350 mm in diameter moved 10s meters in the 2021 melting season. As previously stated, the melting season of 2021 did not have any extreme weather events and can be considered a baseline year. This suggests that during a season of no flooding or any extreme weather, the river still has the competence to move boulders (Hjulstrom, 1935). When the same method was applied in 2020 (Løvaas, 2021), the largest passive tracer placed on the riverbed was 200-250 mm. During the Late July Flooding in 2020 (Figure 61C), massive bedload transport was both heard and observed. Therefore, an assumption that the river transport even larger rocks as bedload during extreme events can be made. The competence of the river is largely dependent on discharge. If climate change were to result in higher discharge and flow velocity, it is likely that the transport of bedload would increase in both size and quantity (Brattli, 2019; Hjulstrom, 1935). The transport of bedload cause erosion as particle crash into each other, causing new particles to roll, slide, and/or saltate. Increased discharge in the river would therefore cause positive feedback of erosion and thereby sediment transport to the depositional area (sink). Should the discharge decrease, it is thought that the opposite would happen.

Suspended sediment concentration (SSC) is hydraulically controlled. Based on observation of all filtered samples, sample A (Figure 62A) represents what a normal suspended sediment sample looked like. Sample B (Figure 62B) represents what a sample looked like in a few samples. In sample A the sediments are mostly fine with a few larger grains (white circle). This indicates that in Longyearelva saltation occurs under normal conditions. Due to the loose hose during sample collection, it is not possible to state whether sample B was a result of extreme saltation or sampling close to the riverbed. It is likely that the mouthpiece (Figure 21B) was close to the riverbed when the sample was taken, which resulted in more saltation particles entering the sample, causing coarser grain sizes ≤ 1,5mm. Although it is possible that discharge was so high that sand was transported as a suspended load. As the samples cannot be compared to the specific discharge at the time, it is not at this moment possible to conclude anything about the connection between grain size, discharge, and sediment load.

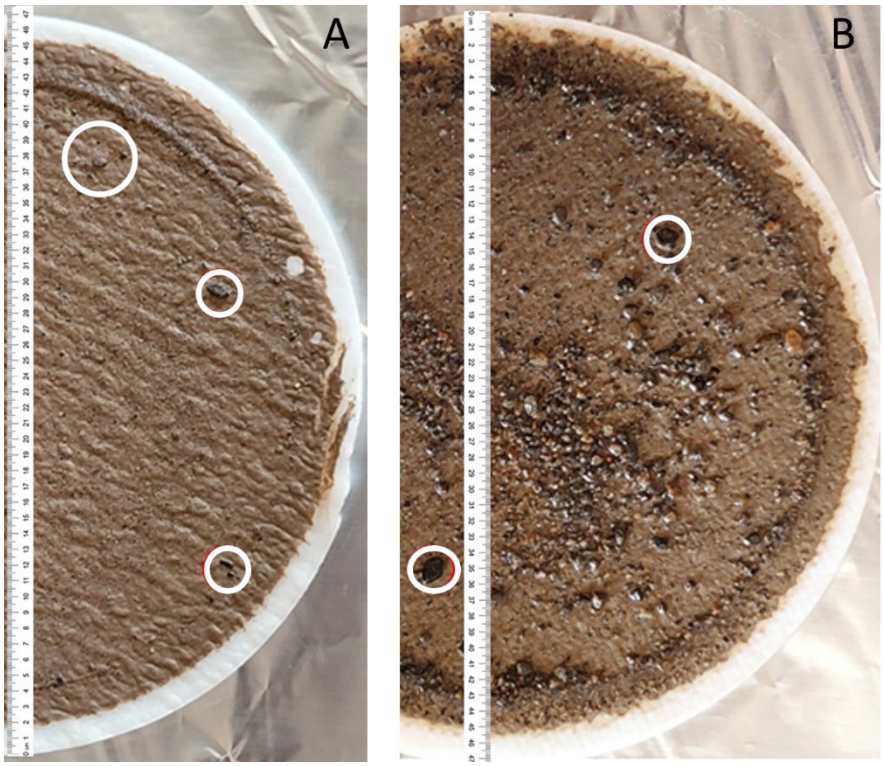

Figure 62 Suspended sediment sample in filter paper from early in the 2021 melting season. Sample A had a normal distribution of grain size ≤ 1,0mm, and sample B had a bimodal distribution of grain sizes ≤ 1,5mm.

5.2.3 The daily sediment cycle and seasonal trends

Temperature increase, quantity of precipitation, groundwater, and solar radiation cause ablation and meltwater (Nowak & Hodson, 2013). These factors influence the occurrence and amount of sediment delivery (Hodson & Ferguson, 1999). Figure 63 shows connections between discharge, suspended sediment concentration (SSC), temperature, and precipitation. The variables display the following characteristics found in each mode interpreted from the 2021 hourly hydrograph:

Mode 1: At the beginning of a melting season there is commonly little available sediment due to frozen ground (Etzelmüller & Frauenfelder, 2009). This corresponds with what was observed in the SSC for the 2021 melting season. For this mode, one small peak in the SSC could be seen (Figure 63). This peak occurs at the same time as a peak in the air temperature and discharge, showing that more sediment becomes available as temperature increases and allows for discharge to transport it. As the temperature and discharge decrease after the peak, so does the SSC. This is typical for early melting seasons where snow- and ice melt dominate the runoff in the system (Scott, 1978).

Mode 2: From mode 1 to mode 2, the average daily air temperature had increased. At the beginning of the mode discharge and SSC increased significantly despite relatively stable temperatures and little precipitation. This might be a result of the system becoming more glacially controlled, and meltwater channels within the glaciers suddenly shifting and releasing more sediment-laden meltwater into the hydrological system (Bogen & Bønsnes, 2003; Hasnain & Thayyen, 1999). From the 18th to the 20th of July, a larger precipitation event occurred. During the event, both discharge and SSC decreased along with the

temperature, supporting the hypothesis that temperature has the largest control on the system. Towards the end of this mode, the temperature increased again while the discharge dropped, and the SSC continued in the same trend seen earlier in this mode. This indicates a switch in the controlling factor of the system as temperature remained stable.

Mode 3: The highest SSC peaks occur in mode 3. The amplitude of the peaks in the SSC is significantly larger than the peaks observed in modes 1 and 2 in light of the relatively low discharge values. As the discharge was low and it was late in the melting season, the high SSC must be a result of other factors than a glacial meltwater-controlled system. Thawing permafrost and an increased active layer make sediment more available for erosion and transport (Nilsson et al., 2015; Scott, 1978). This supports the hypothesis that the modes represent shifts in the system. At the end of the mode, the drop in SSC is possibly a result of depletion in the sediment storage (Orwin et al., 2010) as the system is about to freeze (Bogen & Bønsnes, 2003).

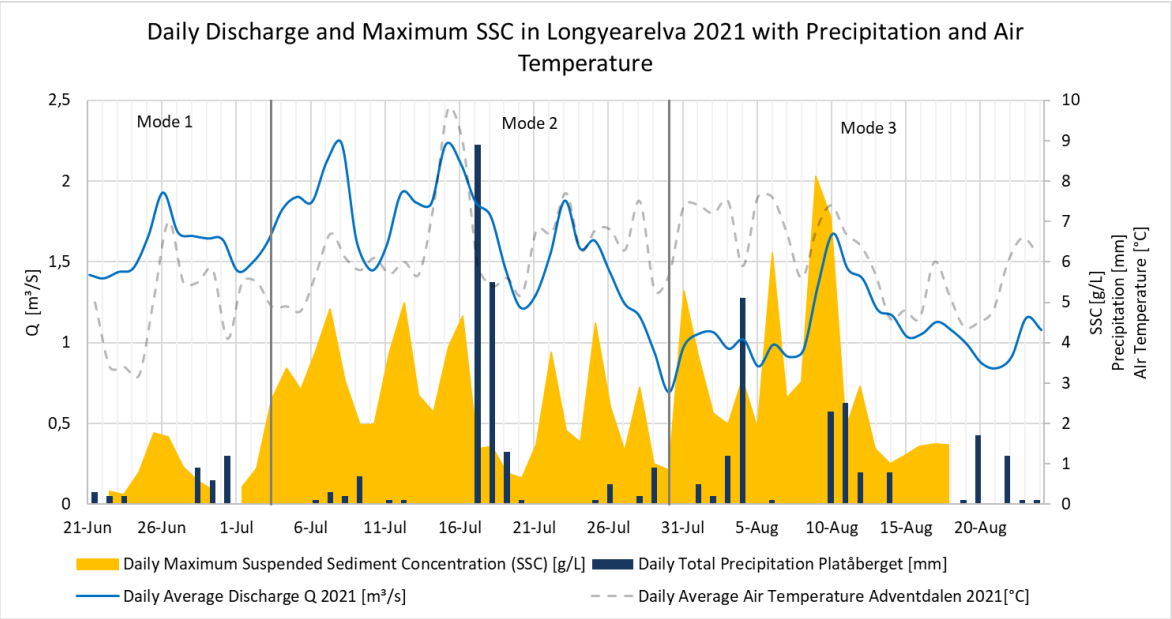

Figure 63 Daily average discharge and suspended sediment concentration in Longyearelva compared with daily total precipitation from Platåberget and daily average air temperature in Adventdalen in 2021.

To further investigate the relationship between the suspended sediment concentration (SSC) and discharge, four scatterplots were made (Figure 64) for; A) the whole monitoring period, B) mode 1, C) mode 2, and D) mode 3. For the whole period the R^2 value was 0,06. Indicating that there was no relationship between the SSC and discharge. A closer investigation of the individual modes reveals stronger associations. For mode 1, the R^2 value was 0,27. The relationship was still considered weak but stronger compared to the whole period. Low sediment availability with rising discharge was likely the reason for the existing but weak relationship. Mode 2 had an R^2 value of 0,41. This reveals a relatively strong linear trend between the SSC and the discharge, likely a result of high sediment availability and high discharge. This supports the hypothesis of higher sediment availability with seasonally thawing ground. In mode 3, the R^2 value was 0,24, showing that the relationship weakened at the end of the melting season. The low association in mode 3 supports the hypothesis that the system shifts from being glacially controlled to being controlled by thawing permafrost. The

result of a thicker active layer was that the sediment input to the river was no longer dependent on discharge but rather the availability of sediments.

The fact that the individual modes show a stronger relationship compared to the whole monitoring period further confirms suspicions that throughout the melting season, different factors dominate the discharge (e.g., snowmelt, precipitation, meltwater, groundwater, etc.) This supports the decision to study and interpret the monitoring data on the basis of three modes. Discharge was the main controller of sediment transport in the beginning and middle of the melting season as a result of snow melt (mode1) and glacier melt (mode 2). At the end of the melting season, thawing permafrost is assumed to be the main controller (mode 3).

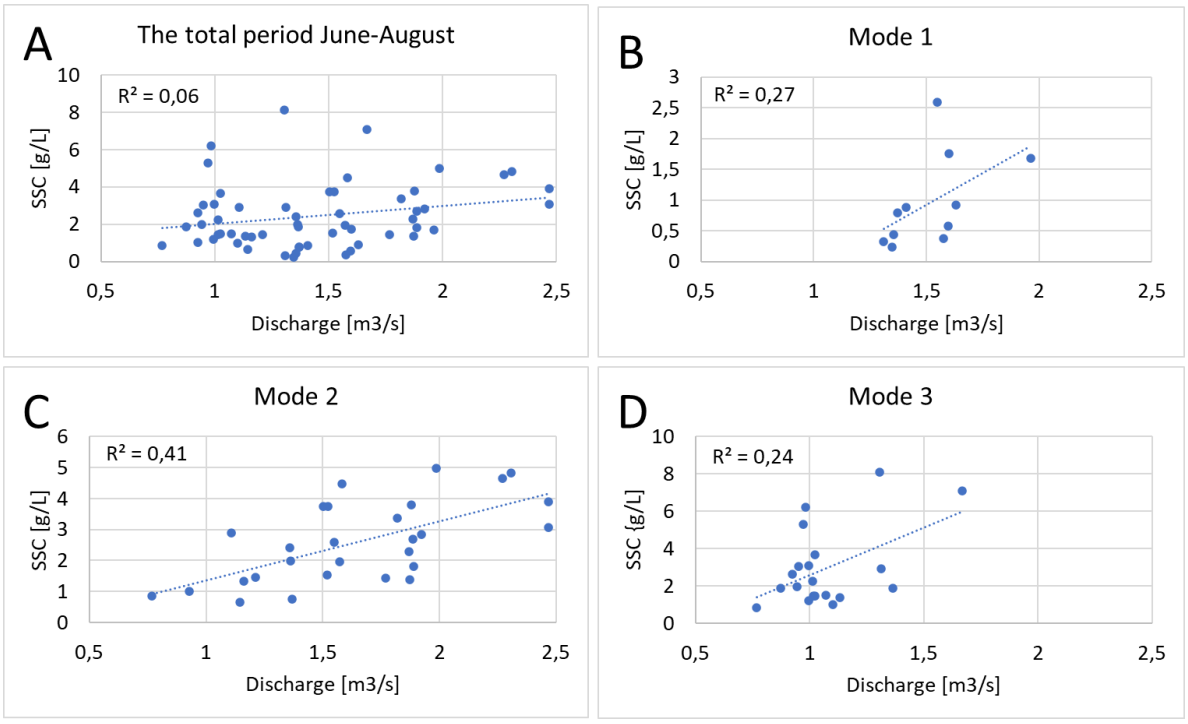

Figure 64 Relationship between maximum suspended sediment concentration (SSC) and daily average discharge for A) the whole period (22/07/21-19/08/21), B) mode 1 (22/07/21 – 04/07/21), C) mode 2 (04/07/21 – 31/07/21) and D) mode 3 (31/07/21 – 19/08/21).

The time of occurrence for the maximum SSC (Figure 34) was most commonly at 20:00 in modes 1 and 2. Around the 31st of July, when the system changed from mode 2 to mode 3, the time of occurrence was observed to change to 14:00. Similarly, the daily maximum discharge mainly occurred between 19:00 and 00:00 in modes 1 and 2. In mode 3 the maximum values more often occurred around 16:00. The discharge peaks, along with the maximum SSC, occurred progressively earlier in the day, resulting in shorter rising limbs and extended falling limbs as a likely result of the glacial drainage system changing through the melting season. This is found possible for both polythermal glaciers (Hasnain & Thayyen, 1999) and cold glaciers (Bogen & Bønsnes, 2003). In glacier-fed meltwaters, diurnal variations in discharge and suspended sediment concentration (SCC) are typical (Hasnain & Thayyen, 1999). The water stage is subject to a change throughout the season. This change is attributed to the degradation of the river channel caused by seasonal melting of the upper permafrost layer (Bogen & Bønsnes, 2003). The change in time of occurrence may also be related to 1) a shift

from meltwater dominated system to a rain- or groundwater-dominated system, 2) days getting shorter, and the sun doesn't warm for that long resulting in lower sediment transport later the day or 3) higher sediment availability late in the melting season due to thawing of permafrost.

The suspended sediment load (SSL) and the discharge from 2020 and 2021 are presented in Figure 65, split into modes as interpreted from the 2021 hydrograph (Figure 59). The SSL shows an estimation of the total amount of sediment transported through the river system for both years. The observed trends for the inter-seasonal sediment variations in 2021 have been described in this chapter by the use of Figure 63, and they are further confirmed in Figure 65A. The low SSL in mode 1 for the 2021 hydrograph was probably a result of low sediment availability. Higher SSL with larger diurnal variations in mode 2 was related to glacier meltwater and higher sediment availability. The SSL remained high regardless of decreasing discharge, likely as a result of thawing ground in mode 3. This caused high availability of easily transported sediment, even though the discharge was reduced. At the end of mode 3, both discharge and SSL dropped as a result of the melting season coming to an end.

The inter-seasonal trends in discharge for the 2020 melting season were described in Chapter 5.2.1. To further study the trends in sediment transport for the Longyeardalen catchment, the SSL from 2020 (Figure 65B) will be compared to the SSL from 2021(Figure 65A). In mode 1, although larger amounts of sediment were transported in 2020 compared to 2021, the overall sediment transport was low. For both seasons, it is assumed to be a result of frozen ground early in the melting season, limiting the sediment availability. In mode 2, the Late July Flooding in 2020 caused significantly elevated values for the SSL and the discharge (marked in gray in Figure 65B). The significance of how strongly the air temperature can affect the snow- and glacier melt, and the control it has on discharge and sediment transport, was reflected by this event. Reoccurring periods of high-low discharge and SSL could be observed for both years. Although the periods do not align perfectly within the mode, similar values in both discharge and SSL could be found in the two years (disregarding the results of the heat wave). This concurs with the hypothesis that mode 2 is dominated by glacier melt (Bogen & Bønsnes, 2003). In mode 3, the SSL was high despite the average discharge being relatively low for both hydrographs. The peak in the 2021 SSL was high compared to the relatively low correlating peak in discharge around the 10th of August. In 2020 the peak in discharge around the 13th of August was higher than the typical peaks seen throughout the melting season. Meanwhile, the peaks in SSL were equal to or lower than the previously observed peaks. The two graphs show a different relationship between the SSL and the discharge for mode 3. This can further corroborate the hypothesis that the discharge (i.e., snow- and glacier melt) is not the main controlling factor in the system at the end of the melting season.

Seeing at the modes fit well with the inter-seasonal trends in suspended sediment transport and discharge for two consecutive years, it might suggest that the inter-seasonal trends observed occur seasonally. The data presented confirm that the theoretical annual sediment cycle described in Chapter 2.2.3 can apply to this catchment. For 2021 the total SSL transported was at least 11 700 tonne. In 2020 Løvaas (2021) found the SSL to be at least 41 050 tonne. The low SSL value in 2021 is an underestimate as the river was not monitored throughout the hydrological year. The large value seen in 2020 was mainly a result of the Late July Flooding (Løvaas, 2021). The suspended sediment concentration in meltwater throughout

the melting season was variable in 2020 and 2021. The variable changes in sediment supply in a glacial system may reflect seasonal pattern of suspended sediment transport (Østrem, 1975).

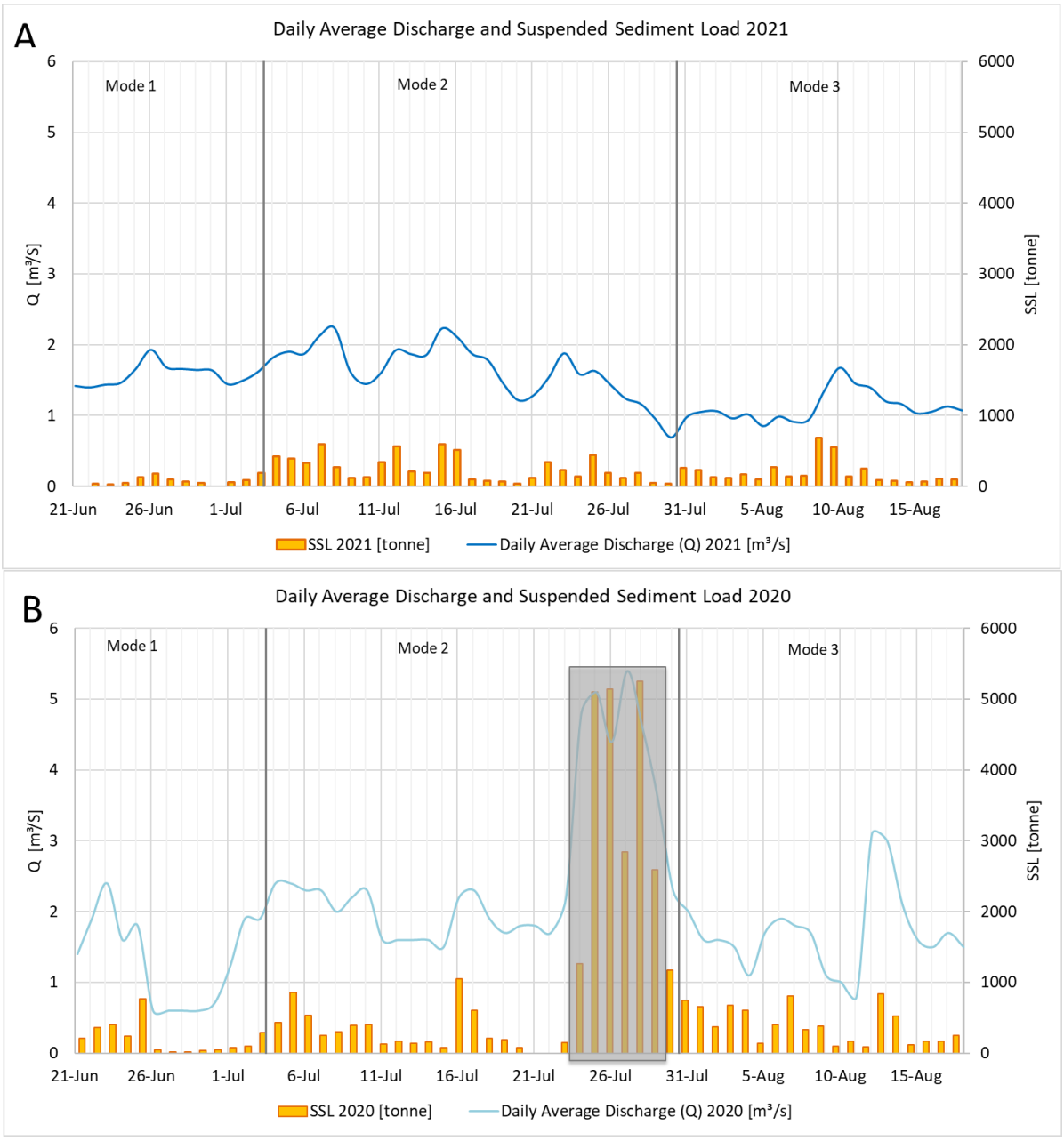

Figure 65 Suspended sediment load and daily average discharge in Longyearelva in A) 2021 and B) 2020. What is here defined as suspended sediment load is equivalent to what Løvaas (2021) defined as suspended sediment yield.

5.3 Delta development over time

So far, we have seen sediment sources and how the sediments are transported to the coastal zone. In this chapter, the main research questions will be discussed. From the Longyeardalen catchment system, the sink is considered to be glaciofluvial-marine sedimentation in the shallow and deeper pars of Adventfjorden (Figure 66), including the beach and delta formations. The final sink is eventually the deep-sea basin.

Figure 66 Flow chart of the Longyeardalen source-to-sink system. This chapter is centered around the sink. The main focus is transport in Longyearelva and sink in the Longyear delta.

To understand the processes currently affecting the delta development and delta front position, it is important to study how it has developed over time. The deglaciation of the west coast of Svalbard began ~13 ka years ago, and around 10 ka years ago the glaciers were withdrawn to fjordheads (see Chapter 2.4.1) (Landvik et al., 1998). As the glacial retreat continued, the Longyeardalen valley was left open for subaerial river processes. The braided meltwater river (Longyearelva) started filling up the previously glacierized valley with sediment (Figure 67). As the shallow valley lies protected from coastal processes, the sediment transported filled the valley relatively fast. During the past glacial, the global sea level was 120 m lower than today (Hanssen-Bauer et al., 2019), but it began to increase the last 10 ka years as the ice sheet melted (Landvik et al., 1998). The marine limit for Adventfjorden is 60-70 m (Rubensdotter et al., 2015). Although the sea level was raised, the glacial isostatic uplift (GIA) (Table 4) resulted in a decreasing trend in the relative sea level (RSL) (Table 5). The GIA is likely continuing to contribute to delta progradation as the RSL was and still is declining (Hanssen-Bauer et al., 2019). When the rapidly prograding river delta reached the sea, it likely began to prograde more slowly due to erosion, longshore transport, and a deeper fjord basin. These factors will be further discussed in the following chapters.

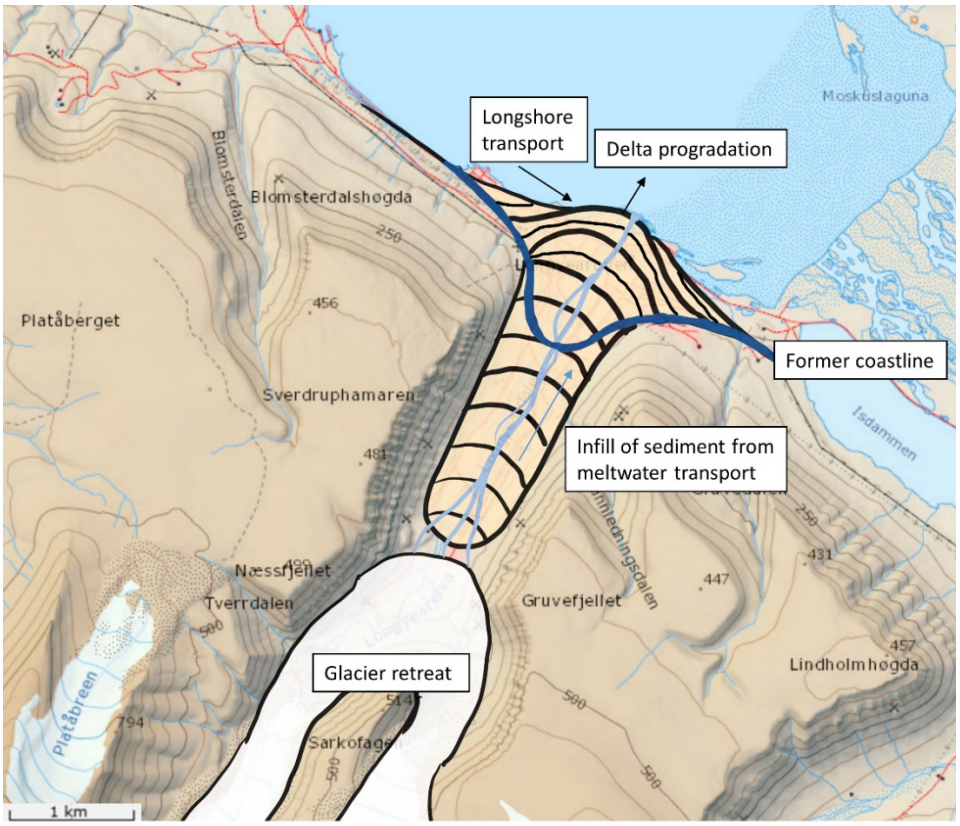

Figure 67 Conceptual sketch of Longyearelva filling up the glacierized valley with sediments, creating a prograding river delta.

5.3.1 Where does sediment in the delta originate?

From the suspended sediment samples (Figure 62) and the bedload monitoring, it was concluded that sediments are transported as suspended particles, saltation, sliding, and rolling to the delta (Nichols, 2009). Even though the results from the passive tracers were limited, they indicated that sediments up to at least 300-350 mm could be transported by the river. In a braided river system, the bedload might be transported slower to the delta due to lateral transport as a result of rapidly switching thalweg and channel paths (Miall, 1977; Nichols, 2009). The bedload monitoring from 2020 (Løvaas, 2021) and 2021 shows that cobbles and boulders can be transported as bedload in the braided section of Longyearelva. Today, large sections of Longyearelva are restricted to a single, straight channel (The Norwegian Water Resources and Energy Directorate, 2020). It is possible that when confining the runoff to a reduced lateral extent, larger grain sizes are transported faster to the delta area because of higher flow speed (Brattli, 2019; Hjulstrom, 1935). The delta is dominated by coarse sediment, indicating that the finer sediment has been washed away by the river and coastal processes (e.g., wave action and tide), to be deposited further out into the fjord or as tidally reworked deposits (Meade, 1972; Nichols, 2009).

The delta will, in theory, collect sediments from the entire catchment, but the sediments with direct contact with the river system are more prone to end up in the delta (Meade, 1972). The delta front was mainly made up of coarse sediments, as seen in grain size distribution curves and photos in Figure 68. The primary source of the sediments in the delta is from Longyeardalen and transported by the river and reworked by the coastal processes. In more

recent years, coarse material has also come from anthropogenic interference. In the delta front, the grain size distribution (Figure 41) lies within the typical ranges for fluvial material and glacio-fluvial material, as they include a lot of sand and gravel (Brattli, 2019). Photos taken at the location of each sample (Figure 68) shows a large variety of grain sizes over a small area. In the river mouth, silt can be observed on the surface as a result of secondary tidewater sedimentation due to the mean tidal difference being approximately 1,1 m (Kartverket, 2020b). Sample 008 (Figure 68E) has characteristics of being more tidewater influenced due to the high content of silt and clay.

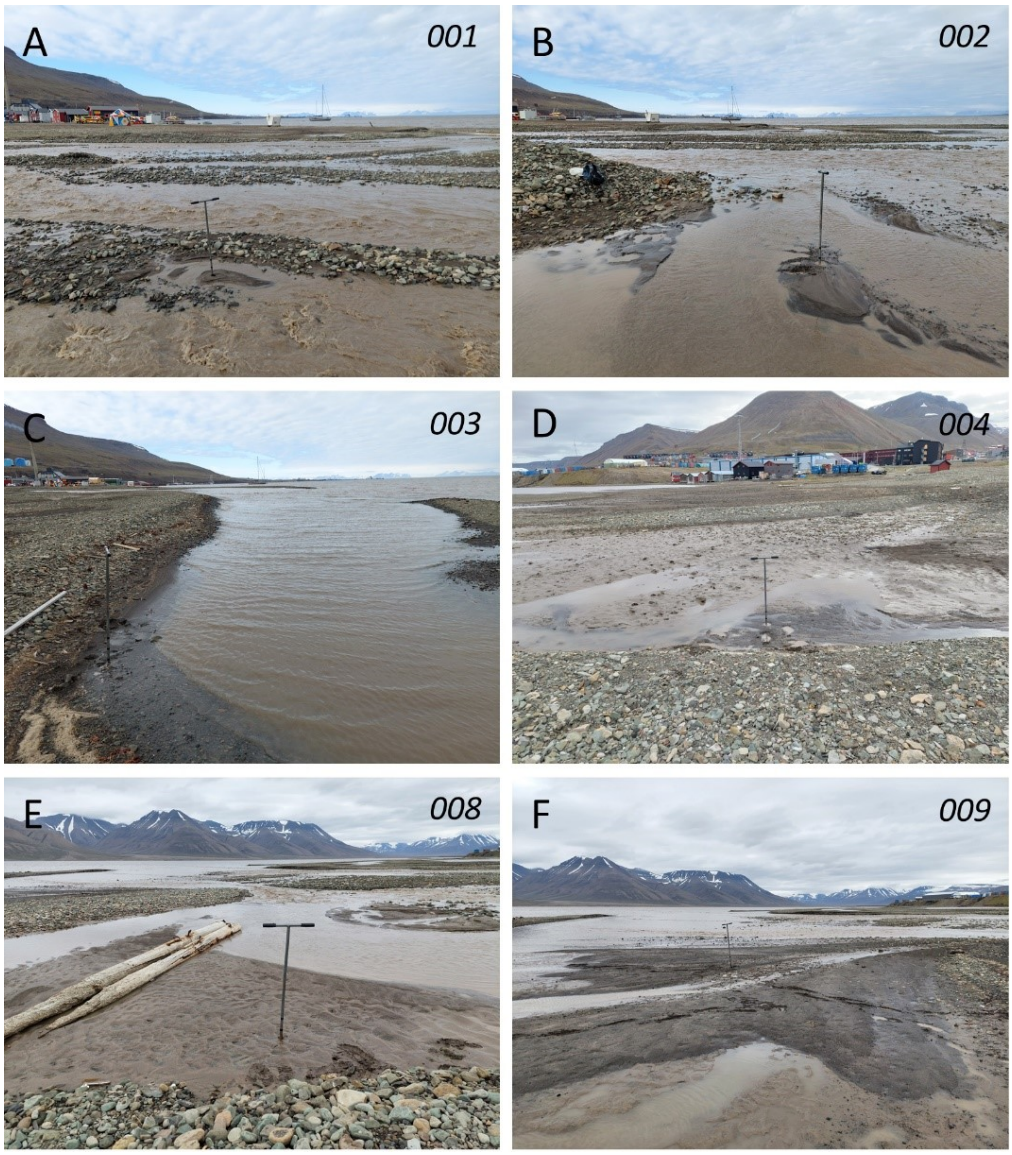

Figure 68 Photos of the location of each sediment sample collected from the Longyear delta. Location and grain size distribution curve can be found in Figure 41. Photo ABC taken towards west, photo D taken towards southeast, and photo EF taken towards east. Sediment probe for scale.

Overwash features were observed on the beach ridges and spits (Figure 69). The sediments deposited in overwash features were of the coarser grain sizes, which indicates that the sediment was from a shallow marine environment and not from a deep marine environment. They were likely created during winter storms when Adventfjorden was ice-free (Nichols,

2009). It is therefore likely to be redeposited river material. Similar structures can be found in aerial imagery from 1936. The reverse grading in the beach ridges by Gruvedalen (Figure 43) is likely to be a result of two different environments where either different energy during deposition caused the reverse grading or depletion of fine-grained sediment leaves coarser grain sizes from primary deposits.

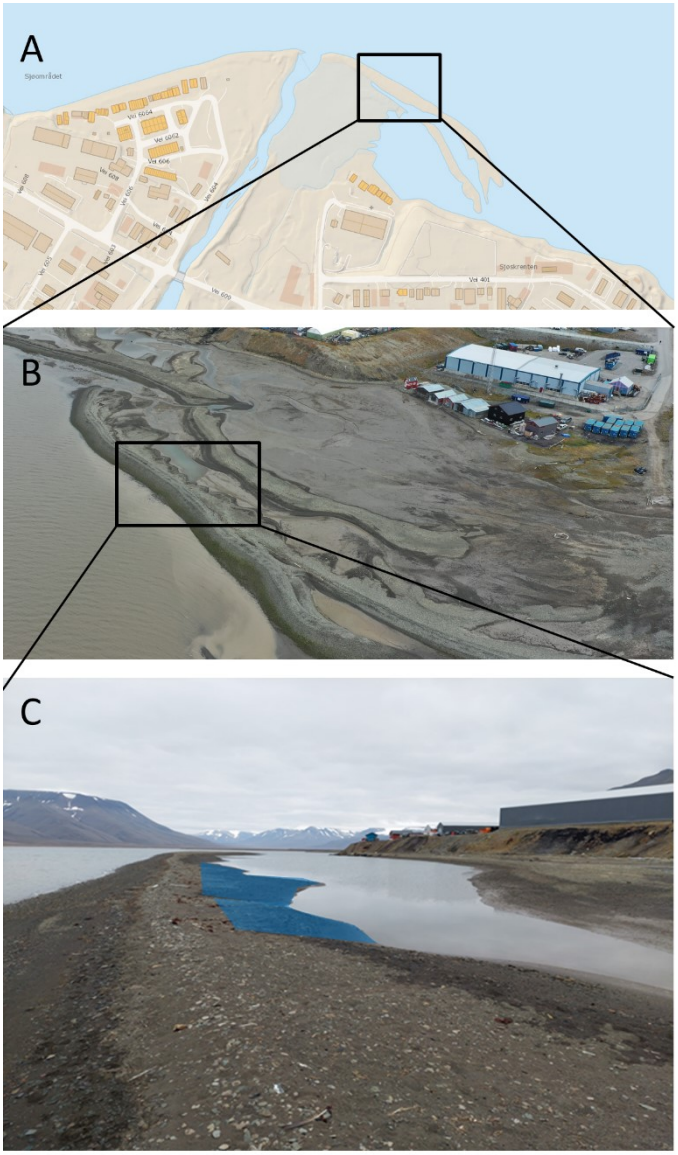

Figure 69 Overwash structures on beach ridge by Søppelfyllinga from August 2021. A) Overview. B) Imagery of overwash structures on a beach ridge. Photo towards southeast C) Blue area represents overwash deposits. Photo towards east.

Longyeardalen is located on the south side of Adventfjorden, with Isfjorden in the west and the Advent delta in the east. The strongest and most frequent waves are coming from Isfjorden (west). This is likely to be a contributor to erosion in the west and accumulation in the east of The Longyear delta. The local population is observing less sea ice in the fjord, and climate predictions suggest the reduction will increase (Hanssen-Bauer et al., 2019; Søreide et al., 2020).

During field observations, it was discovered anthropogenic pink rocks along the Longyeardalen shoreline (Figure 42), with decreasing frequency from the west towards the end of Søppelfyllinga. On the coastline in front of Gruvedalen, they were not present. This confirms the hypothesis that longshore transport occurs along the delta from northwest to southeast, where the rocks from the fill mass at the west of the delta (section 1) have been transported towards Gruvedalen.

It has previously been reported that the delta is exposed to a westward longshore transport (Dill et al., 2021), which is the opposite direction of what was observed in 2021. The study used coal as an indication of the current direction. As coal "dust" is light and easily transported, it is possible that it has been affected by the Adventelva coming from the east and thereby shows signs of being transported from east to west. This also suggests that the depositional zone (section 3, Figure 38) is strongly reliant on the Longyear delta river-to-ocean interactions, at the same time as its being altered by mechanisms related to Adventelva and the Advent delta. Freshwater from Adventelva flows on top of the salty seawater due to differences in density (Meade, 1972), likely creating a weak river current above the longshore transport created from wave action. As coal is low-density material, it has likely been floating in the weak river current as a suspended load. Simultaneously pebbles are being transported from west to east, indicating stronger transport influence from the northwest. The coal can show that actions from Adventelva do affect the Longyear delta, but to a smaller degree than the longshore current.

5.3.2 Delta formation and geometry

The coarser grain sizes accumulating on the delta front can, during one year, develop or accrete up to several spits and beach ridges (Hayes, 1979; Nichols, 2009). Orthophotos have shown that from the beginning to the end of melting season, beach ridges and spits can be eroded, prograding, and redeposited. From the volume calculations of beach ridges 1 and 2 (Figure 40), ca. 462 m^2 was eroded and likely redeposited only within a couple of months. This is illustrated in Figure 70, where a suggested concept of delta progradation is a result of a dynamic relationship between the river and the coastal zone (beach).

Stage A show a prograding delta with a net wave transport direction from left to right. This net wave transport will from here on be referred to as longshore transport. The longshore transport causes depositional landforms as beach ridges and spits to develop on one side of the delta. In stage B, the outer parts of the older depositional features are still being reworked in terms of erosion and accumulation. Meanwhile, the delta continues to prograde causing new depositional features to develop on the seaside of previously developed landforms. In stage C, the delta continues to prograde. Furthermore, the longshore transport causes erosion on the left side of the delta due to the continued progradation outwards into the sea. Erosion leading to an asymmetrical delta. On the right side of the delta the depositional features continue to grow. The innermost landforms are at this point considered to be permanently repositioned, while the outermost is continuously reworked by the coastal mechanisms.

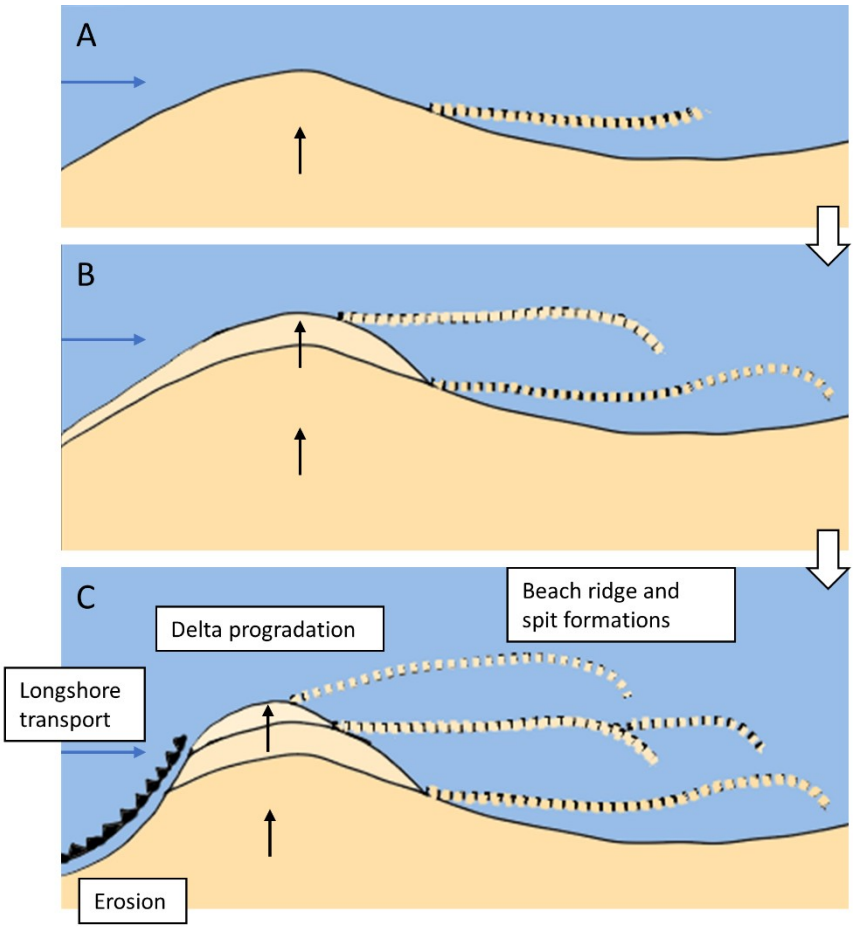

Figure 70 Schematic timeline with three periods (ABC) showing the delta progradation from an overhead view. The progradation is affected by net wave transport direction (longshore transport), and erosional and depositional areas.

The hypothesis that the innermost landforms become permanently deposited is confirmed by the higher amount of weathering found in the beach ridges closest to land. What was also observed was that the outermost beach ridge in the depositional zone by Gruvedalen also consisted of strongly weathered deposits suggesting it has been relatively stable for more than one year. This is despite the fact that it is the outermost beach ridge. It is therefore important to keep in mind that Figure 70 only shows a concept of delta progradation, and that the outermost beach ridge is not necessarily the youngest. Taking into consideration the relative age of the beach ridges the system seems to build out around the delta (Figure 71). Waves erode the west side of the delta and overwash accumulated in the east, which is likely a result of reduced sea ice in the fjord (Søreide et al., 2020).

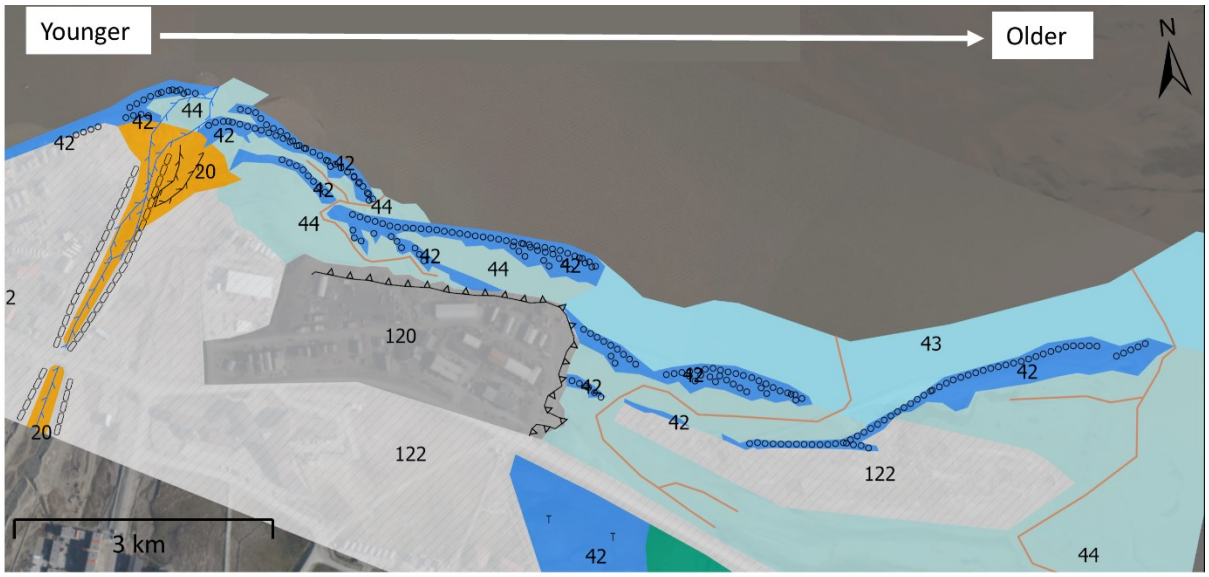

Figure 71 Relative age of beach ridges from the Longyear delta to the depositional area. Clip of Figure 39.

This thesis is mainly restricted to studying the river transport and the delta and coastal zone. Although, it is worth mentioning that a study by Prior et al. (1981) looked at the Longyear delta slope. It was suggested that submarine slopes of the Longyear delta had the potential to be unstable. Their interpretation of a side-scan sonar showed submarine erosion scarps, chutes, ridges, blocks, and depositional fans in the delta slope (Figure 72A). This suggests that sediment was transported and deposited from the upper delta slopes in the deeper parts of Adventfjorden as a result of submarine mass movement (Prior et al., 1981). The quantification of the delta change (see Chapter 4.4.3) in this study has shown that the Longyear delta slope is actively prograding. It is therefore believed that this could have partaken in the formation of the morphological features found in the delta slope (Figure 72A). Larger blocks were interpreted to be transported down the slope (Prior et al., 1981), indicating that the bottom of the fjord consists of more than settling suspended sediment from the surrounding river systems in Adventfjorden (Meade, 1972).

The Longyear delta is steeply inclined (Figure 72B) and has prograded rapidly from 1936 to 2021. The net shoreline movement (NSM) was up to 167 m over the 85-year period (see Chapter 4.4.3). These circumstances can make the Longyear delta susceptible to submarine slope failure. Uneven submarine depth contours from 2020 show indications that chutes are still present on the delta slope. It has been argued that when upfjord-winds (northwest) occur, they can cause surface waves to significantly impact the cyclic loading effects on bar-front sediments of the delta. The mass movement of the bar-front sediments can be the cause of the observed chutes (Prior et al., 1981). Large amounts of snowmelt, precipitation, low tide, and stormy weather can also be contributing causes for submarine landslides (L'Heureux et al., 2010).

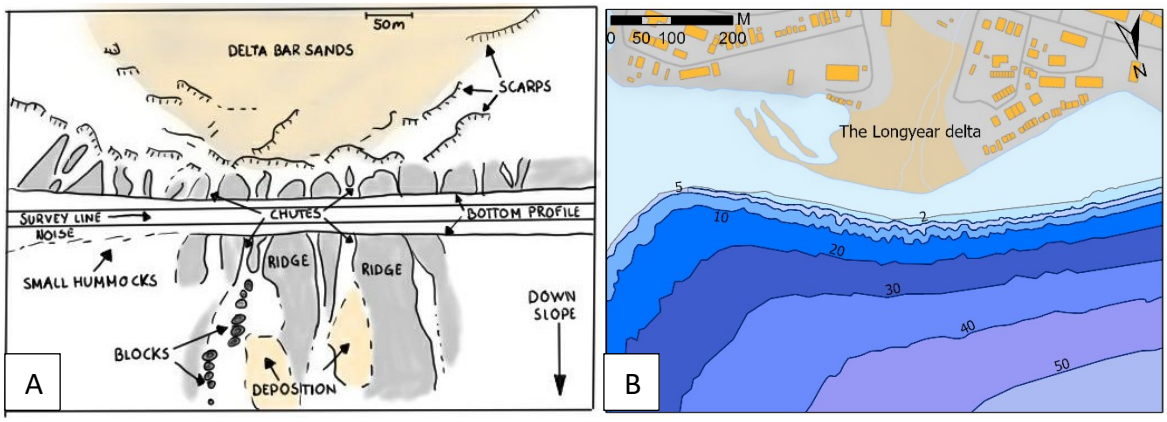

Figure 72 A) An interpretative map of the Longyear delta slope from a side-scan sonar. Modified from Prior et al. (1981). B) Depth countors from 2020 of the Longyear delta slope (Kartverket, 2020a).

5.3.3 The Longyear delta compared to other systems on Svalbard

To put the Longyear delta in perspective, similar systems were introduced in Chapter 4.5. In Adventfjorden two spit systems could be found on opposite sides of the fjord. One related to the Advent delta and the other to the Longyear delta. They were found to be quite similar, with little change over time. Through quantification of the delta change using DSAS, it is known that the coastline by the Longyear delta has changed a lot since 1936, up to 167 m. Despite this, we still do not see massive changes in the spit Longyear system. The biggest changes in the Longyear delta spit system over time were documented closest to the river outlet and in the area where marine deposits had been dug out. Both spit systems were built from the west towards the east, suggesting that longshore transport as a result of net wave movement from Isfjorden affects the whole coastline in Adventfjorden.

In Isfjorden, there are two delta systems with similar conditions. Both Longyeardalen and Vindodden are glacierized catchment systems with approximately the same catchment size. It is expected that since the Longyear delta has two glaciers able to provide sediment to build up the delta, that this would be the larger delta of the two. However, this is not the case, as Vindodden was calculated to be five times bigger than the Longyear delta (see Chapter 4.5.2). The two deltas also have different shapes of delta fronts. Due to the location of the Vindodden delta, it is more exposed to wave action. The mechanisms in the sea for the two systems are likely to be quite different. The Longyear delta is strongly affected by longshore transport of sediments, causing net erosion in the west and net progradation in the east. If the Vindodden system does not experience the same amount of longshore transport but is largely affected by wave action, it can be a part of the explanation for why they look quite different. Different types of ocean processes and the angle at which the forces hit the coast are therefore important for the symmetry of the delta front position. As there is no data on sediment transport in the Vindodden system, it is not possible to make a statement regarding sediment transported to the delta. Other factors such as geology, bathymetry, and anthropogenic interference also contribute to the shape of the delta front (Jensen & Rubensdotter, 2020).

When closer studying the aerial imageries and orthophotos over the Longyear delta, it is possible to draw similarities from the 1936 aerial imagery of the Longyear delta to the 2009 orthophoto of the Vindodden delta. A hypothesis for this is that in 1936 when the Longyear coastline was 167 m further back (inland, in Longyeardalen). It was more protected from the

longshore transport, which acted as the main influence for the asymmetrical shape of the delta front today.

5.3.4 Natural development and anthropogenic interference

The Longyeardalen catchment system is the source-to-sink system strongest affected by anthropogenic interference in Svalbard. Even the oldest aerial imagery (1936) shows signs of human activity.

Throughout this thesis, orthophoto and basemaps from 2009 have been frequently used. Datasets from 2009 have become a standard for many maps over Svalbard, and particularly Longyearbyen. When using these, it is important to consider that the basemaps are an interpretation based on the available data at the time. A consequence of this becomes clear in the depositional zone (Figure 73A) of the coastline by Longyearbyen. In the spit system, beach ridges have been permanently deposited and later anthropogenically disturbed. As a result, the disturbed beach ridges were incoherent, soft, and mixed with tidal mud. Making it close to impossible to walk on. This anthropogenically disturbed sediment has been interpreted as a relatively large barrier island (Figure 73B), which does not reflect the reality of the coastal morphology. The extent of beach ridges and anthropogenically disturbed sediment were mapped in Figure 39.

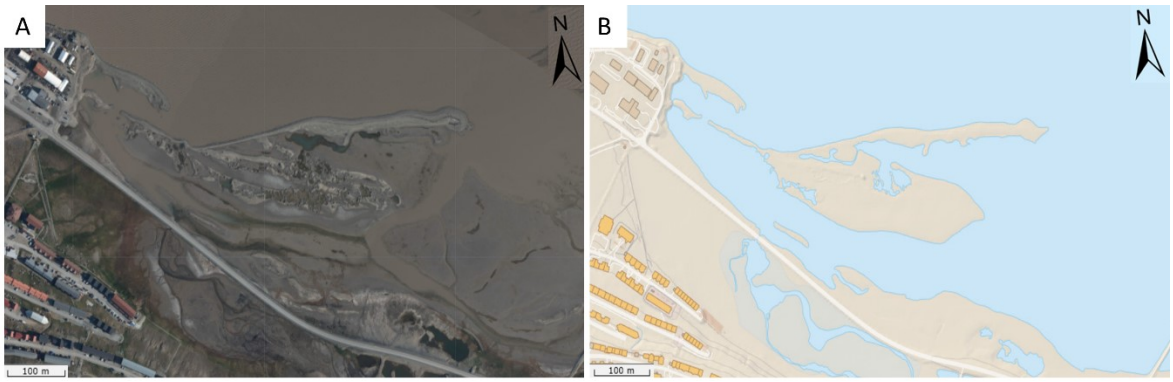

Figure 73 Overview of the depositional zone by Longyearbyen. A) The spit system with anthropogenically disturbed sediment in a clip of the 2009 orthophoto. B) The spit system has been interpreted as a relatively large barrier island in a clip of the 2009 basemap from the Norwegian Polar Institute (n.d.-a).

Periodically and occasionally anthropogenic measures, i.e., mitigation walls, fill mass, building roads, and digging, have been taken to restrict the lateral extent of the river and delta (Longyearbyen Lokalstyre, 2017; The Norwegian Water Resources and Energy Directorate, 2020). An example of how the river and delta have been managed can be seen in Figure 74. Early in the melting season in 1990 (A), Longyearelva has broken through beach ridges created by winter storms on the east side of the Longyear delta. The river mouth had braided features with several small channels leading into the fjord. Buildings (marked with a white circle) can be seen close to the river outlet. Late in the melting season in 1990 (B), Longyearelva was a straight channel with mitigation walls to confine the active channel in the center of the delta. As the river threatened the buildings (A), measures to take control of the river and river outlet were used in an effort to save the constructions on the east side of the delta (B). This illustrates that over just how fast anthropogenic interference can change a system, as the orthophotos were taken a few months apart.

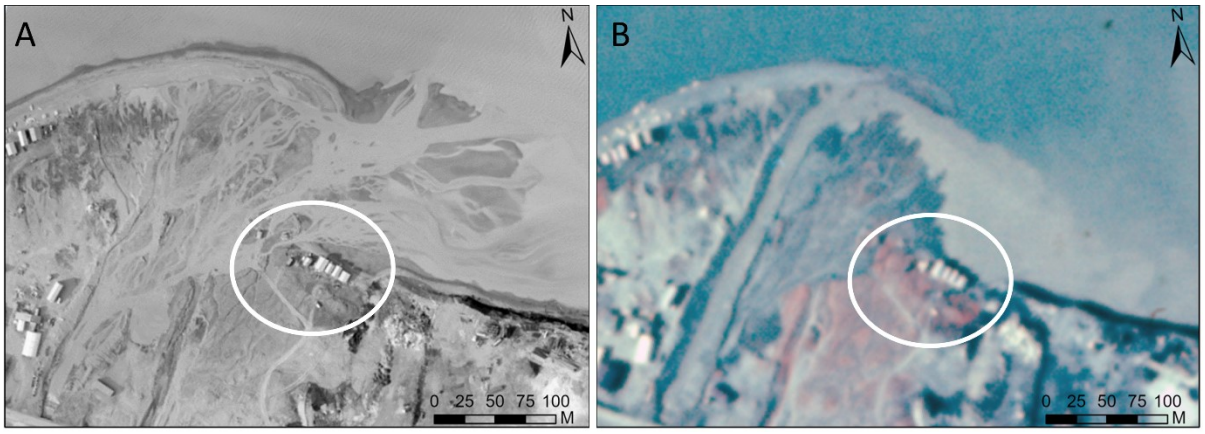

Figure 74 The Longyear delta in 1990. White circles show infrastructure vulnerable to erosion. A) Early melting season$_1$ before drastic measurements were taken in the river mouth. B) Late melting season$_2$ after drastic measurements were taken in the river mouth.

The sediment-laden water from the river outlet was, in both orthophotos (Figure 74), flowing towards the east. This also supports the hypothesis that longshore transport from west to east is a dominating factor in the development of the delta front position. From the available aerial imagery and orthophotos through time (Figure 44), it has been observed that the Longyear delta has changed from a symmetrical delta (1936) to a slightly asymmetrical delta (1990) and eventually to a completely asymmetrical delta (2009). With the restricted availability of older aerial imagery and limited monitoring data, it is difficult to state if the development of the delta front symmetry is solely a result of the processes in the natural system. Nor how large the effect of anthropogenic interference is.

From the quantification of delta change (see Chapter 4.4.3) it was observed that from 1936 to 2021, the net shoreline movement (NSM) was up to 167 m. The Quaternary geological map of the Longyear delta (Figure 39) shows that large areas within the coastal zone are anthropogenically disturbed sediment or anthropogenic fill mass. It is assumed that the fill mass resulted in an anthropogenic progradation of the shoreline, although the development of the delta was naturally prograding. The suspended sediment yield (SSY) for the catchment indicates that large amounts of sediment can be transported to the delta, the relative sea level (RSL) is declining (Table 5), and the isostatic uplift rates are positive (Table 4). All of which contribute to a prograding delta.

5.3.5 Future development

The warming Arctic has already resulted in changes in the glaciers and the glaciofluvial system in the Longyeardalen catchment. Over the past 40 years, it has been reported both increasing temperatures and precipitation, and a reduction in land fast sea ice duration (Hanssen-Bauer et al., 2019; Nowak et al., 2020; Søreide et al., 2020). All these changes strongly affect the river-to-ocean interactions and the delta development on short- and long-term scales. The anthropogenic interference has made the already complex glaciofluvial delta system even more difficult to understand. The data collected in 2021 is considered as a baseline when discussing potential future outcomes.

From the available aerial imagery and orthophotos through time, it has been observed that the Longyear delta has changed from a symmetrical delta (1936) to a slightly asymmetrical delta

(1990) and eventually to a completely asymmetrical delta (2009). Based on landforms and types of sediment in the coastal zone, it is possible to predict which areas are prone to erosion and deposition because of the direct linkage between coastal processes and types of landforms and sediment (Jensen & Rubensdotter, 2020). The Quantification of delta changes along with field observation shows that:

- The west side of the delta (section 1, Figure 38) has experienced erosion over the last 30 years. It will likely continue to do so in the future due to net wave transport from the west, causing longshore transport.
- Although erosion occurs in the west, the delta front (section 2, Figure 38) has been prograding during the same period. Due to fluctuating shorelines, seasonally shifting landforms (e.g., beach ridges and spits), and management of the Longyearelva river mouth, the progradation can be seen to vary from 0m to 116m for a 30-year period. Over an 85-year period the delta has prograded up to 167m, suggesting that the delta front will continue to do so as long as the sediment supply to the delta continues.
- The spit system in the depositional zone (section 3, Figure 38) has seemingly been developing under the same river and coastal processes over the last 85 years. This despite being moved further out in the fjord as a result of both natural development and human interference (i.e., river- and delta front management and disturbances in depositional features). As the depositional landforms are heavily influenced by the river-to-ocean interactions, the future development of the depositional zone is expected to rely on delta development and human activity.

Some important questions to ask when addressing the future development of the Longyear delta and coastline are "*Is the total sediment transport in Longyearelva expected to increase or decrease in the future, and what consequences will it have for the delta and coastline development*?"

If the Arctic continues to warm, it is a possibility that the sediment availability will increase as the permafrost thaws. This may also cause more active slope processes that also function as a sediment source (see twin-study Pallesen (2022)). Whether the sediment gets transported down the system or gets stored depends on the development of discharge. As the climate change trends are likely to continue in the Arctic (Hanssen-Bauer et al., 2019), it is possible that the dominating factors and controls on the hydrological system change, where precipitation, groundwater, and thawing permafrost can change trends observed.

Small arctic catchments in Svalbard have already passed "peak water", thus a decrease in glacial meltwater is expected (Nowak et al., 2020). If this is the case for Longyearbreen and Larsbreen, it is thought that the decrease in meltwater will also contribute to a long-term decrease in sediment load (Overeem & Syvitski, 2008). In addition, it is likely that the competence of the river is reduced due to lower discharge and flow velocity leading to smaller particles being transported as bedload which would further decrease river erosion (Brattli, 2019; Hjulstrom, 1935). This would lead to reduced sediment input to the delta, as well as smaller grain sizes. A reduction of sediment input would slower or potentially halt the propagation of the delta. It is a possibility that the net erosion caused by longshore transport will decrease in intensity should the delta stop prograding. A change in grain size will have an effect on both the delta front position and landforms related to the river-to-ocean interactions. Until today we have seen that the finer sediment is mostly washed away from the delta, and

the coarse sediment builds up the delta front. If the sediment input changes to finer grain sizes, the delta might be exposed to more erosion as a result of ocean processes such as wave action and tidal influences.

Due to the warming of the Arctic, a long-term increase in sediment transport is also a possibility (Orwin et al., 2010). For the Longyeardalen catchment, temperature increase has been observed along with increased precipitation over the last 30 years (Table 11), and it is projected to continue to increase (Hanssen-Bauer et al., 2019). Increasing temperatures will likely cause increasing active layer thickness and thereby increase the amount of material prone to erosion (Guégan & Christiansen, 2017). Twin-study Pallesen (2022) concluded that these factors would, at least on a short-term scale, increase sediment transportation as slope processes accelerate. An increase in sediment input to the Longyear delta will continue and potentially accelerate the progradation into the fjord. A significant increase in sediment delivery through rivers to deltas could offset the impacts of climate-induced coastal erosion in some areas (Rowland et al., 2010). A rapid and increasing progradation can potentially lead to increased erosion west of the delta while the depositional landforms continue to develop.

Projections of increased and higher frequency precipitation suggest that the catchment may experience a shift from being glacially controlled to being precipitation-dominated. This affects the daily and seasonal sediment cycles. High-intensity precipitation can cause flooding and event-based transportation of sediment to the delta. It has already been observed instabilities in the delta slope (Prior et al., 1981), and sudden, high sediment loads might further increase the slope instability causing changes to the delta front position. A higher frequency of precipitation could lead to daily trends, e.g., evening rain. This can result in a more constant sediment transport to the delta, causing a more stable progradation.

Due to the warming in the Arctic, it is expected that the melting season will increase in length. If the melting season starts earlier, a depletion of sediment sources may occur earlier in the season. This is not expected to happen for the Longyeardalen catchment (at least on the short-term scale), as large amounts of sediment are stored in the permafrost. With continued thaw of the permafrost, along with glacial, moraine, and slope processes, sediments are likely to not be depleted before the melt season is over and the system freezes (Pallesen, 2022).

A continued reduction of sea ice will increase wave action, especially during winter storms. This will increase the erosion of the coastline. Even though the wave can create depositional features such as overwash, the erosion is expected to be bigger than the deposition and thereby reduce the progradation of the delta.

The future development of the delta is mainly dependent on sediment supply. Over longer time scales, the isostatic uplift is an important factor along with the relative sea level. Over a short time scale the erosive and depositional forces are more important. A change in sediment supply regarding both size and quantity contributes to the shape and front. Anthropogenic interference has been shown to have a large contribution to delta development as well.

5.4 Uncertainties and potential future studies

The two main uncertainties for this thesis were 1) lack of hydrological monitoring and 2) the restricted availability of older remote sensing. This was known in the beginning, and this study aimed to improve that. It must be acknowledged that the lack of aerial imagery between the mostly natural river and delta system in 1936 and the anthropogenically influenced system in 1990 prevents a thorough understanding and quantification of the delta development. The remote sensing data indicates a significantly altered landscape after human acquisition. From historical sources, it is also known that sediments from the coastline have been used for roads and infrastructure, which means that the delta and beach ridge volumes were underestimated when collecting measurements from today's landscape.

Some potential questions and recommended measures that could be addressed in future studies:

- Continue the long-term monitoring project under RiS ID 11641 to ensure continuity and comparable data, especially in terms of investigating if the Longyeardalen catchment has experienced "peak water" and which consequences it may have for sediment transport. It would be interesting to see how large particles can be transported as suspended load, how high the discharge must be before sand can be transported in suspension, and how large particles can be transported as bedload.
- Monitoring of the active layer in regard to the thickness and water flux to further study the effects of climate change in the Longyeardalen source-to-sink system.
- It is recommended to continue to create orthophotos of the coastline to the same or larger spatial extent as in 2021. This is to monitor the erosion, further document the threat it has on the infrastructure, and quantify the development of secondary sedimentary deposits.
- Further work to document and classify coastlines at smaller and larger scales has already begun. A continued interdisciplinary discussion and data sharing in the coastal dynamics group would be beneficial to get a broader understanding of how climate change can affect the Svalbard coastlines.

6 Conclusion

A long-term monitoring project is set to investigate hydrological and geomorphological changes in Longyeardalen in a changing climate ("Hydrology, sediment transport, and erosion in Longyeardalen" - RiS ID 11641), which has been active since 2018. During the 2021 melting season, the Longyeardalen source-to-sink system was investigated to study the long-term geomorphological development of the arctic Longyear delta in regard to river-to-ocean interactions and sediment input. Twin-study Pallesen (2022) investigated the source and transport in the system.

In the present study, a large collection of aerial imagery, orthophotos, digital elevation models (DEM), and 3D-models was made to study the long-term development of the delta and river system from 1936 to 2021. In addition, a range of field methods was applied between the 22nd of June 2021 and the 25th of August 2021, including hydrological and geomorphological monitoring using water measurements, sediment samples, passive tracers, and drone photogrammetry. It is possible to apply the collected data as baseline data for the catchment system as no extreme weather or event (e.g., temperature, precipitation, flooding) occurred. From geomorphological mapping, a Quaternary map of the Longyear delta was produced.

Key findings from this study:

- Three sections of the coastline were identified: 1) an erosional coastline west of the Longyear delta, 2) a fluctuating shoreline in the Longyear delta, and 3) a depositional coastline east of the delta.
- The approximate volume of sediments in the Longyear delta was calculated to be 48 000 ± 9600 m^3 (excluding the erosive and depositional zones).
- Twelve marine beach ridges were observed related to the river-to-ocean system. From the two most active beach ridges, approximately 460 ± 90 m^3 of sediment was eroded and redeposited over approximately two months.
- The average hourly discharge in the 2021 melting season was 1,3 ± 0,1 m^2/s. In 2020 it was 1,5 m^2/s.
- The maximum discharge in 2021 was 3,2 ± 0,3 m^2/s on the 8th of July 2021.
- The maximum suspended sediment concentration was 8,1 ± 0,8 g/L on the 25th of July 2021.
- The total suspended sediment load was at least 11 700 tonne in 2021. In 2020 it was 41 050 tonne.
- Particles ≤ 1,5 mm in diameter were found in suspended sediment samples.
- 5,8% of the passive tracers were registered after movement from the initial location. The largest moved passive tracer was 300-350 mm in diameter, and the longest transport distance was 74 m.

Primary sediment sources in the Longyeardalen catchment are the glacier system, the moraine system, and aeolian deposition of fine-grained sediments. The main transport mechanisms are the river system (including fluvial transport, -erosion, and temporary storage) and ocean processes (e.g., waves and tide). The sink is the delta formation and marine sedimentation (both shallow and deep sedimentation in the fjord).

Three modes were interpreted from an hourly hydrograph for the 2021 melting season to study the seasonal and inter-seasonal trends in the hydrological system in Longyeardalen.

Based on the interpreted modes, a hypothesis was developed suggesting that throughout the melting season, the dominating control of the hydrological system changed twice. The following dominant controls were concluded for each mode: At the beginning of the melting season (mode 1) the hydrological system was dominated by snowmelt, resulting in little sediment transport as the ground was frozen and partially covered with snow. In the middle of the melting season (mode 2) it was dominated by glacier melt. This is concluded based on a significant increase in discharge and suspended sediment concentration (SSC) and a strong correlation between the two. In the beginning and middle of the melting season (modes 1 and 2), the discharge and sediment transport largely respond to temperature variations as a controlling factor. At the end of the melting season (mode 3), the system was controlled by thawing permafrost in the ground. This was supported by a low correlation between the discharge and the SSC, where relatively high sediment concentrations were transported during relatively low discharge. Thawing ground makes more sediment available for erosion and transport. At the end of mode 3, both discharge and SSC are low as the hydrological system might experience sediment depletion and was about to freeze again.

The delta morphology is a result of transported sediment, depth of the fjord, and transport mechanisms. Two conceptual models of delta development were presented. The first model suggests how the delta prograded over the last 10 ka, after the past glacial. It is assumed a rapid progradation of the delta through Longyeardalen as the valley was a branch of Adventfjorden before the isostatic uplift. Then the delta prograded slower as it was exposed to erosion, longshore transport, and a deeper fjord basin in Adventfjorden. The second model illustrates how the progradation of the Longyear delta became asymmetrical with a large erosional and depositional zone as a result of longshore transport. Net wave action causing longshore transport has led to an asymmetrical delta front position. The innermost beach ridges furthest away from the river mouth had an older relative age compared to the ones close to the river mouth. The two main factors that alter the delta front position are 1) isostatic uplift (for longer time scales) and 2) progradation due to sedimentation in the delta and coastal zone (for shorter time scales).

Short-term analysis (2009-2021) of the delta change shows up to 7 m of net erosion west of the delta and up to 32 m of net progradation in the river mouth. The last 30 years show net erosion up to 21 m west of the delta, a largely fluctuating river mouth, and up to 116 m of net progradation east of the delta. The large net progradation resulted from a shifting river outlet and anthropogenic interference. Over the last 85 years there has been no net erosion. The smallest net progradation (0-10 m) occurred west of the delta, and the highest net progradation was up to 167 m in the river mouth, with relatively high values towards the east. The long-term net progradation is a result of combined natural accretion and anthropogenic interference. The delta has a highly dynamic character related to erosion and deposition, which may result in consequences for the development of infrastructure in the area.

A direct linkage between coastal processes and types of landforms and sediment makes it possible to predict which areas in the coastal zone are prone to erosion and deposition. Areas already experiencing erosion or deposition are prone to experience similar future development. Furthermore, climate change in the Arctic is well established. Continued warming is projected along with increased frequency and intensity of precipitation, and reduced sea ice. Possible consequences of this are changes in trends related to discharge and sediment transport. The hydrological system may become dominated by other factors than

snow- and glacier melt and thawing permafrost, such as precipitation and groundwater. Although this will affect the diurnal and seasonal trends in discharge and thereby transport of sediment to the delta, the short-term change in delta progradation would mainly be depended on a decrease or increase in the total sediment transported. A continued reduction of sea ice will likely increase wave action and thus longshore current, especially during winter storms. This will probably increase the erosion of the coastline in the west. How this will affect the deposition is unsure.

References

Beven, K. J., Wood, E. F., & Sivapalan, M. (1988). On hydrological heterogeneity—catchment morphology and catchment response. *Journal of Hydrology*, *100*(1-3), 353-375.

Bogen, J. (1992). Monitoring grain size of suspended sediments in rivers. *Erosion and sediment transport programmes in river basins*, 183-190.

Bogen, J., & Bønsnes, T. E. (2003). Erosion and sediment transport in High Arctic rivers, Svalbard. *Polar Research*, *22*(2), 175-189. https://doi.org/10.3402/polar.v22i2.6454

Brattli, B. (2019). *Ingeniørgeologi løsmasser*. Akademika.

Brown, G. H. (2002). Glacier meltwater hydrochemistry. *Applied Geochemistry*, *17*(7), 855-883.

Christiansen, H. H., Gilbert, G. L., Demidov, N., Guglielmin, M., Isaksen, K., Osuch, M., & Boike, J. (2020). Permafrost temperatures and active layer thickness in Svalbard during 2017/2018 (PermaSval). *SESS Report 2019*, 237-249.

Court, A. (1957). The Classification of Glaciers. *Journal of Glaciology*, *3(21)*, 2-7. https://doi.org/10.3189/S0022143000024618

Dill, H. G., Jolanta, K., Andrei, B., Sorin-Ionut, B., Stephan, K., & Borrego, A. G. (2021). Organic debris and allochthonous coal in Quaternary landforms within a periglacial setting (Longyearbyen Mining District, Norway)-A multi-disciplinary study (coal geology-geomorphology-sedimentology). *International Journal of Coal Geology*, *233*, 103625.

Dingman, S. L. (2015). *Physical hydrology*. Waveland press.

Esri. (n.d.). *World Imagery*. https://www.arcgis.com/home/item.html?id=10df2279f9684e4a9f6a7f08febac2a9

Etzelmüller, B., & Frauenfelder, R. (2009). Factors controlling the distribution of mountain permafrost in the Northern Hemisphere and their influence on sediment transfer. *Arctic, Antarctic, and Alpine Research*, *41*(1), 48-58.

Etzelmüller, B., Hagen, J., Vatne, G., Ødegård, R., & Sollid, J. (1996). Glacier debris accumulation and sediment deformation influenced by permafrost: examples from Svalbard. *Annals of Glaciology*, *22*, 53-62.

Etzelmüller, B., Ødegård, R. S., Vatne, G., Mysterud, R. S., Tonning, T., & Sollid, J. L. (2000). Glacier characteristics and sediment transfer system of Longyearbreen and Larsbreen, western Spitsbergen. *Norsk Geografisk Tidsskrift - Norwegian Journal of Geography*, *54*(4), 157-168. https://doi.org/10.1080/002919500448530

Favaro, E. A., & Lamoureux, S. F. (2015). Downstream patterns of suspended sediment transport in a High Arctic river influenced by permafrost disturbance and recent climate change. *Geomorphology*, *246*, 359-369. https://doi.org/10.1016/j.geomorph.2015.06.038

Gallagher, S., Fulthorpe, C., Bogus, K., Auer, G., Baranwal, S., Castañeda, I., Christensen, B., De Vleeschouwer, D., Franco, D., & Groeneveld, J. (2017). Expedition 356 methods.

Geological Survey of Norway. (n.d.). *API og WMS-Tjenester*. https://www.ngu.no/emne/api-og-wms-tjenester?fbclid=IwAR1sM9bJ7JWcY4nqYxxiRiNKugD0s_NUXSg6uUNP669nYA4YvHjm7zkA780

Grochowicz, A., Heineken, D., & Wennberg, S. (2021). The reliability of wind power in the Longyearbyen area.

Grønsten, H. A. (1998). *Hydrological Studies and Simulations of a High Arctic Catchment Longyearelva, Spitsbergen* [Master thesis, The University of Oslo/University Centre in Svalbard].
Guégan, E. B., & Christiansen, H. H. (2017). Seasonal Arctic coastal bluff dynamics in Adventfjorden, Svalbard. *Permafrost and Periglacial Processes*, *28*(1), 18-31.
Haldorsen, S., & Heim, M. (1999). An Arctic groundwater system and its dependence upon climatic change: an example from Svalbard. *Permafrost and Periglacial Processes*, *10*(2), 137-149.
Hanna, J. (2019). *Longyear River, lower part*. https://sketchfab.com/3d-models/longyear-river-lower-part-a813f4f25ec44f53a9d95f54c79b854b
Hannah, D. M., Smith, B. P., Gurnell, A. M., & McGregor, G. R. (2000). An approach to hydrograph classification. *Hydrological Processes*, *14*(2), 317-338.
Hanssen-Bauer, I., Førland, E. J., Hisdal, H., Mayer, S., Sandø, A. B., & Sorteberg, A. (2019). Climate in Svalbard 2100 - a knowledge base for climate adaptation. https://doi.org/10.13140/rg.2.2.10183.75687
Hasholt, B., Bobrovitskaya, N., Bogen, J., McNamara, J., Mernild, S. H., Milburn, D., & Walling, D. E. (2006). Sediment transport to the Arctic Ocean and adjoining cold oceans. *Hydrology Research*, *37*(4-5), 413-432.
Hasnain, S. I., & Thayyen, R. J. (1999). Discharge and suspended-sediment concentration of meltwaters, draining from the Dokriani glacier, Garhwal Himalaya, India. *Journal of Hydrology*, *218*, 191-198. https://doi.org/10.1016/s0022-1694(99)00033-5
Hayes, M. (1979). Barrier island morphology as a function of tidal and wave regime. In: Leatherman SP (ed) Barrier Islands. *Academic Press, New York*, *1*, 27.
Hergot, V. G. S. (2021). *Where the Arctic River Meets the Sea; Connections Between Fluvial and Shoreline Processes in Isfjorden, Svalbard* [Master thesis, NTNU].
Himmelstoss, E. A., Henderson, R. E., Kratzmann, M. G., & Farris, A. S. (2021). *Digital Shoreline Analysis System (DSAS) version 5.1 user guide* [Report](2021-1091). (Open-File Report, Issue. U. S. G. Survey. http://pubs.er.usgs.gov/publication/ofr20211091
Hjulstrom, F. (1935). Studies of the morphological activity of rivers as illustrated by the river fyris, bulletin. *Geological Institute Upsalsa*, *25*, 221-527.
Hodgkins, R., Cooper, R., Wadham, J., & Tranter, M. (2003). Suspended sediment fluxes in a high-Arctic glacierised catchment: implications for fluvial sediment storage. *Sedimentary Geology*, *162*(1-2), 105-117. https://doi.org/10.1016/s0037-0738(03)00218-5
Hodson, A., Nowak, A., & Christiansen, H. (2016). Glacial and periglacial floodplain sediments regulate hydrologic transfer of reactive iron to a high arctic fjord. *Hydrological Processes*, *30*(8), 1219-1229. https://doi.org/10.1002/hyp.10701
Hodson, A., Tranter, M., Dowdeswell, J., Gurnell, A., & Hagen, J. (1997). Glacier thermal regime and suspended-sediment yield: a comparison of two high-Arctic glaciers. *Annals of Glaciology*, *24*, 32-37.
Hodson, A. J., & Ferguson, R. I. (1999). Fluvial suspended sediment transport from cold and warm-based glaciers in Svalbard. *Earth Surface Processes and Landforms*, *24*(11), 957-974.
Humlum, O., Instanes, A., & Sollid, J. L. (2003). Permafrost in Svalbard: a review of research history, climatic background and engineering challenges. *Polar Research*, *22*, 191-215. https://doi.org/10.1111/j.1751-8369.2003.tb00107
Jaskólski, M. W., Pawłowski, Ł., & Strzelecki, M. C. (2018). High Arctic coasts at risk-the case study of coastal zone development and degradation associated with climate changes and multidirectional human impacts in Longyearbyen (Adventfjorden,

Svalbard). *Land Degradation & Development*, *29*(8), 2514-2524. https://doi.org/10.1002/ldr.2974
Jensen, M., & Rubensdotter, L. (2020). *Dynamic Svalbard Coastline (DynaCoast)*.
Kartverket. (2020a). *Sjøkart - Dybdedata 20201001*.
Kartverket. (2020b). *Tidevannstabeller for den norske kyst med Svalbard* (0801-2024).
Killingtveit A, Kane D.L, & D., Y. (2004). Water balance studies in two catchments on Spitsbergen, Svalbard.
King, C. A. (1970). Feedback relationships in geomorphology. *Geografiska Annaler: Series A, Physical Geography*, *52*(3-4), 147-159.
Klimaservicesenter, N. (n.d., April 2021). *Klimaprofil Longyearbyen2022-04-06*. Norsk Klimaservicesenter. Retrieved 15/04 from https://klimaservicesenter.no/kss/klimaprofiler/longyearbyen
L'Heureux, J.-S., Hansen, L., Longva, O., Emdal, A., & Grande, L. (2010). A multidisciplinary study of submarine landslides at the Nidelva fjord delta, Central Norway-Implications for geohazard assessment. *Norwegian Journal of Geology*, *90*(1-2), 1-20.
Ladegaard-Pedersen, P., Sigsgaard, C., Kroon, A., Abermann, J., Skov, K., & Elberling, B. (2017). Suspended sediment in a high-Arctic river: An appraisal of flux estimation methods. *Sci Total Environ*, *580*, 582-592. https://doi.org/10.1016/j.scitotenv.2016.12.006
Lafrenière, M. J., & Lamoureux, S. F. (2019). Effects of changing permafrost conditions on hydrological processes and fluvial fluxes. *Earth-Science Reviews*, *191*, 212-223. https://doi.org/10.1016/j.earscirev.2019.02.018
Lambert, S. J. (2004). Changes in winter cyclone frequencies and strengths in transient enhanced greenhouse warming simulations using two coupled climate models. *Atmosphere-Ocean*, *42*(3), 173-181. https://doi.org/10.3137/ao.420302
Landvik, J. Y., Bondevik, S., Elverhøi, A., Fjeldskaar, W., Mangerud, J., Salvigsen, O., Siegert, M. J., Svendsen, J.-I., & Vorren, T. O. (1998). The last glacial maximum of Svalbard and the Barents Sea area: ice sheet extent and configuration. *Quaternary Science Reviews*, *17*(1-3), 43-75.
Lecher, A. L. (2017). Groundwater discharge in the Arctic: A review of studies and implications for biogeochemistry. *Hydrology*, *4*(3), 41.
Longyearbyen Lokalstyre. (2017). *Arealplan for Longyearbyen planområde 2016 - 2026* 2016/929). https://www.lokalstyre.no/arealplan-2016-2026.486570.no.html
Lønne, I., & Lysså, A. (2005). Deglaciation dynamics following the Little Ice Age on Svalbard: implications for shaping of landscapes at high latitudes. *Geomorphology*, *72*(1-4), 300-319.
Lønne, I., & Nemec, W. (2004). High-arctic fan delta recording deglaciation and environment disequilibrium. *Sedimentology*, *51*(3), 553-589. https://doi.org/10.1111/j.1365-3091.2004.00636.x
Løvaas, M. A. S. (2021). *Management of a High Arctic River* [Master Thesis, NTNU]. Trondheim.
Major, H., & Nagy, J. (1972). Geology of the Adventdalen map area: With a geological map, Svalbard C9G 1: 100 000.
Meade, R. H. (1972). Sources and sinks of suspended matter on continental shelves. *Shelf sediment transport: Process and pattern*, 249-260.
Miall, A. D. (1977). A review of the braided-river depositional environment. *Earth-Science Reviews*, *13*(1), 1-62.
Miller, G. H., Brigham-Grette, J., Alley, R., Anderson, L., Bauch, H. A., Douglas, M., Edwards, M., Elias, S., Finney, B., & Fitzpatrick, J. J. (2010). Temperature and

precipitation history of the Arctic. *Quaternary Science Reviews*, *29*(15-16), 1679-1715.
Moore, L. J. (2000). Shoreline Mapping Techniques. *Journal of Coastal Research*, 111-124.
Moreno-Ibáñez M, Hagen JO, H. C., Lihavainen H, & A, Z. (2021). *SESS report 2020*. S. I. A. E. O. System.
Nichols, G. (2009). *Sedimentology and stratigraphy* (2nd ed.). John Wiley & Sons.
Nicu, I. C., Rubensdotter, L., Stalsberg, K., & Nau, E. (2021). Coastal Erosion of Arctic Cultural Heritage in Danger: A Case Study from Svalbard, Norway. *Water*, *13*(6), 784.
Nicu, I. C., Stalsberg, K., Rubensdotter, L., Martens, V. V., & Flyen, A.-C. (2020). Coastal erosion affecting cultural heritage in Svalbard. A case study in Hiorthhamn (Adventfjorden)—An abandoned mining settlement. *Sustainability*, *12*(6), 2306.
Nilsson, C., Polvi, L. E., & Lind, L. (2015). Extreme events in streams and rivers in arctic and subarctic regions in an uncertain future. *Freshwater Biology*, *60*(12), 2535-2546.
Norwegian Polar Institute. (n.d.-a, 19/05/2020). *Norwegian Polar Institute Map Data and Services*. https://geodata.npolar.no/
Norwegian Polar Institute. (n.d.-b). *Svalbardkartet*. https://geokart.npolar.no/Html5Viewer/index.html?viewer=Svalbardkartet
Nowak, A., Hodgkins, R., Nikulina, A., Osuch, M., Wawrzyniak, T., Kavan, J., Lepkowska, E., Majerska, M., Romashova, K., Vasilevich, I., Sobota, I., & Rachlewicz, G. (2020). From land to fjords: The review of Svalbard hydrology from 1970 to 2019 (SvalHydro). *SESS Report 2020*, 176-201. https://doi.org/10.5281/zenodo.4294063
Nowak, A., & Hodson, A. (2013). Hydrological response of a High-Arctic catchment to changing climate over the past 35 years: a case study of Bayelva watershed, Svalbard. *Polar Research*, *32*(1), 19691.
Orwin, J. F., Lamoureux, S. F., Warburton, J., & Beylich, A. (2010). A Framework for Characterizing Fluvial Sediment Fluxes from Source to Sink in Cold Environments. *Geogr. Ann.*, *92*(2), 155-176. https://doi.org/10.1111/j.1468-0459.2010.00387.x
Overeem, I., & Syvitski, J. P. M. (2008). Changing sediment supply in Arctic rivers. *IAHS Publ.*, *325*.
Pallesen, L. (2022). *Sediment source-to-sink in a warming Arctic; Thawing moraines, slope processes and river erosion in Longyeardalen, Svalbard* [Master thesis, NTNU]. Trondheim.
Peirce, S., Ashmore, P., & Leduc, P. (2018). The variability in the morphological active width: Results from physical models of gravel-bed braided rivers. *Earth Surface Processes and Landforms*, *43*(11), 2371-2383.
Prior, D. B., Wiseman, W. J., & Bryant, W. (1981). Submarine chutes on the slopes of fjord deltas. *Nature*, *290*(5804), 326-328.
Radulović, M., Radojević, D., Dević, N., & Blečić, M. (2008). Discharge Calculation of the Spring Using Salt Dilution Method – Application Site Bolje Sestre Spring (Montenegro).
Riger-Kusk, M. (2006). *Hydrology and hydrochemistry of a High Arctic glacier: Longyearbreen, Svalbard* [Master thesis, University of Aarhus/The University Centre in Svalbard].
Rowland, J., Jones, C., Altmann, G., Bryan, R., Crosby, B., Hinzman, L., Kane, D., Lawrence, D., Mancino, A., & Marsh, P. (2010). Arctic landscapes in transition: responses to thawing permafrost. *Eos, Transactions American Geophysical Union*, *91*(26), 229-230. https://doi.org/https://doi.org/10.1029/2010eo260001
Rubensdotter, L., Romundset, A., Farnsworth, W. R., & Christiansen, H. H. (2015). *Landskapsformer og løsmasser, Bjørndalen-Vestpynten, Svalbard. Kvartærgeologisk kart, 1:10 000*. Norges geologiske undersøkelse.

Sahu, N., Reddy, G. P. O., Kumar, N., & Nagaraju, M. S. S. (2015). High resolution remote sensing, GPS and GIS in soil resource mapping and characterization-A Review. *Agricultural Reviews*, *36*(1). https://doi.org/10.5958/0976-0741.2015.00002.1

Scott, K. M. (1978). *Effects of permafrost on stream channel behavior in arctic Alaska*. Department of the Interior, Geological Survey.

Serreze, M. C., & Barry, R. G. (2014). *The Arctic Climate System*. https://doi.org/10.1017/cbo9781139583817

Stenius, S. (2016). Flomberegning for Longyearelva, Spitsbergen, Svalbard (400). In: NVE-Oppdragsrapport.

Store Norske. (n.d.). *Historie*. Retrieved 25/10 from https://www.snsk.no/historie

Svalbard Museum. (n.d.). *Kultur og historie*. Retrieved May from https://svalbardmuseum.no/no/kultur-og-historie/

Søreide, J. E., Pitusi, V., Vader, A., Damsgård, B., Nilsen, F., Skogseth, R., Poste, A., Bailey, A., Kovacs, K., & Lydersen, C. (2020). Environmental status of Svalbard coastal waters: coastscapes and focal ecosystem components (SvalCoast). *Svalbard Integrated Arctic Earth Observing System. SESS report*, 142-175.

The Norwegian Meteorological Institute. (n.d.). *Seklima: Observations and Weather Statistics*. https://seklima.met.no/?fbclid=IwAR2FeYDOGrhOy6a3I2H7-zoBPQ2nc6r2PDf8BJKRUVN7im6lP00dp15kDUw

The Norwegian Water Resources and Energy Directorate. (2020). *Forsterking av bunnsikringer og forlengelse av flom og erosjonssikringsanleggene* 201601388).

Vegvesen, S. (2016). *R210 Laboratorieundersøkelser* (978-82-7207-693-0).

Węsławski, J. (2011). Adventfjorden Arctic Sea in the backyard. *Institute of Oceanology PAS*.

Weslawski, J. M., Szymelfenig, M., Zajaczkowski, M., & Keck, A. (1999). Influence of salinity and suspended matter on benthos of an Arctic tidal flat. *ICES Journal of Marine Science*, *56*, 194-202.

Woo, M.-k. (2012). *Permafrost Hydrology* (1 ed.). Springer. https://doi.org/10.1007/978-3-642-23462-0

Østrem, G. (1975). Sediment Transport in Glacial Meltwater Sstreams. *Glaciofluvial and Glaciolacustrine Sedimentation*, *SP23*.

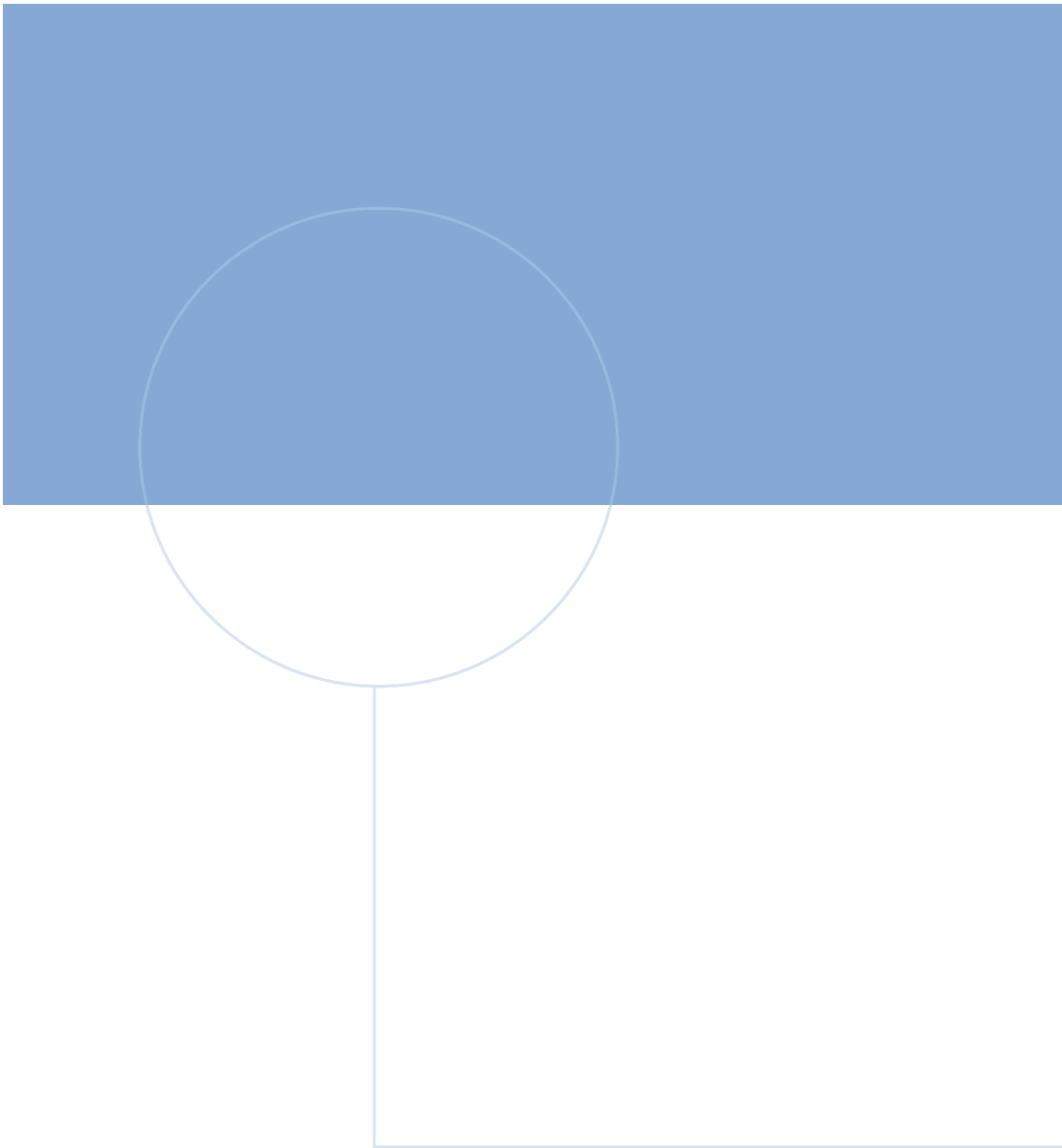

NTNU
Norwegian University of
Science and Technology

UNIS
The University Centre in Svalbard